CRANFIELD UNIVERSITY

LETIAN WANG

DEVELOPMENT OF BATTERY MANAGEMENT SYSTEM FOR HYBRID ELECTRIC PROPULSION SYSTEM

SCHOOL OF AEROSPACE, TRANSPORT AND MANUFACTURING

MSc Thesis
Academic Year: 2016.12 – 2018.04

Supervisor: Al Savvaris
April 2018

ABSTRACT

Because of the high overall efficiency and low emissions, Hybrid Electric Propulsion System (HEPS) have become an attractive research area. In this research, a parallel HEPS architecture is adopted and a Hardware test platform is constructed. As a relative new power source in powertrains, battery system plays an important role in HEPS. Hence, a Battery Management System (BMS) is investigated in this research. Battery pack State of Charge (SOC) is a key feedback value in HEPS control. In order to estimate SOC, firstly, an operation-classification adaptive battery model is proposed for Li-Po batteries. Considering the fact that model parameter accuracy is of importance in model-based system state estimation method, an event triggered Adaptive Genetic Algorithm (AGA) is applied for online parameter identification. Secondly, the Extended Kalman Filter (EKF) is applied for single battery cell SOC estimation. Finally, a fuzzy estimator is proposed for battery pack SOC estimation based on maximum/minimum cell voltages and SOC values. Experimental results show that the proposed AGA can effectively track battery parameter variation and SOC estimation error for single cell as well as for the battery pack are both less than 1%. Moreover, considering the Li-Po battery characteristics, a converter based battery cell balancing method is proposed. Simulation result shows that proposed balancing method can be effective in balancing battery cells. In addition, in relation to safety and reliability concerns, a Discrete Wavelet Transform (DWT) based battery circuit detection method is proposed and simulation results showing its feasibility are presented.

Keywords:

Hybrid electric propulsion system, Adaptive battery model, Hardware test platform construction, Battery management system

ACKNOWLEDGEMENTS

I would like to express my appreciation to Dr. Al Savvaris and Prof. Antonios Tsourdos for their inspiring guidance and kind support; to my friends and colleges for their comprehension and help.

Thanks to my family and who loves me. I love you so much.

CONTENTS

LIST OF FIGURES

LIST OF TABLES

LIST OF EQUATIONS

LIST OF ABBREVIATIONS

AGA	Adaptive Genetic Algorithm
BVLOS	Beyond Visual Line Operation System
BMS	Battery Management System
CAN	Controller Area Network
CWT	Continuous Wavelet Transform
DP	Dynamic Programming
DWT	Discrete Wavelet Transform
ECM	Equivalent Circuit Model
ECMS	Equivalent Consumption Minimisation Strategy
ECU	Engine Control Unit
EKF	Extended Kalman Filter
FLE	Fuzzy Logic Estimator
GUI	Graphic User Interface
HEPS	Hybrid Electric Propulsion System
HIL	Hardware-in-the-Loop
ICE	Internal Combustion Engine
MG	Motor/Generator
NN	Neural Network
OCV	Open Circuit Voltage
PDC	Periphery Direct Communication
PDE	Partial Differential Equation
PF	Particle Filter
PWM	Pulse Wide Module
RC	Resistance And Capacitance
RMSE	Root Mean Squared Error
SDP	Stochastic Dynamic Programming
SOC	State of Charge
SOH	State of Health
SVM	Support Vector Machine
UARTS	Universal Asynchronous Receiver/Transmitters
UKF	Unscented Kalman Filter

1 Introduction

1.1 Background

A report indicates that the total number of flights may reach 12.8 million by 2035 as compared to 8.85 million in 2014 due to the continuing development in the aviation industry [1]. This trend on the one hand promises great convenience for traveller and for global freight, but on the other hand has led to ever-increasing concerns to its environment impact.

Aviation has environmental impacts. Flights generate noise and emit greenhouse gas (CO2), NOx and particulates. In relation to the ever increasing demands for aviation transport, European Commission in their 2016 European aviation environment report [1] forecasted that CO2 and NOx emission would have 25.7% and 24.7% increases respectively compared with that in 2014. However, more stringent environmental legislation has been introduced in order to achieve long-term sustainability. For example, the EU is required to cut its carbonate emissions by 40%, as compared to1990 levels by 2030.

During the last few years, many methods have been proposed and investigated for mitigating the environmental pressure caused by aviation sector. In 2000, Airbus along with other organisations launched the CRYOPLANE project which aimed at developing a practical design for low pollutant emission liquid hydrogen fuelled aircrafts. Also, NASA has proposed a hybrid wing-body electric aircraft prototype (NASA NX-3) for improving fuel efficiency and producing lower noise and emissions. For the same purpose, Boeing and Airbus have proposed their own hybrid aircraft concepts and designed the SUGAR-Volt and the E-thrust respectively. Moreover, in the small aircraft area, a number of companies, such as Hypstair, Siemens and AXTER Aerospace are developing their own electric power plants for gliders and ultralight aircraft.

However, while aircraft in nowadays are more advanced and more environmental friendly, there is global agreement that more effort should be made to meet the future environmental and commercial challenges.

Compared with traditional internal combustion and turbo engines, electric motors have relatively high efficiency and lower operating noise. Hybrid Electric Propulsion System (HEPS) aircraft, which is comprised of Internal Combustion Engine (ICE) and electric motor/generator, can be regarded as an eclectic design for improving energy efficiency without drastically reducing performance which can be used as a stopgap before purely electric-powered aircraft become commercially viable. However, there are still many challenges involved in developing commercial HEPS aircrafts.

One challenge in developing HEPS is the design of supervisory controller. As mentioned before, a HEPS has two power sources (ICE and electric motor). The output power of the system at any time is that of the combination of the two powertrains. It is necessary to design a suitable supervisory controller to allocate power requirement to ICE and electric motor so that the system can achieve satisfactory efficiency and performance. In addition, with the Boeing 787 Li-ion battery failure problems still in recent memory [2], an effective Battery Management System (BMS) is necessary in order to meet the airworthiness and safety requirements [3] - [5]. The precondition of designing a reliable BMS is accurate battery state estimation [6] - [9]. For example, compared to 1% error in battery energy estimation, 5% error is easier to incur battery overcharge which can reduce battery life cycles or lead to permanent damages [10]. Moreover, other challenges such as HEPS weight optimization, aircraft design and aviation regulation are also important for applying HEPS in the commercial aviation sector.

1.2 Research content

This research is an on-going work as a part of the AIRSTART project, a collaborative research and development project developing key technologies for supporting BVLOS and long-endurance aircraft operations. Cranfield University is working on the hybrid propulsion system. Our objectives are to complete a HEPS system design, build a test rig to verify the proposed system, and develop an energy management system.

The project can be decomposed as following: the conceptual design including HEPS design, components selection, and energy management system development is undertaken by analysing the power requirement of the specific flight mission; the system verification requires the designed HEPS is to be tested in a Hardware-in-the-Loop (HIL) system of which the high-level schematic is shown in Figure 1-1.

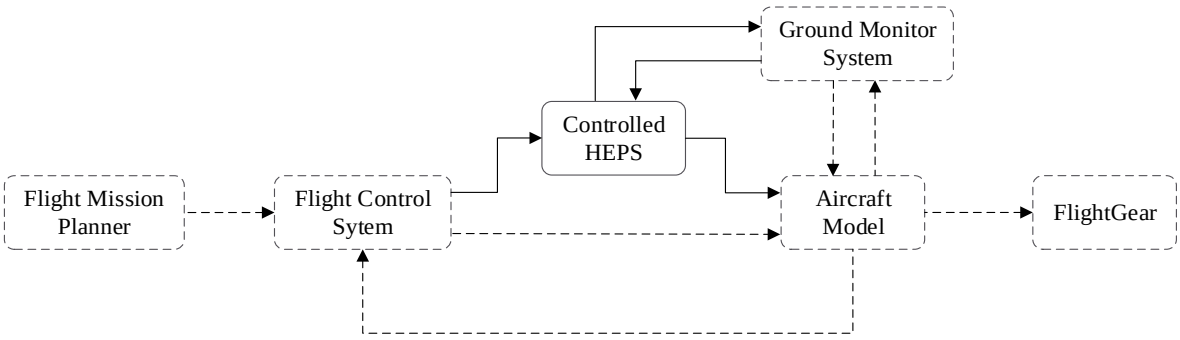

Figure 1-1 Structure of the HIL system for HEPS

The solid lines in Figure 1-1 imply that the connection or block is hardware, whereas the dashed line stands for the software part. Starting from the beginning, the flight control system decodes mission instruction from flight mission planner and determines the control command, based on the feedback information derived by the aircraft model. The control command can be divided into two parts: the power requirement for the controlled HEPS and the control value for the six degree-of-freedom aircraft model (The aircraft model also receives thrust and torque commands from HEPS). To display and monitor the status of both HEPS and aircraft, the FlightGear (software) is utilized and a ground monitoring system is developed.

As a part of the project, the research work in this thesis focuses on the development of HEPS hardware platform and energy management system. The hardware platform development part is about building a communication path among supervisory controller (built in MATLAB), hardware components (test rig) and ground monitoring system. More specifically, the hardware platform design can be divided into three sections:

1) Select a suitable real-time controller and related electronic device.
2) Develop code for each communication interface port on the embedded board. Meanwhile, data format and a simplified Graphic User Interface (GUI) should be defined and implemented.
3) Integrate the hardware components of the HEPS, and test them as a whole, including:
    I. Data collection and analysis for each component;
    II. Low-level component control (torque/speed reference following);
    III. Test of the complete HEPS system with a constant load but without it being connected to the engine and motor generator.

The energy management system design includes battery pack SOC estimation, cell balancing and battery fault detection.

1.3 Aims of the project

The aim of this project is to develop a reliable HEPS system and this can be achieved via the following three steps:

1) Develop a hardware test platform for HEPS verification based on the proposed Simulink model.
2) Develop a battery model and a battery SOC estimation algorithm.
3) Design a BMS which covers battery pack SOC estimation, cell balancing and fault detection.

1.4 Thesis methodology and structure

The thesis outline can be summarised as follows:

Chapter 2 is the literature review. This review covers hybrid propulsion architecture, supervisory controller control strategy and some methods used in BMS design.

The development of the HEPS hardware test platform is introduced in Chapter 3. HEPS hardware components, signal exchange protocol, and the performance of the platform are described in this chapter.

The details of the battery modelling process can be found in Chapter 4. In this chapter, both the offline and the online model parameter methods are described. The offline parameter identification can be used as reference and the effectiveness of the online parameter estimation algorithm is verified by experiment.

In Chapter 5, the concepts of Extended Kalman Filter (EKF) and Particle Filter (PF) are introduced. The performances of these two model-based algorithms are evaluated via the simulation results. Finally, the experimental results show that the proposed single cell SOC estimation method is accurate and effective.

Chapter 6 first describes the extension of the single SOC estimation method to the HEPS battery pack application. In addition, battery cell balancing and battery system fault detection are also covered in this chapter.

Chapter 7 is a summary of this thesis. It also gives possible future directions in developing HEPS.

2 Literature review

The Hybrid Electric Propulsion System (HEPS) is typical of more advanced electric aircraft technology which combines an electric powertrain and a conventional ICE to provide propulsion power. Advantages of the hybrid configuration include: 1) lower emissions and noise; 2) better overall efficiency and low-speed performance; and 3) lower maintenance requirements. These benefits make HEPS an attractive research into powered transportations.

2.1 System architecture

The architectures of the HEPS can be divided in three categories: serial, parallel and power-split [11].

The serial hybrid architecture is shown in Figure 2-1. In this architecture, the power for the whole system comes from the ICE. The ICE output powers a generator to produce electric power. The generator drives an electric motor which is connected to the mechanical payload directly. In this architecture, the ICE can be controlled to running at maximum efficiency and the battery is used as a buffer, providing and storing power as necessary. The serial HEPS system has the advantages of easy implementation and control simplicity, but it needs an extra generator which will increase the system's weight.

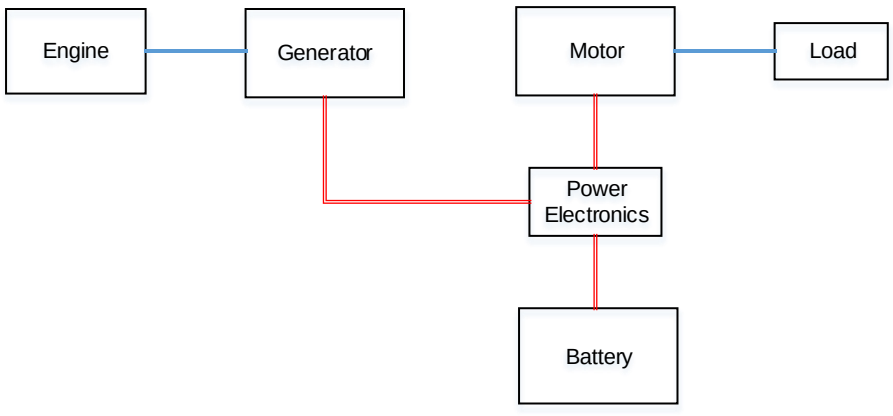

Figure 2-1: Serial hybrid architecture

In the parallel architecture (shown in Figure 2-2), the power for the mechanical payload is provided directly from both ICE and electric motor. The main

difference between parallel and serial architectures is that there is a mechanical connection between ICE and electric motor in the parallel architecture. The electric motor can also be used as a generator for battery charging, depending on the control strategy. Since an independent generator is not required in parallel HEPS, this architecture is usually lighter than serial arrangement but cannot ensure optimal operation of the engine and needs complex a control strategy to divide the power requirements for engine and motor respectively.

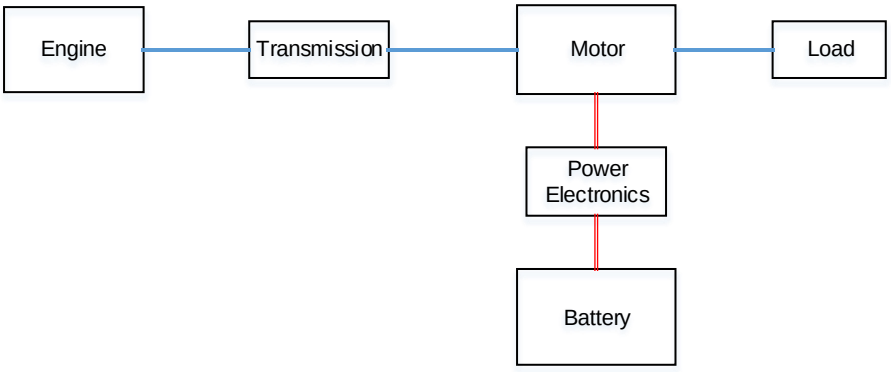

Figure 2-2: Parallel hybrid architecture

The power-split architecture is shown in Figure 2-3. This architecture combines the advantages of both serial and parallel architectures and thus has the highest efficiency. However, since it has two power flows so that it requires a significantly more sophisticated control system which limits its application.

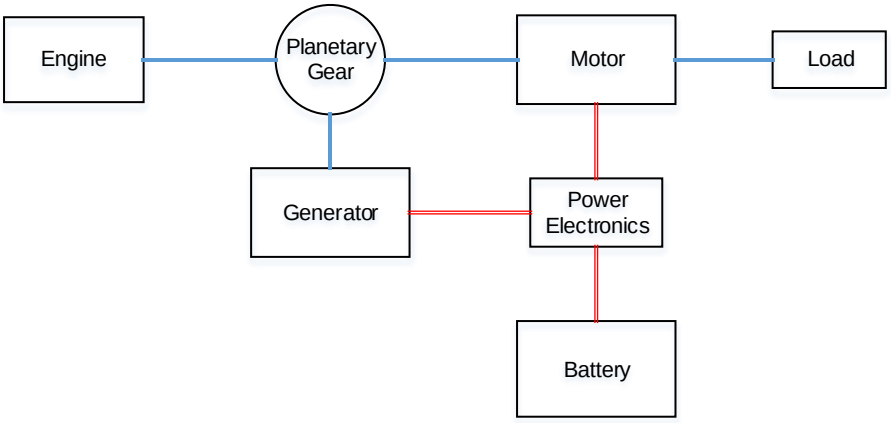

Figure 2-3: Power-split hybrid architecture

In this project, parallel hybrid architecture is chosen in this project.

2.2 Supervisory Controller

The role of the supervisory controller in HEPS is to determine the power split. Reviewing the HEPS development, there are two main types of controllers. One is rule-based and the other is optimization based [12]. Each category consists of various control methods. An illustration diagram is shown in Figure 2-4.

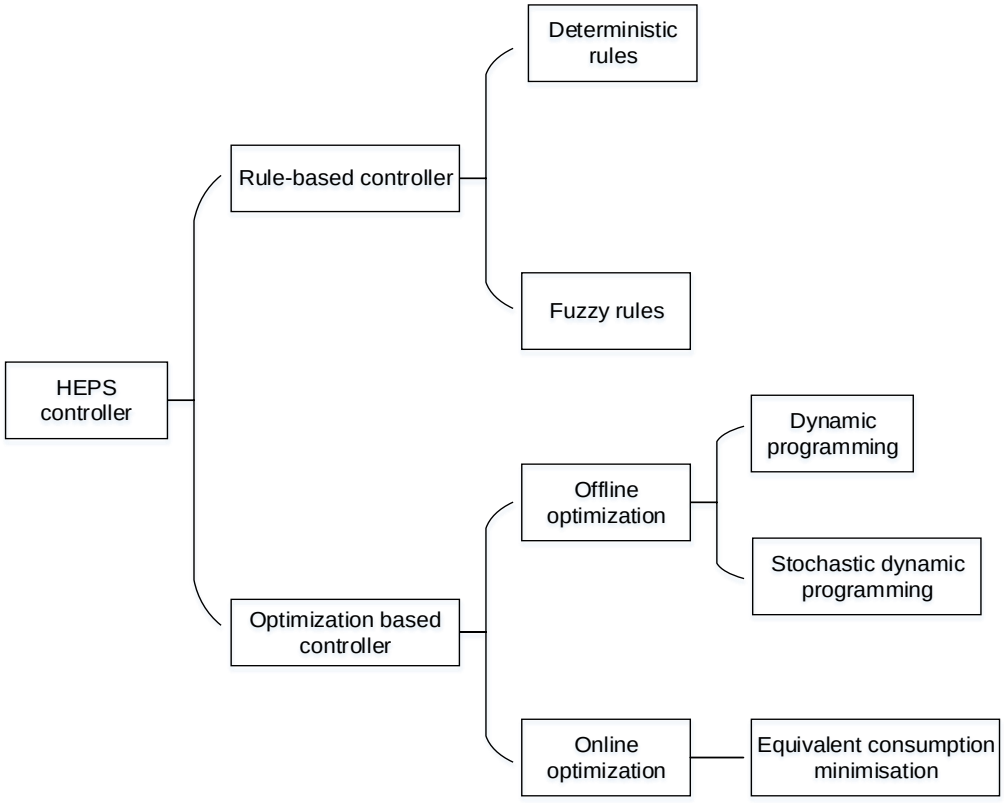

Figure 2-4: Categories of hybrid power system supervisory controllers

In terms of pre-defined logic protocols, control outputs of a rule-based controller are determined by current state of the system, such as power requirements, SOC of the battery, etc. The control strategy of rule-based controllers can be described as a flow chart in which there are some verdict logic boxes. As an illustration, part of a typical rule-based HEPS control strategy is displayed in Figure 2-5. The control logic is designed based on the user's experience. For example, the "Charge_SOC" in Figure 2-5 is 20% in our application. This is a relative conservative value since ensuring operation safety and reliability is important in the initial stage of system development.

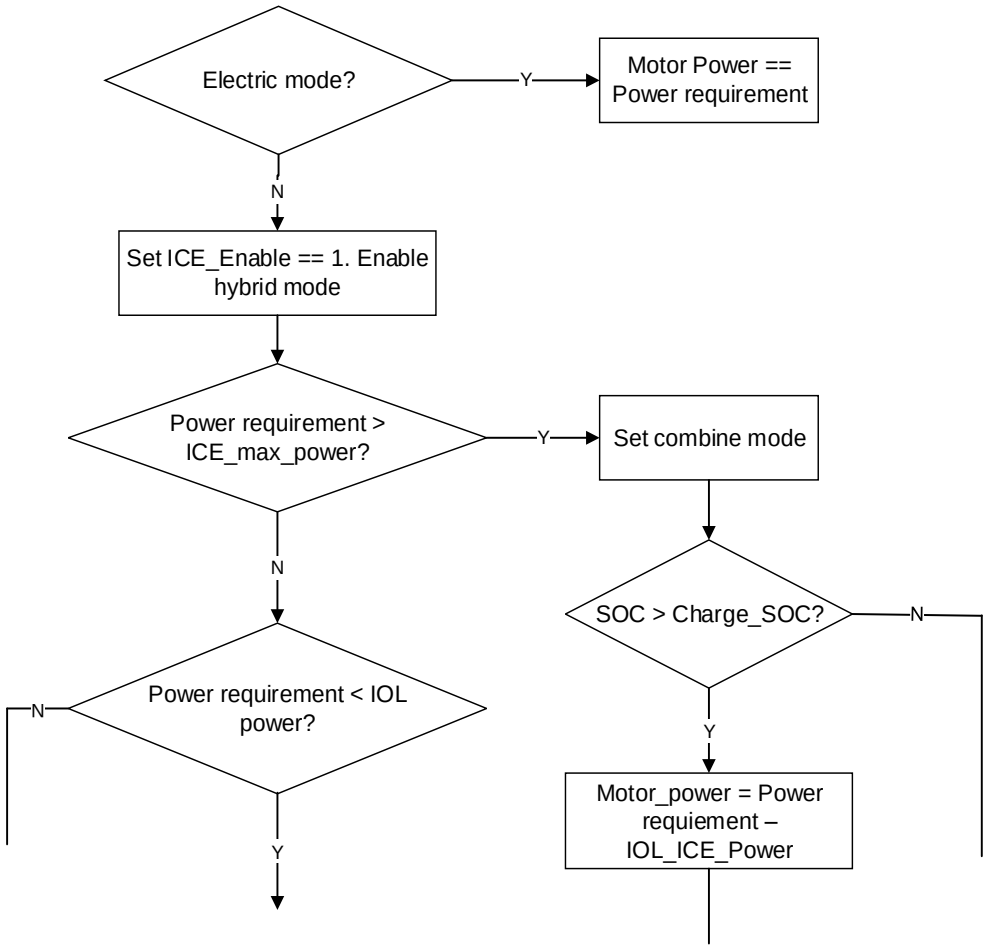

Figure 2-5: An example of rule-based HEPS controller

For classical rule-based controllers, verdict boxes in the control flow are deterministic, which means, for an arbitrary HEPS state vector $\boldsymbol{x}$, there exists one and only one precise set S_i such that $\boldsymbol{x} \in S_i$. Supposing the number of all precise sets is N, $\bigcup_{i=1}^{N} S_i$ can be used for describing all possible system states and $S_i \cap S_j = \emptyset$ holds for any $i \neq j$ $(i, j = 1,2, \ldots, n)$.

The fuzzy logic controller is also a kind of rule-based controller and has exhibited its advantages in promoting HEPS fuel efficiency, reducing toxic emissions and many other applications [13].

Compared with the classical rule-based strategy, the main difference in the fuzzy logic controller is the use of fuzzy sets for handling input states. With fuzzy logic, the answer on whether a variable belongs to a certain set is never a Boolean value but depends on continuous membership functions. In other

words, a variable can belong to both set S_i and set S_j simultaneously in fuzzy logic.

It is noteworthy that handling input variables by fuzzy logic can decreases the effects due to environment disturbance and system uncertainty, which gives the fuzzy logic controller a natural robustness.

Although rule-based controllers have advantages of simplicity and adaptiveness, it cannot guarantee achieving optimality mathematically. On the contrary, optimization controllers relying mathematic models of system make it possible to figure out the optimal strategy if a specific cost function is established. Dynamic Programming (DP) is frequently used for optimisation problems and is usually taken as the reference for other optimal algorithms. However, the overall information requirement of DP limits its performance in variable driving applications [14]. To overcome this limitation of DP, Stochastic Dynamic Programming (SDP) is investigated in [15] and [16]. However, the transition possibility in SDP still relies on the historical database and a driving pattern reorganization algorithm is necessary to abstract the actual transition possibility. In order to implement the online optimal energy management controller, Paganelli proposed the Equivalent Consumption Minimisation Strategy (ECMS) which is based on minimising the combined cost of fuel and electricity instantaneously [17]. ECMS is able to meet real-time control requirements and to get the near optimal results [18][19]. However, the performance of ECMS relays on the equivalence factor that is difficult to be estimated [20].

2.3 Battery management system

The Battery Management System (BMS) is a key part of the electric powertrain in HEPS. The objectives of BMS usually include: 1) monitoring system voltage and current; 2) estimating battery pack SOC; 3) balancing battery cells; 4) predicting battery life based on State of Health (SOH); 5) monitoring battery voltage and current and protecting the battery system from overcharge and over-discharge; 6) thermal management; 7) logging data; 8) communicating

with other parts such as supervisory controller and charger [21] - [23]. Among those objectives, SOH estimation requires experiment data that cover battery's whole life span; thermal management is more relative to environment information instead of battery internal states. Thus, pack SOC estimation, cell balancing, and fault detection are selected for studying in this thesis.

2.3.1 Battery SOC estimation methods

The battery residual energy, which can be regarded as the potential hybrid propulsion, is an essential factor in determining the power split strategy. Unlike petrol whose volume can be easily obtained, estimating the residual energy in batteries is not a trivial exercise because of the inherently complicated electro-chemical reactions and the uncertainty caused by external factors [24].

Accurate estimation of battery SOC not only provides information of the current and remaining performance of the battery but also ensures a reliable and safe operation in HEPS [25].

SOC is a common value used for representing the energy in a battery and is defined as the residual capacity in battery, see equation (2-1).

$$SOC(t) = SOC_0 - \int_0^t \frac{i}{Q} dt \qquad \textbf{(2-1)}$$

where Q is the battery capacity, SOC_0 the initial SOC value in each run and i the battery current that is positive when in discharging and negative when in charging.

Due to the importance of SOC many researches have been devoted to improve SOC estimation performances.

The relationship between Open Circuit Voltage (OCV) and SOC has been used for SOC estimation via a look-up table at the primary stage. Although this lookup table offers an accurate correspondence between OCV and SOC, it is not really suited for real-time application since a long rest time or constant current load is required for a stable terminal voltage [26]. In addition, some

battery types such as Li-Sulphur battery which has a relatively flat OCV-SOC curve [27] making it impossible to use the OCV-SOC curve to estimate SOC.

The ampere-hour counting (Ah-counting) method is another approach to estimate SOC. By logging the current value at each sample point, this method calculates SOC directly according to the SOC definition. This is an easy-to-implement method with low calculation complexity. It is the most practical way for SOC estimate [24][25] but it is also an open-loop method and may result in significant inaccuracy when there are disturbances and noise. For example, the accumulated current measurement error may affect SOC tracking process. Moreover, the initial SOC and the nominal battery capacity in the equation are hard to determine in the later stages of a long operation life-span. In fact, Ah-counting method can be used as references for evaluating SOC estimation method only if in laboratory environment where initial states of batteries and disturbances are known accurately and minimized.

To overcome those drawbacks in the above mentioned estimation methods, on the one hand, some efforts are devoted to improving battery capacity estimation [28] - [30] and obtaining a more accurate initial SOC value [31][32] for Ah-counting method. On the other hand, machine learning and model-based method have been studied and used for SOC estimation. Tong and et al proposed a load-classification Artificial Neutral Network (ANN) for SOC estimation in [33] and yielded a 3.8% average estimation precision. Taking voltage, current and temperature as inputs, Juan, and et al presented a SOC estimation method based on Support Vector Machine (SVM) [34]. Those data driven methods have the merits of easy implementation and good adaptive but they also require lots of computer memory to store training data [35]. Besides, training data selection is also critical in data driven methods and inappropriate data selection may cause additional problems in SOC estimation [36].

Model-based methods can be used to describe battery dynamic characteristics and offer a voltage reference for SOC estimation. In [37], Demenico used electrochemical model to estimate SOC. Other model-based technics such as H infinity [38][39], sliding mode [40], and Proportional-Integral observer [41] have

aslo been applied in SOC estimation. In addition, some filter methods such as Particle Filter (PF) [42][43], Extended Kalman Filter (EKF) [44], and Unscented Kalman Filter (UKF) [45][46] liaised with battery model are used and obtained accepted estimation accuracy. A comparison of the abovementioned SOC estimation methods is shown in Table 2-1.

Table 2-1: Performance comparison of different SOC estimation methods

Name	Error (%)	Advantages	Disadvantages
OCV	-	• Easy to use • High accuracy	• Require long rest time that is not suitable for real-time applications
Ah-counting	-	• Easy to implement • Very high accuracy in lab environment	• Sensitive to disturbance and noise • Require high accuracy initial value estimation
ANN	3.8 [33]	• Capable of working in battery non-linear condition	• Require large memory unit • Modelling is time consuming
SVM	6 [34]	• Performs well in nonlinear system and high dimensional model	• Complex computation • training data selection
H infinity	2.5 [38]	• Satisfactory performance in terms of accuracy, computation cost and time efficiency	• Rely on battery model accuracy
PF	4 [43]	• High accuracy • Adaptive to different noise distributions	• Need complex mathematic tools
EKF	3 [44]	• High accuracy • Initial estimation error correction	• Sensitive to model Parameter
UKF	3 [46]	• Performing well in highly nonlinear model • Adaptive to different noise distributions	• Poor robustness and sensitive to disturbances

Battery SOC estimation is the key point in this research. The architecture of the proposed battery pack SOC estimation method can be roughly descripted in Figure 2-6.

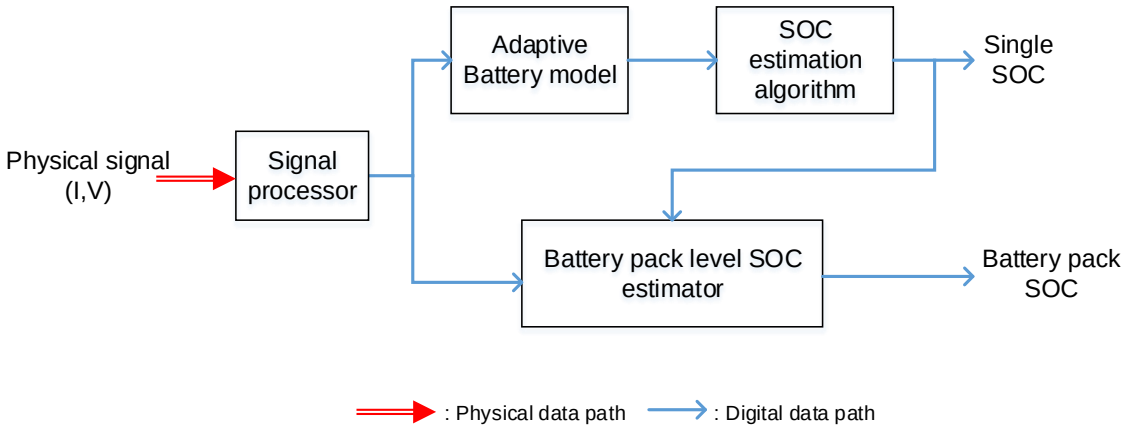

Figure 2-6: Architecture of the proposed battery pack SOC method

This method can be divided in two stages: The first stage is single cell SOC estimation and the second stage is battery pack level SOC estimator. The second stage relies on the output of the first stage (SOC of single battery cell).

2.3.2 Battery cell balancing methods

Cell imbalance can be caused by the inevitable manufacturing variations in manufacturing (storage capacity and impedances) and the uneven operating environment of battery packs such as heat gradient and unequal charge/discharge rates. Without a balanced system, cell voltages in the battery system will drift apart and the battery will surfer a faster capacity fade and even fail permanently. For preserving battery life, a cell balance system is a necessary part in the BMS. A number of battery balancing methods have been described in and their topologies are presented in Figure 2-7 [47].

In the passive balancing method, the extra energy in high voltage cells will be consumed by the resistances. However in the active balancing method, the energy in high voltage cells will be transferred to the lower ones or the entire battery pack. The advantages and disadvantages of several balancing methods are listed in Table 2-2.

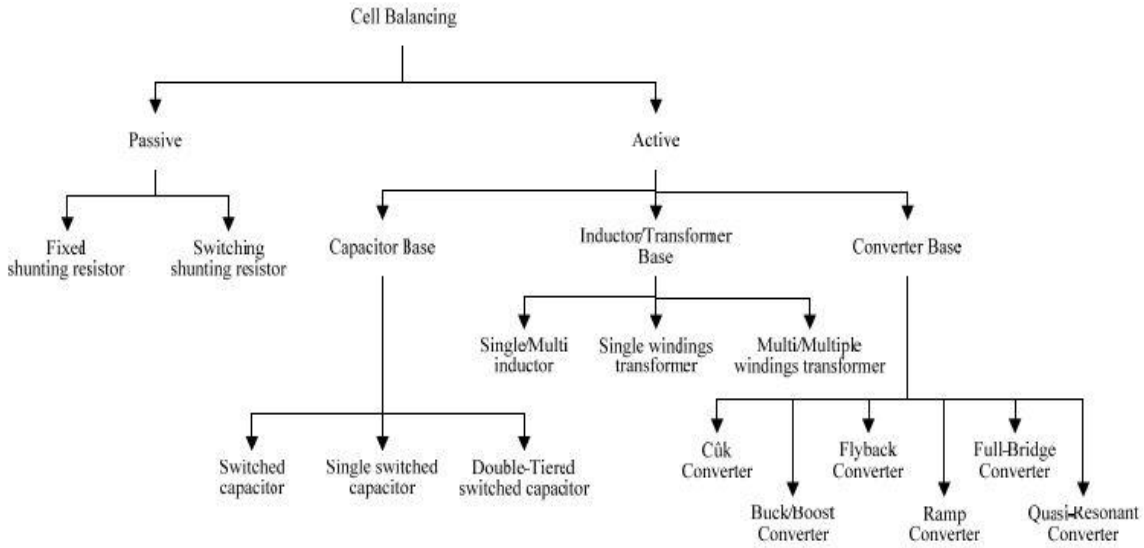

Figure 2-7: Battery cell balancing system topologies

Table 2-2: Comparison of different battery balancing methods

Balancing method	Advantages	Disadvantages
Passive method	• Easy to implement • Reliable • Good equalization speed	• Energy loss • Requires good heat management • May shorten battery capacity when use in discharge mode • Long equalization time
Capacitance based method	• Simple architecture • Control strategy needed but not complex • Effective (few energy loss)	
Inductor/Transformer based method	• Fast equalization speed	• Need extra capacity filter • Magnetic energy loss
Converter based method	• Fully controllable • Effective • Good equalization speed	• Complex architecture • High cost

2.3.3 Battery system fault detection methods

In order to achieve satisfying performance over a long lifespan, special attention is required in Li-ion battery usage to avoid any physical damage, aging or thermal runaways [48]. Faults in battery system are mainly due to over-charge/discharge, abnormal temperature, circuit sparking and aging.

Irreversible loss of active material has been observed at 150% overcharged and distraction of anode and cathode at 200% over-discharged. Over-discharge battery cells accelerates aging under normal use cycles [49][50]. Hence, the maximum and minimum cell voltages and SOC values should be always monitored during HEPS running.

Abnormal temperature in system not only causes battery efficiency fade but also is hazardous. Ramadass has shown that high temperatures will accelerate battery capacity fade [51]. However, low temperatures also affected energy and efficiency, which dropped to 60% of that at room temperature when operated at -20℃ [52]. Fire can be caused accidentally due to the high temperature generated in battery pack.

Given the complexity of the operating scenarios, not only battery faults but also peripheral circuit fault can impair battery system performance. For example, poor connections may be caused by vibration or ageing and introduce a spark or discontinuity into the battery system. These abnormal electric inputs may shorten battery life or even cause system failure.

In order to prompt system safety and reliability, some methods have been studied for fault diagnosis. By comparing measured and predicted data model-based methods can use a residual signal for fault detection [53] - [55]. The fault can also be determined by a signal processing method. Representative of this kind methods are spectrum analysis [56], possibility distribution function and [57] impulse response method [58]. Faults can also be asserted by the knowledge based method by reference to databases [59] - [61]. Because of the good performance of online fault diagnosis, the signal processing approach has been chosen in this research for BMS fault detection.

3 HEPS hardware platform development

Using HIL system, one can test the performance of a particular hardware in a system while the rest of the system is modelled in the simulator. Compared with typical simulation, HIL simulation is closer to the reality and can be a verification technique for the proposed system. This technology is able to mitigate the gap between software model and final hardware product making it possible to test safety related real-time system (e.g. aerospace system, automotive system) without endangering humans or natural environment [62][63].

In order to achieve the objective of project AIRSTART, the HEPS hardware platform is developed for using in the HIL verification. The designed architecture of the HEPS hardware platform is shown in in Figure 3-1.

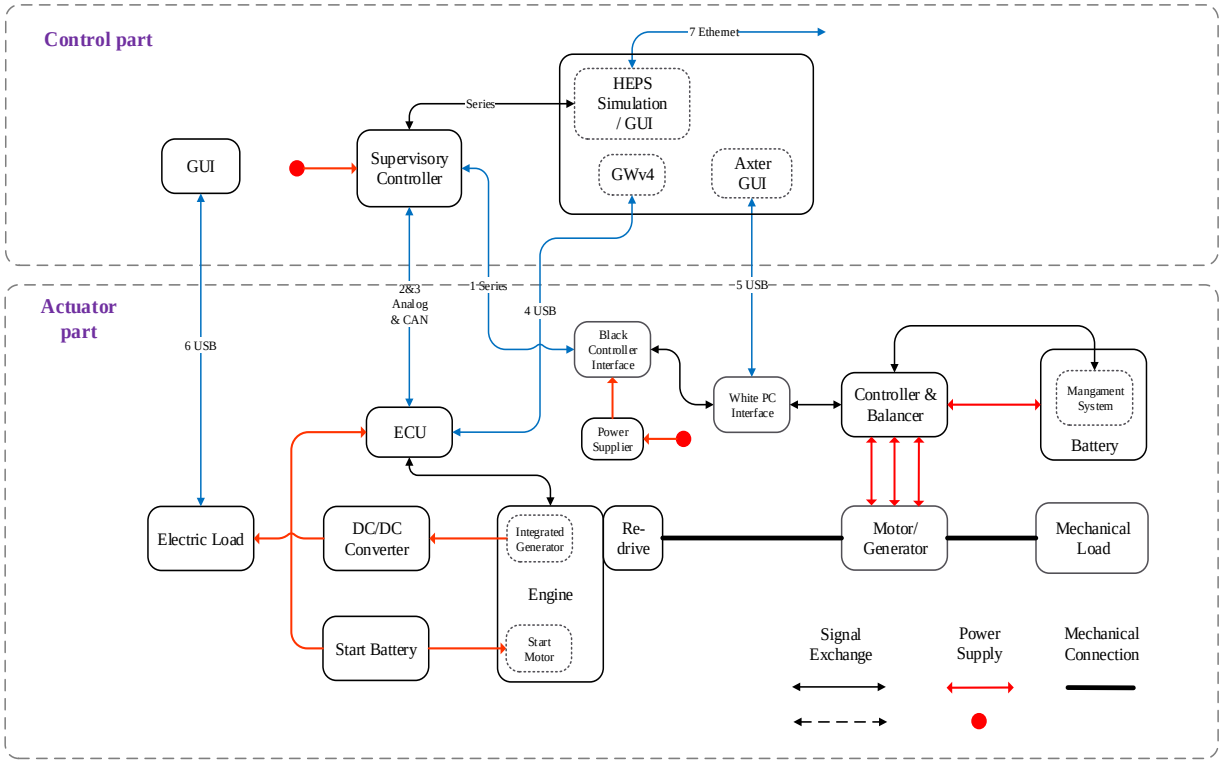

Figure 3-1: Diagram of the HEPS hardware platform

As shown in Figure 3-1, the parallel hybrid architecture is adopted in this project due to its relative lighter weight and higher reliability. In this architecture, the whole system is comprised of two parts which are control part and actuator part.

The two parts are integrated by a real-time controller via CAN bus and serial communication. In the actuator part, on-shelf hardware is chosen to build the hybrid propulsion system test rig. The mechanical load refers to propeller in this project while the electric load is to represent the gauge, sensor and other electric devices may be used in aircrafts. In the control part, HEPS controller in Simulink works for optimizing the power allocation for engine and electric motor. Also, a comprehensive GUI is developed in this part for system information display and data log. Besides, some official software such as the ECU official software Gwv4 is also used for components calibration.

This chapter is organised as following: First, the simulation model is introduced. This model acts as a reference for HEPS hardware platform design and the supervisory controller in the model controls the components in the hardware platform. Second, the test rig, the developed GUI, and data exchange protocols are introduced. In the end, the hardware platform is verified by experiments.

3.1 Simulation model

A simulation model is developed in Simulink and its high-level architecture is shown in Figure 3-2.

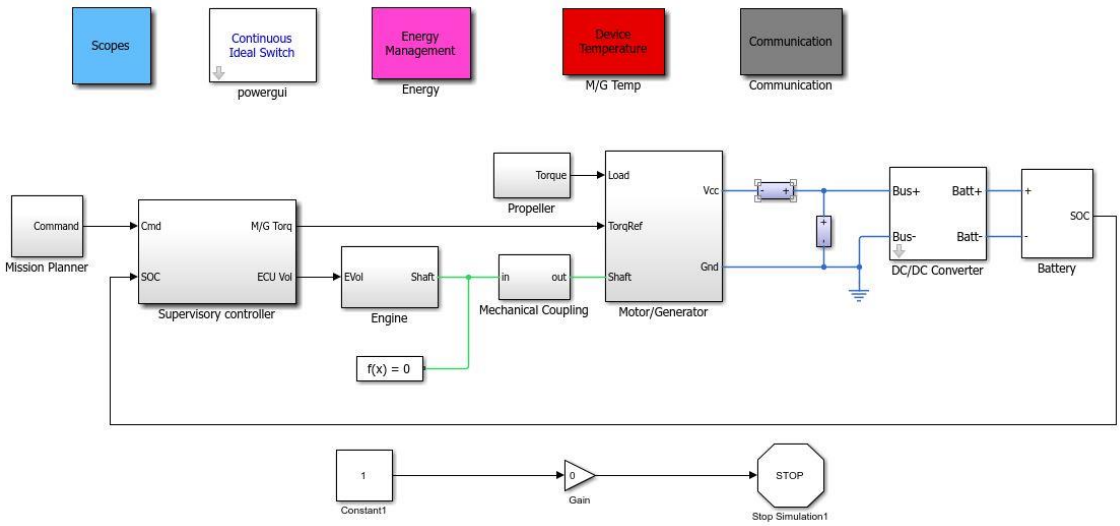

Figure 3-2: High-level architecture of the simulation model

In the simulation model, the Mission Planner stores the pre-defined power requirement profile. The supervisory controller is rule-based one which is able

to determine the power split ration between ICE and electric Motor/Generator (MG). The feedback signal for the supervisory controller is the battery pack SOC that computed by the BMS.

Moreover, in order to simulate the practical experiment environment and promote model accuracy, a SIMSCAPE thermal model is built for simulating the thermal effects and shown in Figure 3-3. Considering the fact that in our platform engine and power electronics have own cooling system, the motor power loss is regarded as the main heat source. The power loss is calculated according to the efficiency lookup table which is obtained from the motor producer ENSTROJ [64].

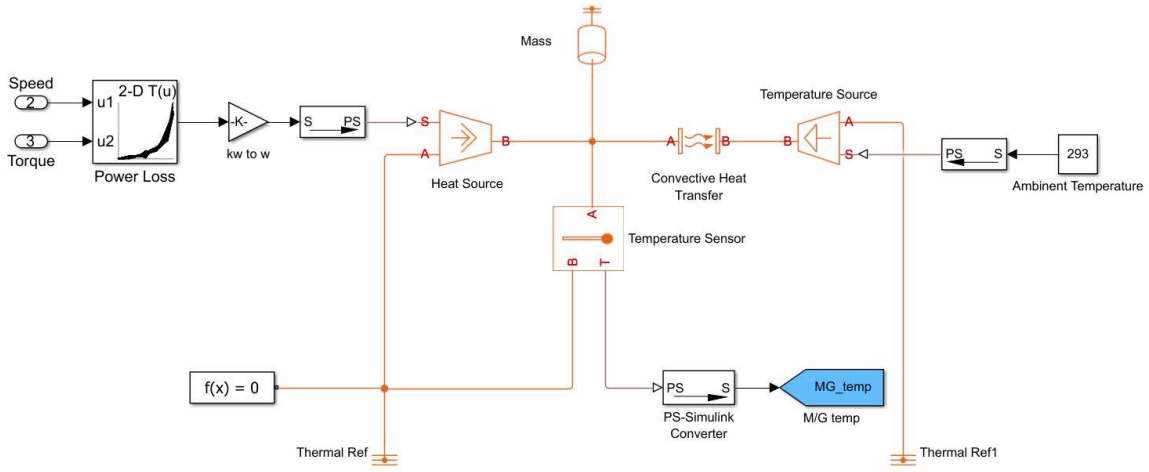

Figure 3-3: Simulation module for the thermal effect

Since ICE has its own cooling system to manage the heat, the power loss of MG is considered as the main heat source. This power loss is calculated by a two dimension lookup table. Convective heat transfer and ambient temperature is also considered in this thermal model.

According to the system design shown in Figure 3-1, Simulation model uses serial communication sending commands to the supervisory controller. As a result, a serial communication module is added in Simulink model as well for signal transition. The details of the communication module are shown in Figure 3-4. Two switches are added here for switching the control mode between automatically (according to a predefined profile) and manually.

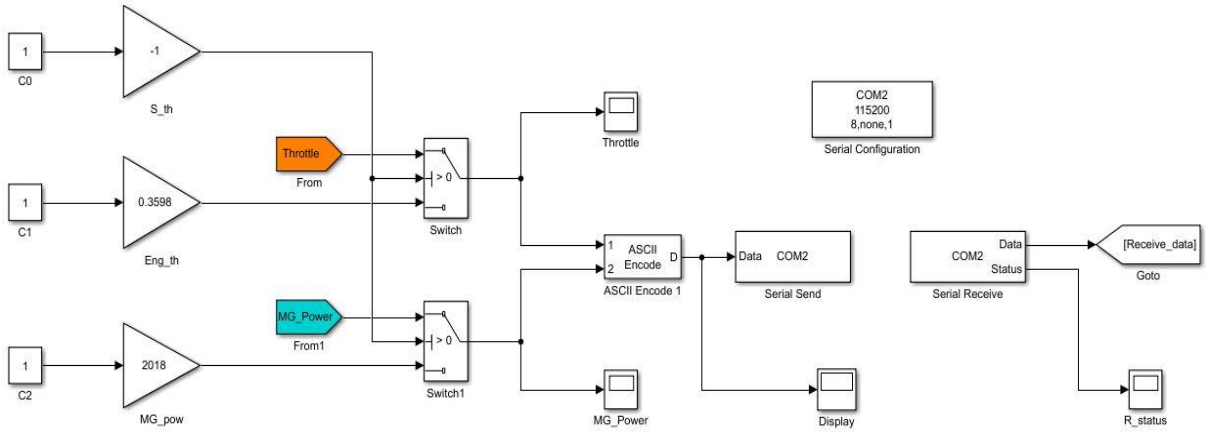

Figure 3-4: Communication module in Simulink model

3.2 HEPS test rig design

A transportable test rig is designed by a PhD student and manufactured by Rotron Ltd. The CAD diagram of the rig is shown in Figure 3-5.

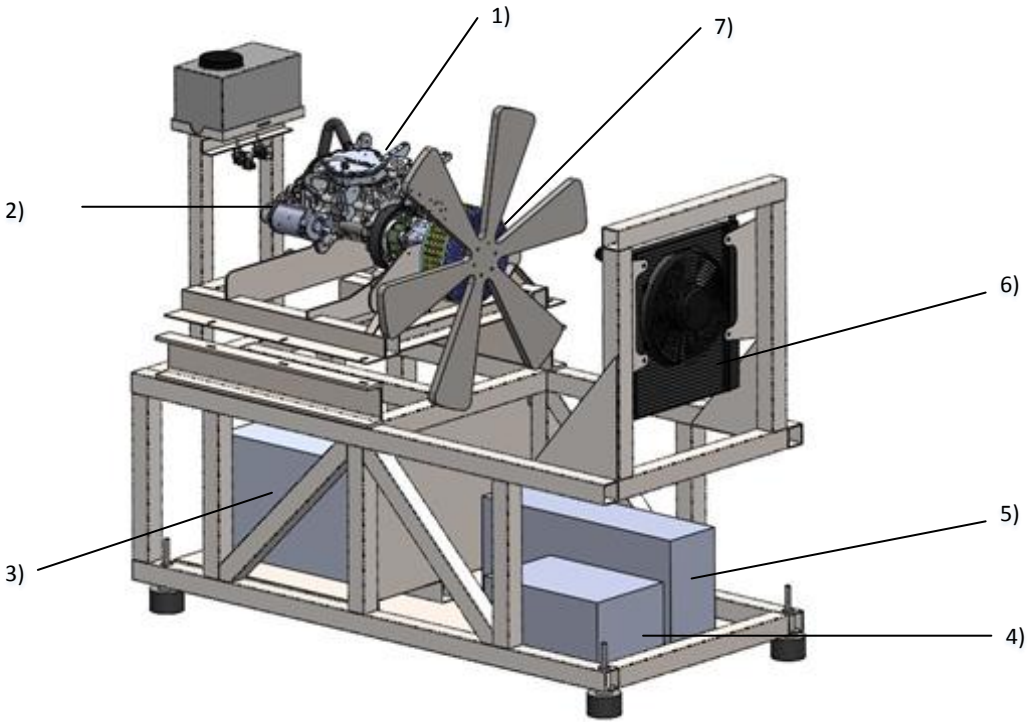

Figure 3-5: Diagram of the test rig

Components and their functions in this HEPS test rig are:

1) Combustion engine. Gasoline engine RT600 is a rotary engine with two rotors and displacement of 600cc. The continuous power output at 6500 RPM is 54 horsepower.
2) Start motor. This device is used for starting engine and powered by a start battery. The battery voltage is required to be above 12 volts when try to start the engine.
3) Fuel tank. A 40 litres fuel tank is used in this test rig.
4) Power electronics (DC/DC converter, sensors and motor/generator controller). Power electronics are used to ensure functions of switching between motor and generator, monitoring electric parameters and communicating with other devices. The power electronics has two interface modules: the white box can be connected to upper computer by USB for data display; the black box is used as the communication interface for control value input and real-time feedback value output.
5) Battery pack. This device is the energy pool for the electric powertrain. The rated power of this battery pack is 30 kW. The voltage of the battery is 302.4 V when fully of charged and promises maximum 3000 RPM for the motor when output power.
6) Radiator. This device is used for dissipating heat of the liquid coolant and enforcing the coolant cycle.
7) Motor/Generator. An AC motor is connected to the engine mechanically via the re-drive gear box and used as the second powertrain in this HEPS. The output power of this electric part is up to 30 kW.

There are also some components that do not be exhibited in Figure 3-5 but still very important:

1) Exhaust and silencers. This device is used for guiding the emission of engine and reducing the engine noise.
2) Integrated generator. When engine is running, this device offering electric power for payloads.
3) Engine Control Unit (ECU). ECU is a specialized controller for engine control. It consists of many mapping relationships which decide the engine performance. The input of the ECU is an analogue value which

corresponds to the throttle position. The engine running status can be obtained by other devices via CAN bus. The ECU is powered by the 12V start battery.

4) Data exchange controller. Atmel SAM4E development board is chosen as the data exchange controller due to its rich on-board hardware resources (embedded CAN controller, Ethernet, USART and et al.) and high running frequency.

5) Other auxiliary components. Two manually control panels are also developed for engine and MG respectively. With control panels, operator can choose to turn on certain component only for debugging or fault diagnosis. For example, we can choose to turn on the ECU only instead of starting the engine for CAN bus communication validation.

3.3 GUI development

For displaying system status better and operation convenience, a GUI is developed based on AppDesigner in MATLAB 2016b and shown in Figure 3-6. Based on this GUI, user can control the experiment and monitor the process.

Figure 3-6: GUI panel

The GUI has 3 parts which are data display sector, curve display sector and commands sector.

1) Command sector: this sector includes main control commands, such as throttle value, system running mode, start and stop. These control commands enable user control input parameters to simulate disturbance or emergency events like motor failure when the Simulink is running. Besides, it is able to set environment parameters such as ambient temperature, humidity via command panel, which can be used for analysing the performances of HEPS in different environment conditions.
2) Data display sector: this sector exhibits some variables' current values. These values are used for indicating the running status of the HEPS. The data display sector also has alert function. When a value exceeds it limitation, for example the battery cell temperature exceeds 60℃, this value will turn to red.
3) Curve display sector: these curves help to display continuously variables that are always used for appraising the system's performance. Those values can help us analysis the dynamic characteristics of the HEPS.

The GUI is able to complete the following task:

1) Collecting, displaying and logging HEPS data online;
2) Monitoring the operating conditions of HEPS;
3) Start and end the HEPS;
4) Tuning component control parameters of HEPS online.

3.4 Communication interface development

3.4.1 Interface unit selection

An embedded board is required for process data coming from ECU, battery power electronics, upper computer and output control signal. Under this situation, rich on board hardware resources and high floating calculation performance are essential when selecting the board. Some possible platforms with their characteristics are shown in Appendix A and finally the Atmel

SAM4E16E development board is chosen for the data exchange controller development because of following reasons:

1) It has lots of on-board interface resources: one Ethernet port, two 9-pin serial interfaces, and two CAN bus communication ports.
2) Core controller ARM Cortex M4 is a powerful controller and widely used in many industrial area.
3) It has official library which can simplify code development.

3.4.2 CAN bus

Controller Area Network (CAN) is a multi-master network developed by Bosch in order to reduce the complex signal wiring architecture among electronic devices in automotive sector. In 1991, NXP semiconductor built the CAN communication protocol CAN 2.0 A/B and from then on, the CAN bus is widely used in automotive, aviation, industry control and monitoring sectors due to its high reliability, high transmission speed and economy [65].

Because of abovementioned benefits, CAN bus is chosen in this HEPS system for spreading engine status in real-time.

3.4.2.1 CAN bus data structure

CAN bus has mainly four kinds of frame: data frame for carrying data information, remote frame for asking remote node sending data, error frame for reporting data checking fails, and overload frame for adding additional time delays.

Data frame is the most common frame on CAN bus. It carries engine information in our application. The structure of data frame is shown as following:

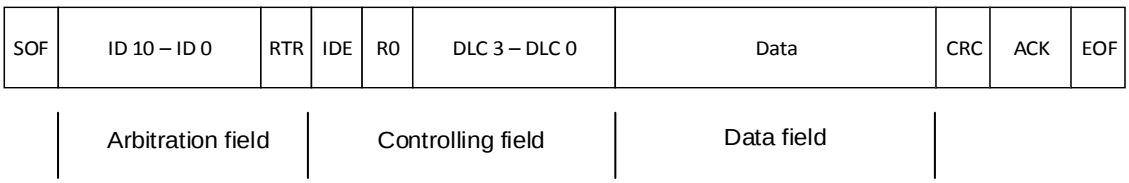

Figure 3-7: Structure of the CAN Bus data frame

As shown in Figure 3-7, one data frame is consisted of arbitration field which is 12 bits length indicating the destination address, controlling field which contains the data length and data field. When receiving a CAN bus message, we need to filter the CAN bus data based on this structure.

The engine feedback data for the HEPS controller includes engine speed, air temperature, battery voltage and throttle. Detailed CAN bus data format can be found in Appendix B.

3.4.2.2 CAN bus connection

Data bit on the CAN bus is a differential voltage signal between two wires CAN-High and CAN-Low. Logic “0” is dominance which means that the voltage on CAN-High is higher than it on CAN-Low and logic “1” is when CAN-High and CAN-Low have the same voltage. A 120 ohm resistance is required between CAN-High and CAN-Low.

3.4.3 Serial communication

Serial communication is widely used in point to point communication scenarios due to its simplicity and high transmission speed.

In order to simplify system structure and fully utilize on-board resources, we use two universal asynchronous receiver/transmitters (UARTs) to implement the serial communication among the Simulink supervisory controller, the data exchange controller and the power electronics. The connection diagram of them can be found in Figure 3-1.

There is a fact that in this HEPS, the data volume in each communication is fixed. Thus Periphery DMC Controller (PDC) is used in this application to simplify program logic structure. In this case, when data communication is required, the PDC will call corresponding periphery devices to finish the task automatically.

3.4.4 Integration

The integrated work flow of ATMEL embedded board is shown in Appendix B and the hardware connection is shown in Figure 3-8. A 10 Hz timer is used as

trigger signal for control output and data updating. Messages in this controller are handled in relative interrupt functions.

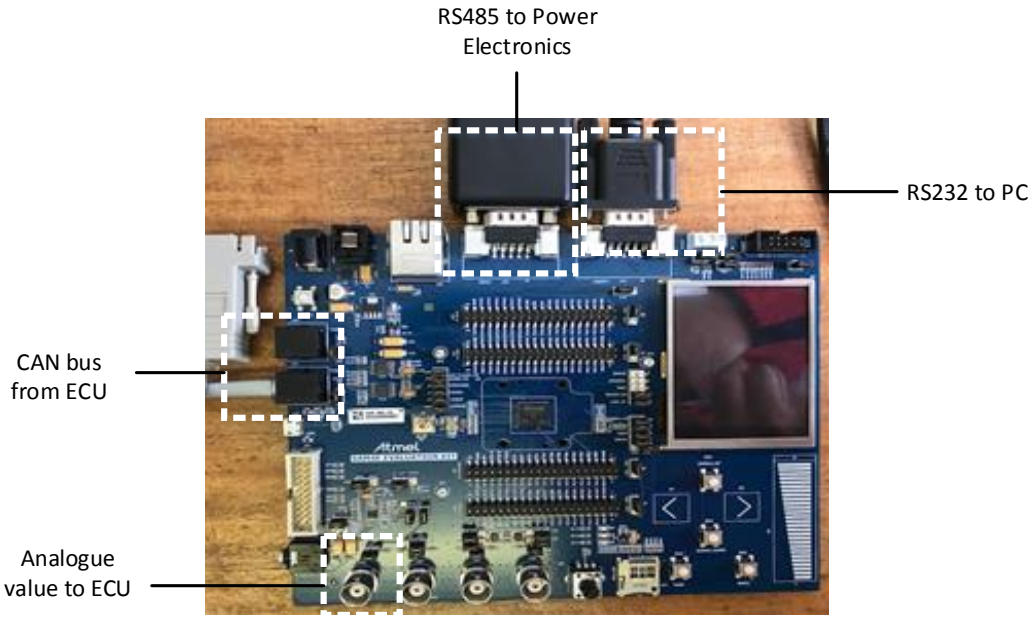

Figure 3-8: Interfaces on the controller and their corresponding devices

3.5 Hardware platform verification

The hardware platform is tested outdoor in Cranfield University to verify the system operation, electric connection and integration. The configuration of the initial test is shown in Figure 3-9. Mechanical load is not connected to the test rig at this stage for safety reasons.

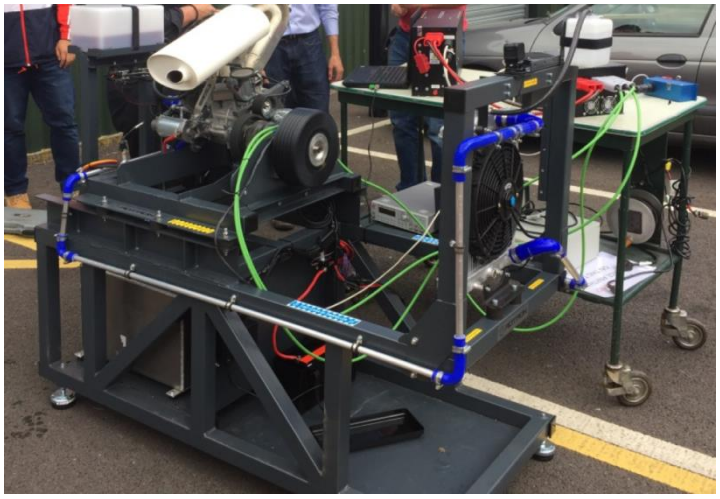

Figure 3-9: Verification test for the HEPS hardware platform

Validation of the whole system can be divided into feedback value validation and control value validation.

3.5.1 Feedback path validation

The feedback path is tested by a throttle signal. The ECU throttle input is set manually via the engine control panel and shown in Figure 3-10 (a screenshot from the ECU official software). The ECU is set to echo the throttle value by CAN bus. At the same time, a scope module is used in Simulink to read and display the system feedback. The received throttle value is shown in Figure 3-11.

Figure 3-10: Throttle input of the ECU

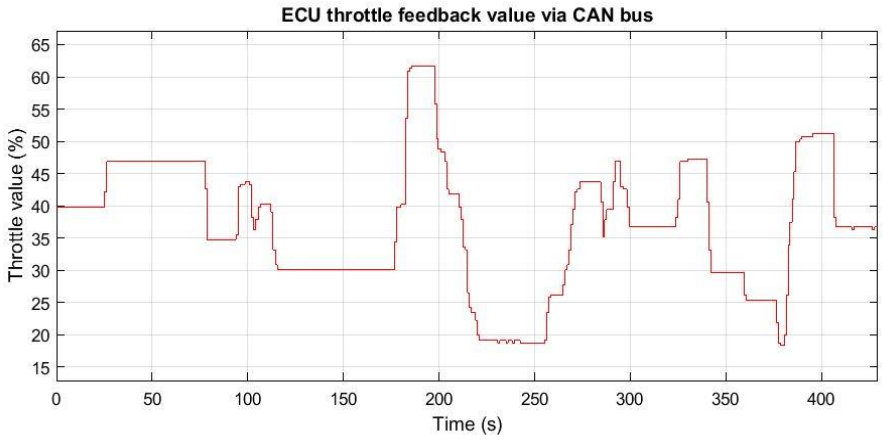

Figure 3-11: Throttle feedback read in Simulink

By comparing Figure 3-10 and Figure 3-11, it is safe to say that the supervisory controller can receive the throttle from ECU and actuator via CAN bus and serial communication. In other words, the feedback path is verified.

3.5.2 Control path verification

In the control path test, a pre-defined motor output power profile is set in the Simulink supervisory controller and the motor running state is logged. The experiment result is shown in Figure 3-12.

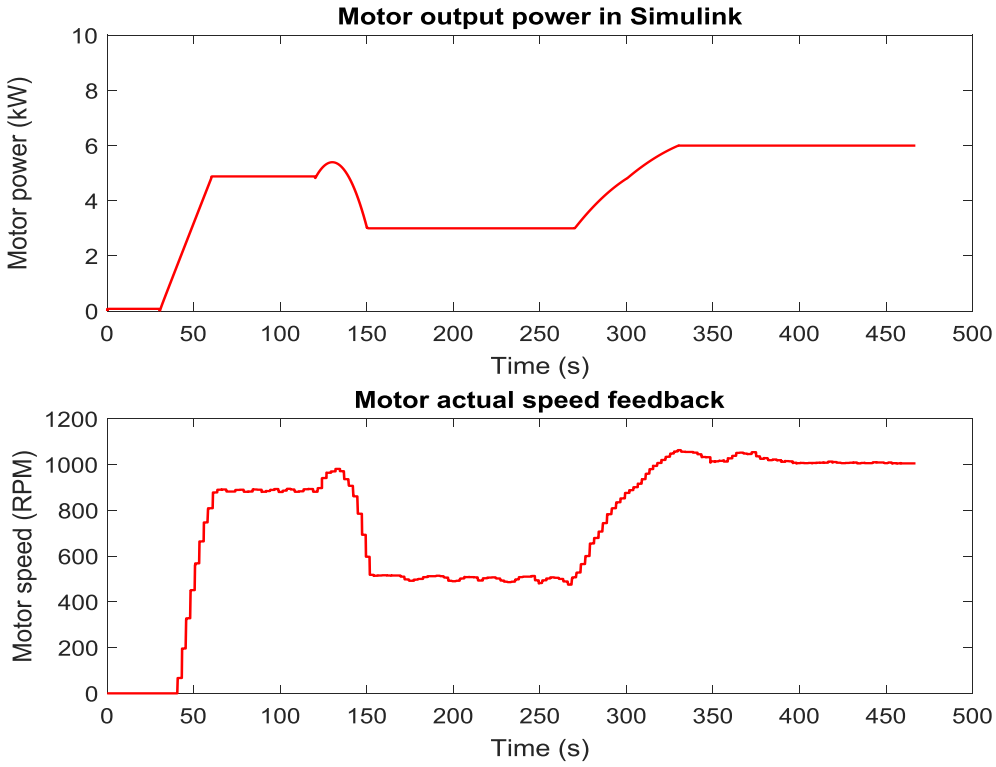

Figure 3-12: Result of the control path verification test

The motor is unloaded in the initial test due to the safety requirement. In this case the motor speed would follow the pre-defined power profile which is straightforward for the control path verification. According to Figure 3-12, the motor speed curve is similar to it in the power profile. Thus we can safely get the conclusion that the control signal is sent from Simulink to motor controller successfully.

3.6 Conclusion

HIL simulation can be used for real-time system test and offer high confidential feedback for next stage development. In order to finish the HIL simulation for AIRSTART, a hardware platform is required for the HEPS.

In this chapter, the Simulink model and the hardware components of the HEPS are introduced. In addition, a signal exchange controller is developed. CAN bus and serial communication are chosen in the HEPS hardware platform for control and feedback signal exchanges in terms of the communication requirements and on board resources. The developed hardware platform is verified by experiments.

4 Adaptive battery model

Due to the high power density, Li-Po battery has been utilized as the power source in many applications. A Li-Po battery is composed of Negative electrode, Positive electrode, and Separator. Negative and positive electrodes are connected to negative and positive terminals respectively [66]. There are composite porous materials in electrodes to reside Lithium ions which are charge carries. The separator isolates the negative electrode from positive one electronically and is filled with electrolyte. The charge and discharge of the battery occur when the transference of lithium ions happens between the positive and negative electrodes through the electrolyte medium. In charge process, the Li ions are extracted from the positive electrode and are inserted into the negative electrode while reverses in the discharge process. [67]

In this chapter, details of different Li-Po battery models are introduced and a two-order equivalent model is chosen for the battery that we use in the HEPS. By sensitive analysis, the important role of battery model parameters is identified. In order to improve the model accuracy, a new event triggered online parameter identification method is proposed. This method adopts Adaptive Genetic Algorithm (AGA) and its feasibility is proofed by experiments.

4.1 Battery model

4.1.1 Electrochemical battery model

Electrochemical model is usually a set of Partial Differential Equation (PDE) and aims to describe the details of battery reaction in electrodes and electrolytes. This model often has high accuracy but is also complex and has a large number of unknown parameters. Hence PDE-based battery model is not suitable for battery state estimation in the real-time application of HEPS [24].

4.1.2 Empirical battery model

Empirical battery model utilizes experimental data to represent batteries. Representatives in this group are combined model in [68], the Shepherd model in [69] and the ANN based battery model in [70].

4.1.3 Equivalent circuit model

Equivalent Circuit Model (ECM) usually consists of 1) OCV source whose value is a function of battery SOC, 2) an inner resistor and 3) several resistor and capacitor (RC) groups for representing battery dynamic characteristics such as polarization effect, double layer effect and etc. Compared with electrochemical battery model, ECM is simple with fewer unknown parameters and can be used in real-time application [24][25]; compared with empirical battery model, ECM has physical meaning and is more deterministic [71].

In the ECM development, there are mainly three kinds of battery models that are RC model, PNGV model, and Thevenin model.

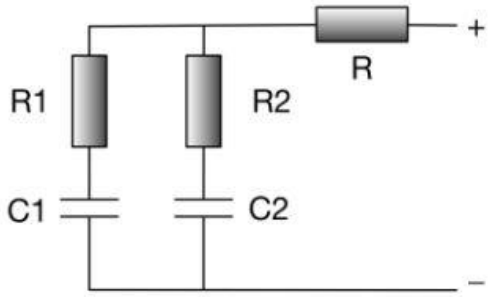

Figure 4-1: RC model

The RC model is shown in Figure 4-1. In this model, the battery cell is represented as two parallel connected RC series. This RC battery cell captures battery diffusion effect, surface and end resistance [72].

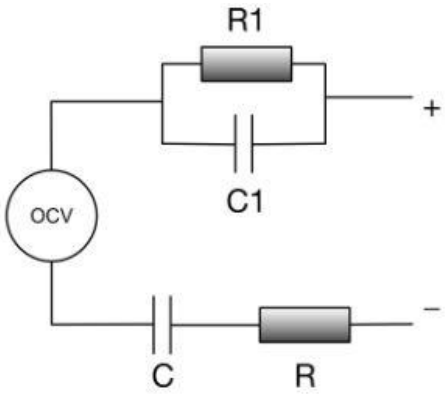

Figure 4-2: PGNV model

In PNGV model (shown in Figure 4-2), a constant voltage source and a serial connected capacitor are used to represent battery OCV. The serial connected capacitor describes the effect of SOC. The parallel connected resistance and capacitance represents the polarization effect.

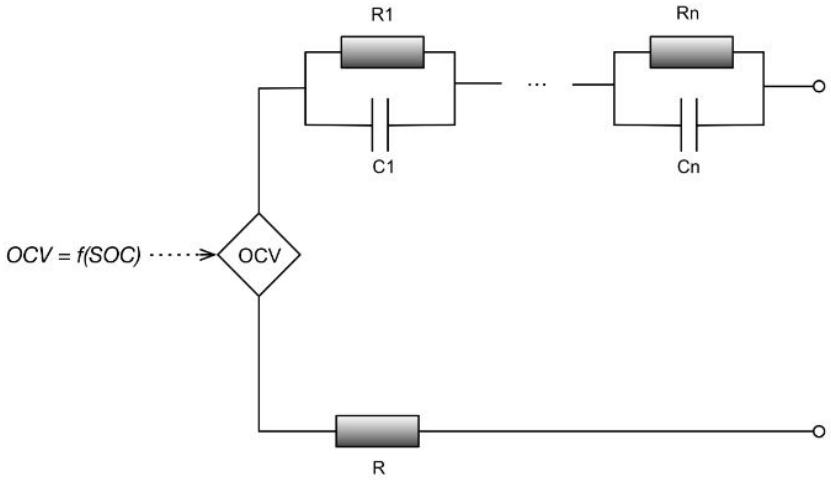

Figure 4-3: Thevenin battery model

In Thevenin model shown in Figure 4-3, OCV is described as a controllable voltage source and the parallel connected RC networks are used for representing battery dynamic responses. This model can be regarded as the linear approximation of the nonlinear physical battery model. Adding more RC networks to the battery model may improve its accuracy. However, the more RC networks model adopts the more complex the system will be, which may exert unnecessary burden to the real-time BMS [73].

In this research, Thevenin model is chosen to describe our Li-Po batteries and a battery dynamic response experiment is used here in order to find the satisfying model order.

In the dynamic response experiment, the battery is incited by a step current and the battery terminal voltage is logged. Theoretically, the model order is fixed after selected thus the initial energy level of the battery in this experiment can be arbitrary. However, the battery SOC for this experiment is recommended to be within 20% to 80% since this range is commonly used in HEPS operation.

After experiment, the current-voltage data is analysis based on the MATLAB curve fitting application. Based on experimental data, we can see from Figure 4-4 that the two order EEC model has an acceptable precision for capturing the battery dynamics.

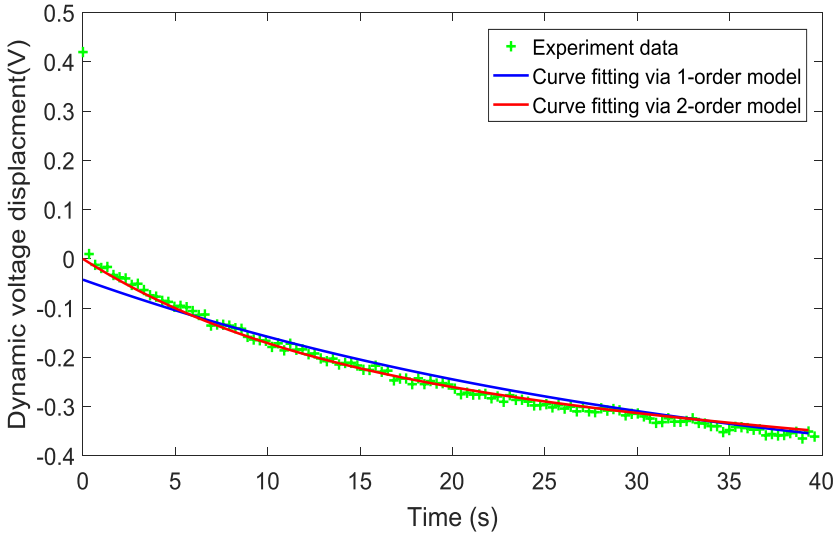

Figure 4-4: Dynamic response of two different RC models

Based on the architecture in Figure 4-3 and the dynamic response experiment, the state space representation of the battery model is shown in (4-1)

$$\begin{bmatrix} \dot{u}_{C1} \\ \dot{u}_{C2} \\ \dot{SOC} \end{bmatrix} = \begin{bmatrix} -\frac{1}{C_1 R_1} & 0 & 0 \\ 0 & -\frac{1}{C_2 R_2} & 0 \\ 0 & 0 & 0 \end{bmatrix} \begin{bmatrix} u_{C1} \\ u_{C2} \\ SOC \end{bmatrix} + \begin{bmatrix} \frac{1}{C_1} \\ \frac{1}{C_2} \\ -\frac{1}{Q} \end{bmatrix} i \qquad \textbf{(4-1)}$$

$$y = f(SOC) - u_{C1} - u_{C2} - R_0 i$$

where $f(SOC)$ is the OCV function and Q is the battery capacity. Furthermore, by defining

$$A_c = \begin{bmatrix} -\frac{1}{C_1 R_1} & 0 & 0 \\ 0 & -\frac{1}{C_2 R_2} & 0 \\ 0 & 0 & 0 \end{bmatrix} \quad B_c = \begin{bmatrix} \frac{1}{C_1} \\ \frac{1}{C_2} \\ -\frac{1}{Q} \end{bmatrix} \qquad \textbf{(4-2)}$$

and sample interval T, the discrete state space equations of battery, which is used in online SOC estimation and battery regulation, can be obtained by $A = e^{A_c T}$ and $B = \int_0^T e^{A\tau} B_c d\tau$ and are:

$$\begin{bmatrix} u_{C1,k+1} \\ u_{C2,k+1} \\ SOC_{k+1} \end{bmatrix} = \begin{bmatrix} e^{-\frac{T}{C_1 R_1}} & 0 & 0 \\ 0 & e^{-\frac{T}{C_2 R_2}} & 0 \\ 0 & 0 & 1 \end{bmatrix} \begin{bmatrix} u_{C1,k} \\ u_{C2,k} \\ SOC_k \end{bmatrix} + \begin{bmatrix} \frac{1}{C_1} - R_1 e^{-\frac{T}{C_1 R_1}} \\ \frac{1}{C_2} - R_2 e^{-\frac{T}{C_2 R_2}} \\ -\frac{T}{Q} \end{bmatrix} i_k \quad \textbf{(4-3)}$$

$$y(k) = f(SOC_k) - u_{C1,k} - u_{C2,k} - R_0 i_k$$

The OCV function $f\big(SOC(k)\big)$ can be obtained by an offline experiment.The experiment adopts a constant current as the input to charging and discharging battery cell in order to obtain the relationship between OCV and SOC. Specification of the tested battery is listed in Table 4-1.

Table 4-1: Specification of the tested battery

Type	Li-ion Polymer
Nominal capacity	5 Ah
Maximum voltage	4.2 V
Cut-off voltage	3.5 V
Nominal voltage	3.8 V
Temperature range	0 - 60℃

In this experiment, firstly, the battery cell is fully charged by a 1C constant current. Then after two-hour rest, the battery is discharged via constant 5A current till the terminal voltage is reach its cut-off voltage. After another two hours rest, the battery cell is fully charged by 1C constant current again. Repeat this test for five different but same labelled battery cells and the averaged

discharge and charge OCV-SOC curves of the five experiments are used for abstracting the coefficients in the function $OCV = f(SOC)$. Due to the obvious difference between discharge and charge curve, the coefficients of $f(SOC)$ in HEPS application will switch between the two groups of coefficient according to the current direction. The experiment result is shown in Figure 4-5.

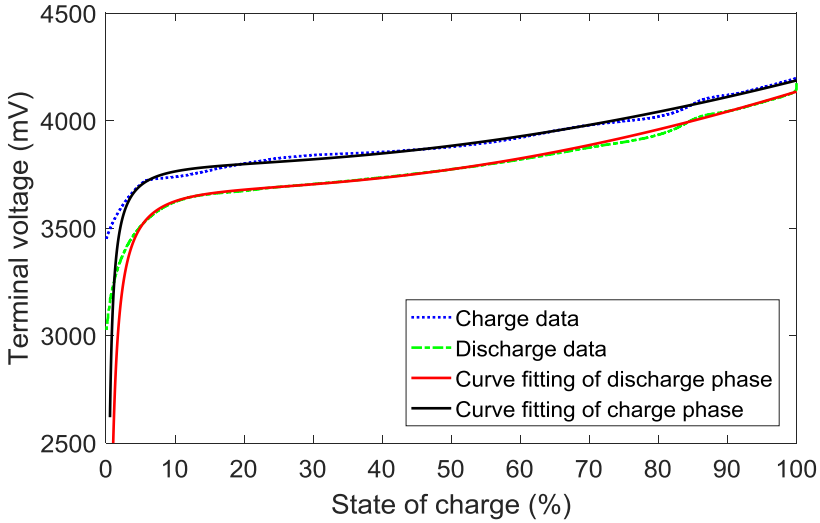

Figure 4-5: Discharge and charge curve

By the Robust Trust-Region curve fitting algorithm in MATLAB curve fitting application, the coefficients in $OCV = f(SOC)$ can be obtained and list in (4-4) .

$$f(SOC) = 3.791e^{-0.0071SOC} + 0.02285 \cdot SOC - 1.347\frac{1}{SOC} \quad (I > 0)$$
$$f(SOC) = 3.849e^{-0.0058 \cdot SOC} + 0.02053 \cdot SOC - 0.7121\frac{1}{SOC} \quad (I < 0) \qquad \textbf{(4-4)}$$

The Root Mean Square Error (RMSE) for discharge curve fitting and charge curve fitting are 6.452 (mV) and 13.27 (mV) respectively.

4.2 Battery model parameter sensitivity analysis

In order to improve the overall battery model accuracy in the whole battery operation range, the model sensitivity is studied in this section. In the sensitivity analysis, each parameter of the battery is adjusted separately and corresponding model performance is evaluated.

Since the SOC is the mostly concerned in a battery system, this sensitive analysis uses SOC estimation precision as the evaluation criterion. The SOC estimating method here is chosen as Extended Kalman Filter (EKF). However, it should be noted sensitivity analysis results do not depend on the SOC estimation algorithm.

The results display the effects of parameter variations in battery modelling according to the SOC estimation error and are shown in Figure 4-6.

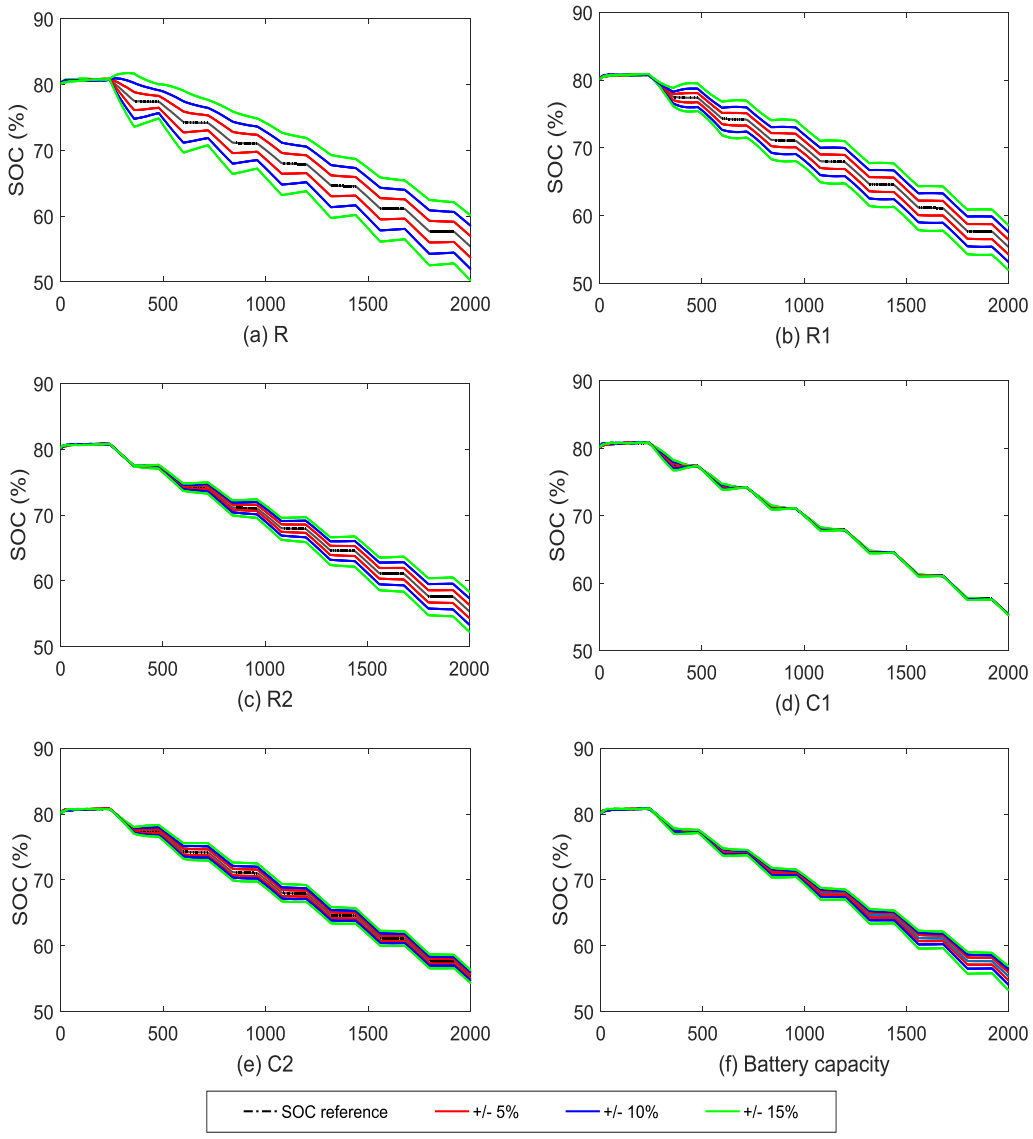

Figure 4-6: Result of the battery model parameter sensitive analysis

Moreover, the RMSE of SOC estimation due to parameter variation is listed in Table 4-2: RMSE in battery model parameter sensitive analysis.

Table 4-2: RMSE in battery model parameter sensitive analysis

	+5%	-5%	+10%	-10%	-15%	+15%
R	1.321	1.339	2.626	2.709	3.925	4.057
R1	0.894	0.887	1.799	1.767	2.729	2.663
R2	0.582	0.589	1.180	1.161	1.831	1.704
C1	0.101	0.074	0.147	0.133	0.216	0.214
C2	0.373	0.377	0.703	0.675	1.090	1.047
Capacity	0.298	0.319	0.643	0.541	1.080	0.772

According to the sensitivity analysis, it is necessary to design an online parameters identification method to improve model accuracy. Furthermore, it can be seen Figure 4-6 and Table 4-2, that the SOC estimation result is more sensitive to resistances while less sensitive to capacitances and battery capacity. In addition, compared with battery capacity which is the inherent attribute of batteries, resistance and capacitance in the ECM are easier to be influenced by environment changes and disturbances. Thus, the resistance and capacitance values (refer to electric parameters in later content) are selected for online parameter identification.

4.3 Offline model parameter identification

Parameters in battery model are the function of SOC. For improving the model accuracy and offering a reference for the online parameter identification, an offline parameter identification method is necessary to determine model parameters at different SOC values.

Least Square is an effective optimal method for linear system identification. It is easy to be implemented for that it only relays on the relationship between system input and measured output.

Considering the OCV and SOC relationship, the output equation in (4-3) can be linearized as:

$$f\big(SOC(k)\big) = f\big(SOC(k_0)\big) + f'|_{SOC(k0)} \cdot \big(SOC(k) - SOC(k_0)\big) + \varepsilon \quad \textbf{(4-5)}$$

where ε here is a bounded linearization error. For offline application, $SOC(k_0)$ is a constant and by denoting $\theta_0 = f\big(SOC(k_0)\big) + f'|_{SOC(k0)} \cdot SOC(k_0) + \varepsilon$ and $\theta_1 = f'|_{SOC(k0)}$ the output equation is rewritten as:

$$y(k) = \theta_0 + \theta_1 SOC - u_{C1}(k) - u_{C2}(k) - R_0 i(k) \quad \textbf{(4-6)}$$

The relationship between current and measured voltage can be obtained via on the Z-transfer function in (4-3).

$$\frac{Y - \theta_0}{I} = \frac{\alpha_3 Z^{-3} + \alpha_2 Z^{-2} + \alpha_1 Z^{-1} + \alpha_0}{\beta_3 Z^{-3} + \beta_2 Z^{-2} + \beta_1 Z^{-1} + 1} \quad \textbf{(4-7)}$$

Thus the relationship between the k-th sampled input and output can be described as followed differential equation.

$$y_k = -\beta_1 y_{k-1} - \beta_2 y_{k-2} - \beta_3 y_{k-3} + \alpha_0 i_k + \alpha_1 i_{k-1} + \alpha_2 i_{k-2} + \alpha_3 i_{k-3} + (\beta_1 + \beta_2 + \beta_3 + 1)\theta_0 \quad \textbf{(4-8)}$$

The mapping relationships between coefficients in transfer function and real electric parameters are given in (4-9).

$$
\begin{aligned}
\alpha_0 &= R_0 \\
\alpha_1 &= \left(\frac{1+T}{C_1} - R_1 + \frac{1+T}{C_2} - R_2 + \theta_1 \frac{T}{Q}\right) - R_0\beta_1 \\
\alpha_2 &= \lambda_0 - \left(\frac{1+T}{C_1} - R_1 - \frac{1+T}{C_2} - R_2\right) - \theta_1 \frac{T}{Q}(\beta_1 - 1) - R_0\beta_2 \\
\alpha_3 &= \theta_1 \frac{T}{Q}\beta_3 + \lambda_0 - R_0\beta_3 \\
\beta_1 &= -(3 - \frac{T}{R_1C_1} - \frac{T}{R_2C_2}) \\
\beta_2 &= 2 - \frac{T}{R_1C_1} - \frac{T}{R_2C_2} + (1 - \frac{T}{R_1C_1})(1 - \frac{T}{R_2C_2}) \\
\beta_3 &= -(1 - \frac{T}{R_1C_1})(1 - \frac{T}{R_2C_2}) \\
\lambda_0 &= \left(\frac{1+T}{C_2} - R_2\right)\left(1 - \frac{T}{R_1C_1}\right) - \left(\frac{1+T}{C_1} - R_1\right)\left(1 - \frac{T}{R_2C_2}\right)
\end{aligned}
\tag{4-9}
$$

Considering the fact that R_1C_1 and R_2C_2 are relatively large, Maclaurin equation is applied here for simplifying calculation.

$$
\begin{aligned}
e^{-\frac{T}{R_1C_1}} &\approx 1 - \frac{T}{R_1C_1} + o(\frac{T}{R_1C_1}) \\
e^{-\frac{T}{R_2C_2}} &\approx 1 - \frac{T}{R_2C_2} + o(\frac{T}{R_2C_2})
\end{aligned}
\tag{4-10}
$$

From equation (4-9), it is easy to obtain that $\beta_1+\beta_2+\beta_3 = -1$. According to equation (4-8), it can be known that the uncertainty θ_0 does not affect system identification performance. In other words, LR can be used to identify battery parameters offline accurately even linear approximation existing.

An experiment is used here for offline battery model parameter identification. The input of the test is pulse current. A part of the current profile and corresponding battery terminal voltage is shown in Figure 4-7.

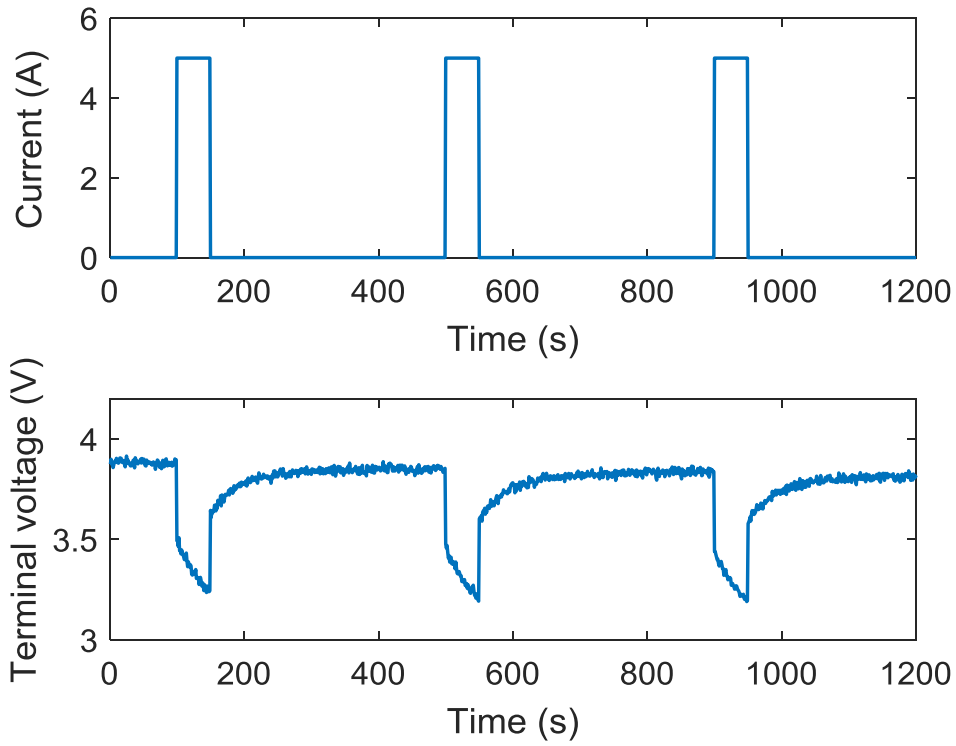

Figure 4-7: A part of current profile in the offline parameter identification

The experiment procedure is listed as follow:

First the battery is charged to 100% SOC. Then three 5A current pulses are applied to the battery to incite the battery dynamic response. Finally, a constant current discharge is applied to the battery until it reaches the next SOC sample point. 30-minute rest is given between each step to ensure the battery is in stable state. Repeat the second and third steps until every SOC sample point is reached.

In the offline experiment, SOC is calculated via Ah-counting method, since in this test the initial condition of battery is deterministic and the experiment environment is controllable in the laboratory. SOC sample points in this experiment are $[5, 10, \ldots, 100]$.After the experiment, the battery parameters can be determined at each SOC sample point. This experiment is executed in $20℃$ room temperature. The results of this test are plotted in Figure 4-8.

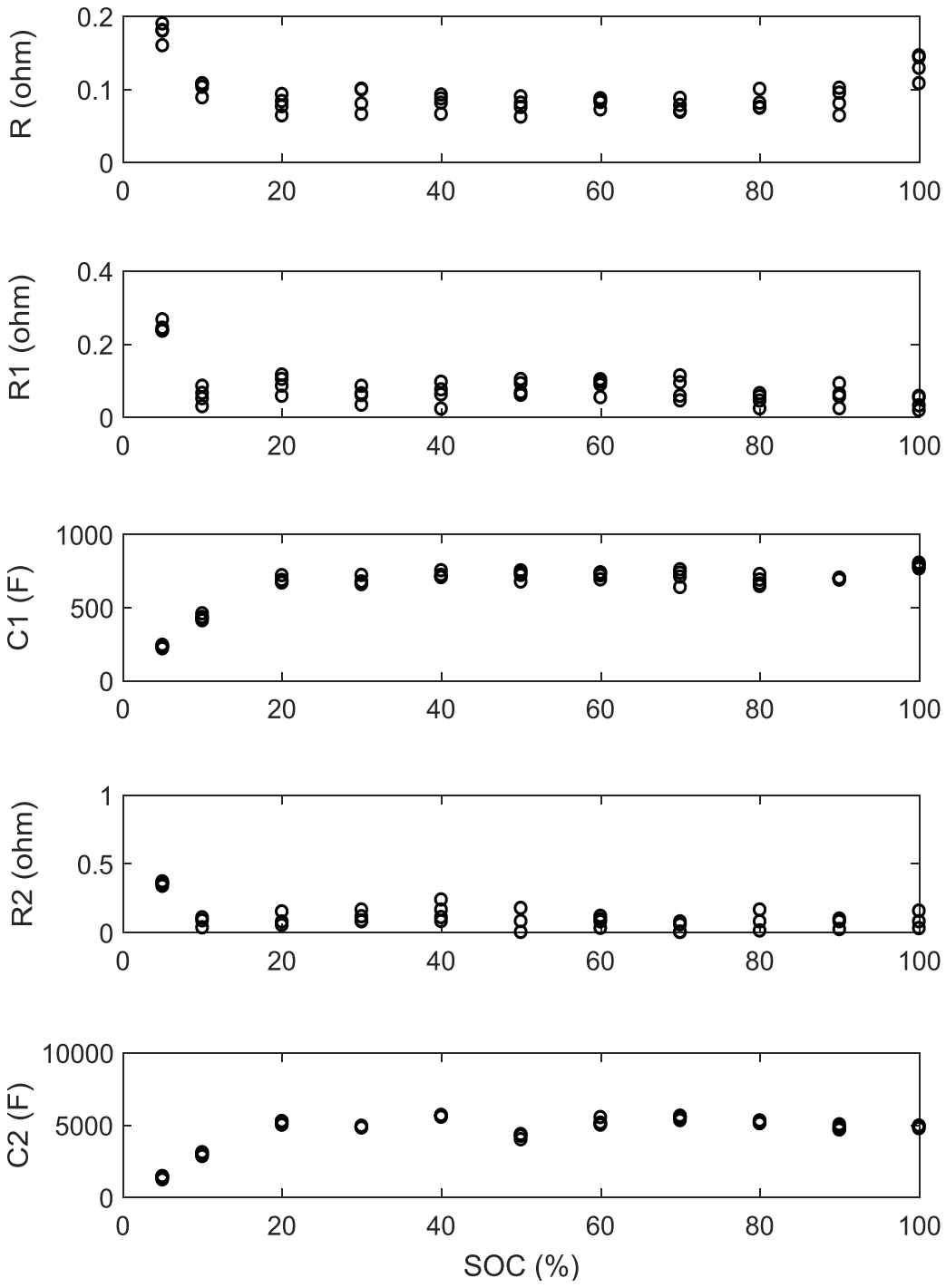

Figure 4-8: Model parameter variation versus battery SOC

4.4 Event triggered online parameter identification method

Model accuracy is important in model-based SOC estimation algorithm [74][75]. However, battery parameters are environmental sensitive [24]. Temperature,

aging effect, and current load may cause parameter variation. For example, Dubarry showed in [76] that the Lithium-ion battery resistance in 60℃ is much greater than it in 25℃. In addition, parameter varies in the battery pack due to manufacturing tolerance. These abovementioned facts place difficulties for SOC estimation of the battery pack in which many battery cells are combined and heat gradient exists.

Considering abovementioned facts, an Adaptive Genetic Algorithm (AGA) is used here for online battery parameter updating. However, it should be noted that in a physical application, with thermal management methods and many other protections, all-time parameter identification is unnecessary and may even cause unexpected time delay due to high calculation complexity. Hence, an event triggered online parameter identification mechanism is proposed in this research. The AGA parameter identification procedure will be called only when a certain event is triggered.

The event is based on a data queue that consists of 60 measured and estimated voltages. The data queue is updated at every sample time and the AGA algorithm is called when the following condition is satisfied:

$$E(|v_m - v_{es}|) > \delta_{th} \tag{4-11}$$

where $\mathrm{E}(\cdot)$ is the expectation and δ_{th} is a pre-defined threshold.

A simulation is used to illustrate that the event triggered mechanism can be used for representing parameter changes. The simulation result is plotted in Figure 4-9.

In this simulation, electric parameters in the battery model have 12% variation versus their actual values at 1000 seconds. It can be seen from Figure 4-9that the expectation of terminal voltage error has an obvious difference after model parameter changed. In other words, the event described by (4-11) can effectively indicate battery parameter changes.

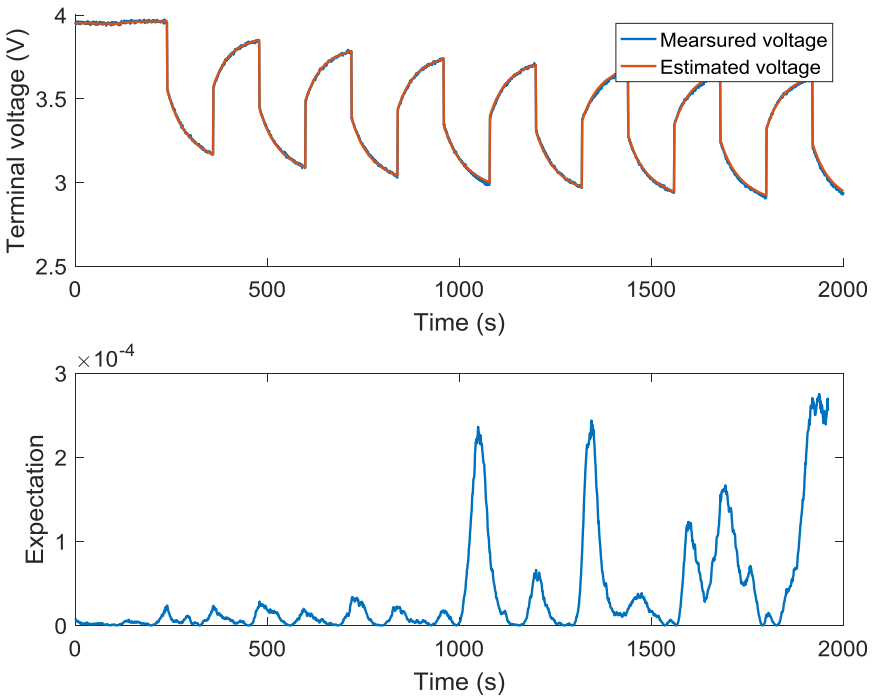

Figure 4-9: Expectation of terminal voltage error

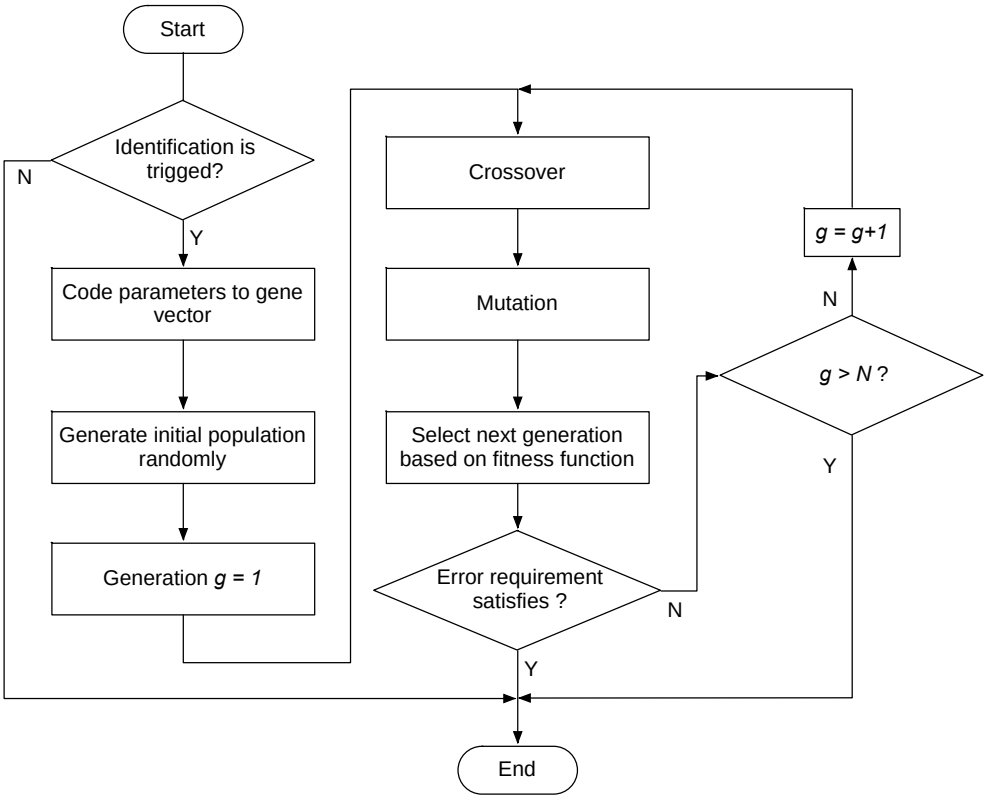

Figure 4-10: Implementation flowchart of GA algorithm

AGA consists of four operators namely encode, crossover, mutation and selection. The flow chart of the AGA is shown in Figure 4-10.

Details of each operator are listed as follow:

1) Encode. For the two-order battery model, there are five parameters for identification which are R_1, C_1, R_2, C_2, R. Considering the reasonable range, an 8-bit binary vector is used for each parameter and one individual can be represented as $\mathbb{C}_i = \left[R^i,\ R_1^i,\ R_2^i,\ C_1^i,\ C_2^i\right]$. The population can be written as $\Sigma = [\mathbb{C}_1,\ \mathbb{C}_2,\ \ldots\ ,\ \mathbb{C}_{2N}]$
2) Crossover. In each generation N pairs of individual will crossover and generator N individuals.
3) Mutation. Mutation may happen in each individual. An adaptive mutation rate is applied in AGA to ensure the initial population diversity and the stability later. Suppose the maximum and minimum mutation rates are $\bar{R}_M = 0.3$ and $\underline{R}_M = 0.01$ respectively. In order to maintain the population diversity, the covariance of each population is evaluated:

$$d = \frac{Var(\Sigma^T)}{1000} \tag{4-12}$$

where 1000 is the normalization coefficient. Generation number N_g is also considered in the adaptive mutation rate. Hence, the mutation rate R_M is defined finally in (4-13).

$$R_M = \frac{1}{1 + d + 0.5N_g}\left(\bar{R}_M - \underline{R}_M\right) + \underline{R}_M \tag{4-13}$$

The mutation bit is selected by two random position vectors, which correspond to electric parameter selection and parameter code bit selection.

4) Selection. Based on iterative prediction-error minimization method, the Fitness function for selection is

$$F = \frac{1}{1 + \sum_{i=1}^{n} \sqrt{e_i^2} + \sum_{i=1}^{n-1} \sqrt{\Delta e_i^2}} \times 100\% \quad \textbf{(4-14)}$$

where e is the error between the measured and the predicted terminal voltage. Δe_i in equation (4-14) equals $e_{i+1} - e_i$. With the introduction of Δe_i the GA is able to reach stable faster.

In order to test the performance of proposed AGA based parameter identification, a simulation is conducted and the result is shown in Figure 4-11.

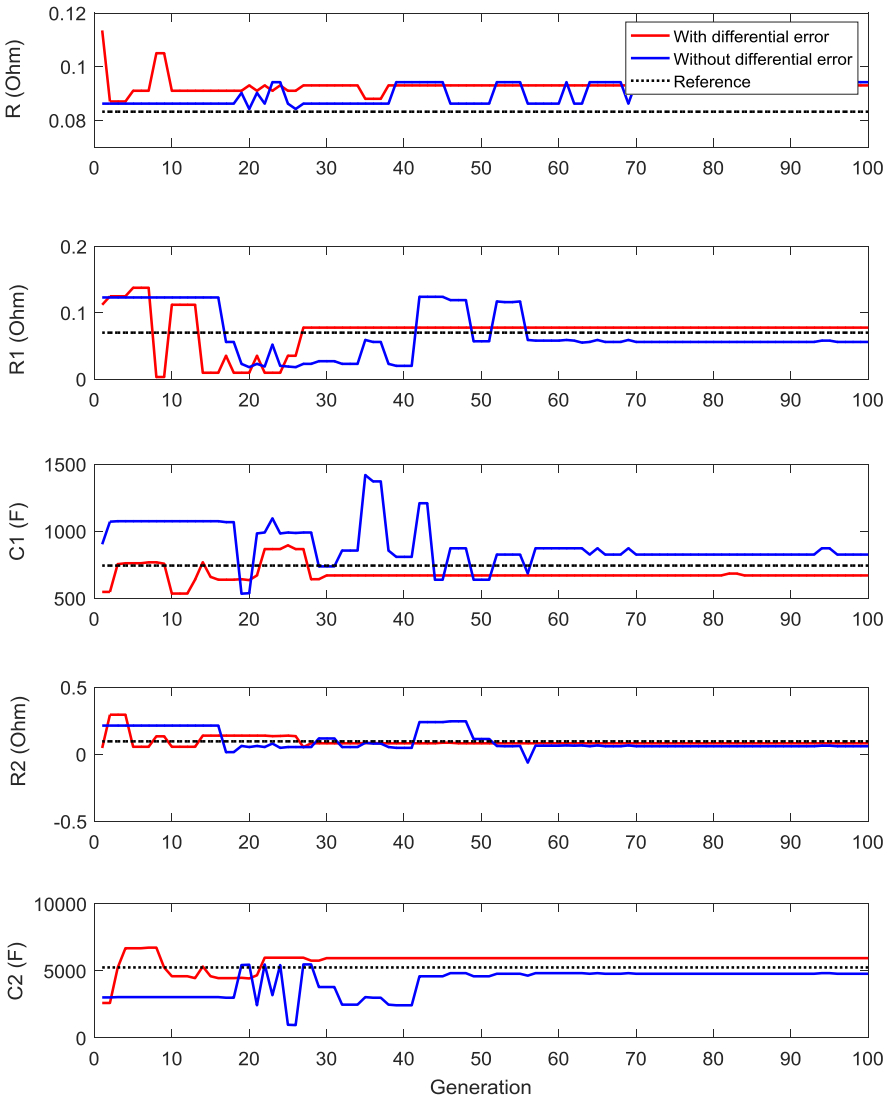

Figure 4-11: Parameters estimated by AGA

The simulation results show that AGA is able to find the reference parameter values after some generations. It can also be obtained that with differential error introduced in fitness function, the generation number for convergence decrease.

Moreover, a hardware experiment is used for evaluate the proposed AGA in real-time parameter identification. In this test, a square pulse current whose period is 1 minute is applied to a battery cell. The experiment results are shown in Figure 4-12.

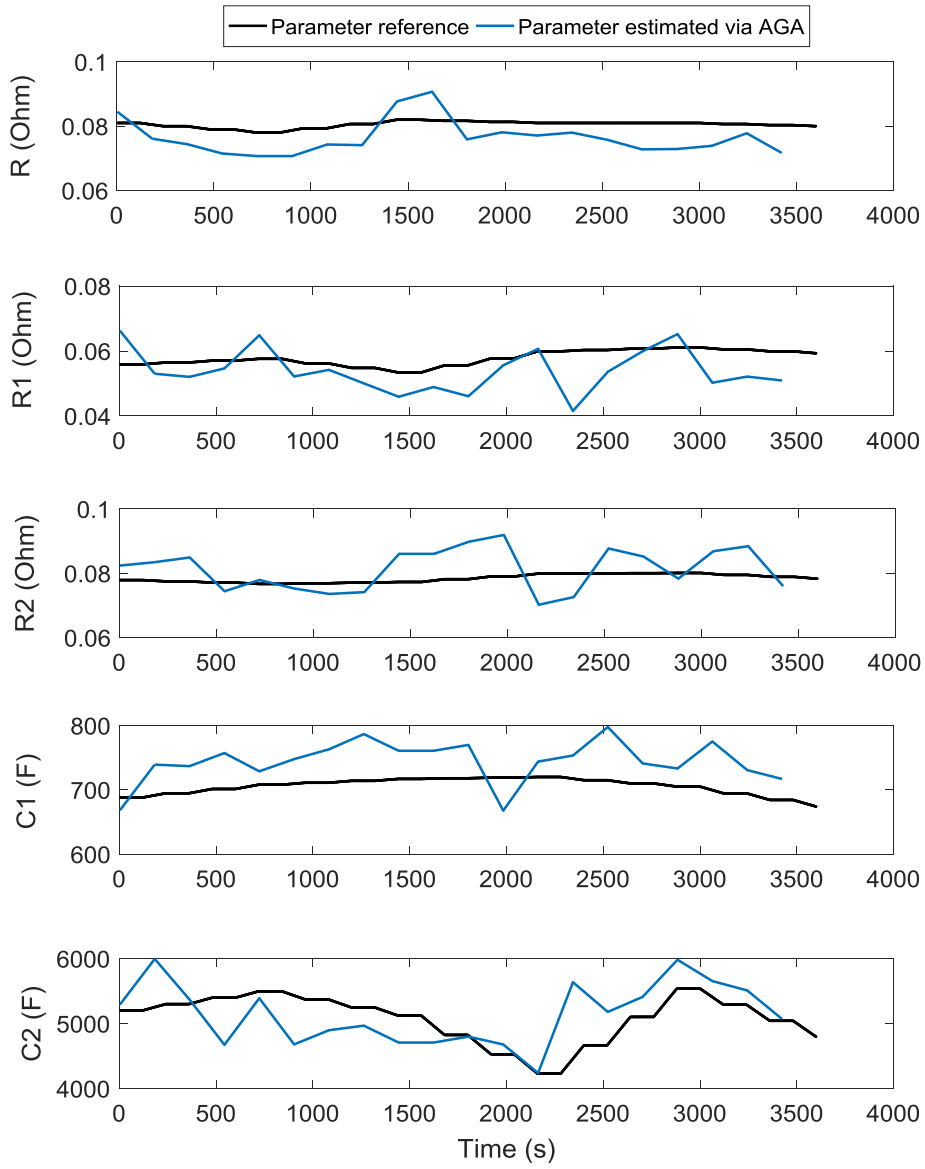

Figure 4-12: Online event trigged parameter identification

The event triggered AGA algorithm was called 20 times in the 1 hour discharge experiment. Other data points in blue lines are added by linear interpolation method. In this experiment, the SOC values are also calculated by Ah-counting method and the reference for each electric parameter is obtained according to the offline parameter identification experiment and current SOC value. As shown in Figure 4-12, the evolving trend of AGA estimated parameters roughly approximates that of the references which for the case under here is acceptable.

4.5 Conclusion

In this chapter, a two-order equivalent circuit battery model is applied for SOC estimation. The relationship between open circuit battery voltage and SOC is obtained based on constant current charge and discharge process via the curving fitting method.

Parameters are of importance for battery state estimation. In order to determine battery model parameter, two parameter identification methods (Least Square and GA) are proposed for offline and online use respectively. With a new fitness function and adaptive mutation rate, AGA is able to converge to the optimal values faster so that can help reduce the parameter identification time. Moreover, an event triggered method is used to determine if parameters should be re-identified at a certain time.

5 Single cell SOC estimation method

State of charge (SOC), defined as the percentage of remain capacity to battery nominal capacity, is usually used to indicate the residual energy in a battery. SOC is a key feedback in HEPS. Accurate SOC estimation can help improving HEPS overall efficiency and be used as an important criterion for BMS control. However, to estimate SOC is not an easy task due to the complex battery dynamic characteristics, sensitive OCV-SOC relationship, and noises.

According to the introduction of kinds of SOC estimation algorithm in the literature review section, model-based SOC estimation method has been chosen in this research for our HEPS development.

Some assumptions should be noted before utilizing model-based SOC estimation method:

1) For any given time k, system noises come from environment disturbance $\xi_k$and measurement noise η_k which are independent.
2) The ideal battery system is observable
3) For any given time k, system state x_k based only on the state at time $k-1$, which is x_{k-1}. In other words, the single battery running process is a Markov process.

Based on those assumptions, the processes of battery SOC estimation in the HEPS can be represented by the hidden Markov model (HMM).

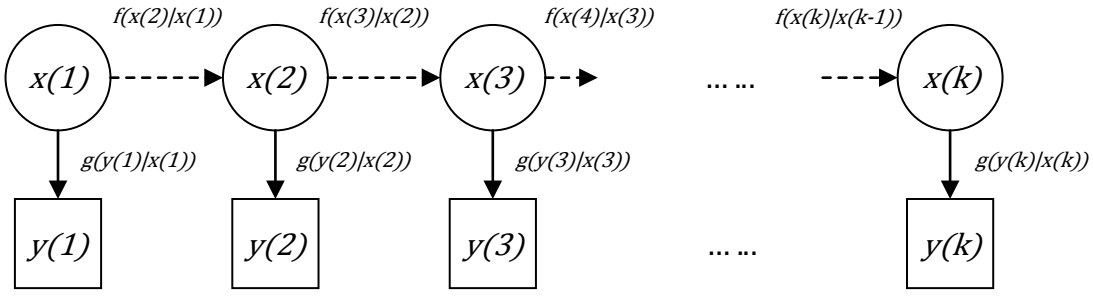

Figure 5-1: Hidden Markov model

As shown in the Figure 5-1, HHM has two layers which are observable layer and hidden layer. $f(x_k|x_{k-1})$ and $g(y_k|x_k)$ are state probability transition

functions and output probability transition function respectively. For Li-ion batteries, y_k is the battery terminal voltage and x_k is the system state vector comprised of two battery dynamic responses and SOC.

This chapter is organized as follow: firstly the theories of EKF and PF are introduced and their performances of SOC estimation are compared. Then based on the adaptive battery model proposed in Chapter 4, an EKF based single cell SOC estimation method is proposed. Finally, the physical experiment demonstrates that the new proposed SOC estimation method has a good accuracy.

5.1 Extended Kalman filter

System state estimation of a stochastic process is actually an optimal problem. The best estimated state $\hat{x}_k$ can be derived from measured output v_i (output space) . This optimal problem can be written as it indicated in [77]

$$\min\{tr\|x_k - \hat{x}_k\|^2, \hat{x}_k \in \overline{span}(v_0, v_1 \dots v_k)\} \quad \textbf{(5-1)}$$

where the $\|\cdot\|$ is defined as:

$$\|x\|^2 = Var(x) = E[(x - E(x)(x - E(x)^T)] \quad \textbf{(5-2)}$$

If we can find a serial of orthonormal basis e_i of the space spanned by v_i and considering the HMM, the optimal state estimation is

$$\begin{aligned} \hat{x}_k = \sum_{i=0}^{k} \langle x_k, e_k \rangle e_i = \sum_{i=0}^{k-1} \langle f(x_{k-1}, x_k), e_i \rangle + \langle x_k, e_k \rangle e_k \\ = f(\hat{x}_{k-1}, x_k) + \langle x_k, e_k \rangle e_k \end{aligned} \quad \textbf{(5-3)}$$

where $f(x_{k-1}, x_k)$ is the state transition function.

Based on these, Kalman Filter (KF) is built and by an extra system linearization process, we can obtain the Extended Kalman Filter (EKF) for nonlinear system state estimation.

Considering the noise effect, we can rewrite system (4-3) into a more general form for description briefness:

$$\begin{aligned} x_{k+1} &= A_k x_k + B_k u_k + \Gamma_k \xi_k \\ y_k &= \Phi(x_k, u_k) + \eta_k \end{aligned} \quad \textbf{(5-4)}$$

The EKF based SOC estimation algorithm for the two-order battery system can be thus build by (5-5).

$$\begin{aligned} &P_{0,0} = \mathrm{Var}(x_0) \\ &\hat{x}_0 = \mathrm{E}(x_0) \\ &P_{k,k-1} = \mathrm{A}\, P_{k-1,k-1} A^T + \Gamma_{k-1} Q_{k-1} \Gamma_{k-1}^T \\ &G_k = P_{k,k-1}[\frac{\partial \Phi}{\partial x}(\hat{x}_{k|k-1})]^T \left[\left[\frac{\partial \Phi}{\partial x}\left(\hat{x}_{k|k-1}\right)\right] P_{k,k-1} \left[\frac{\partial \Phi}{\partial x}\left(\hat{x}_{k|k-1}\right)\right]^T + R_k\right]^{-1} \\ &P_{k,k} = \left[I - G_k \frac{\partial \Phi}{\partial x}\left(\hat{x}_{k|k-1}\right)\right] P_{k,k-1} \\ &\hat{x}_k = \hat{x}_{k|k-1} + G_k\left(y_k - \Phi\left(\hat{x}_{k|k-1}, u_k\right)\right) \end{aligned} \quad \textbf{(5-5)}$$

where $\mathrm{G_k}$ is the Kalman gain matrix, $\mathrm{P_{k,k}}$ the state estimation covariance and $\hat{\mathrm{x}}_\mathrm{k}$ the optimal state estimation. The linearized output matrix is given by $\frac{\partial \Phi}{\partial x}$ which is:

$$\frac{\partial \Phi}{\partial x}\left(\hat{x}_{k|k-1}\right) = [-1 \quad -1 \quad f'(SOC_{k|k-1})] \quad \textbf{(5-6)}$$

5.2 Particle filter

From another point of view, the state estimation at time k can be regarded as the exception of the posterior distribution $p(x_k|y_{1:k})$. Hence the optimal state estimation is the expectation of the posterior distribution.

$$E\big(f(x_k)\big) = \int f(x_k)\frac{p(x_{1:k}|y_{1:k})}{q(x_{1:n})}q(x_{1:k})dx_{1:k}$$
$$= \frac{\int f(x_k)\frac{p(x_{1:k},y_{1:k})}{q(x_{1:k})}q(x_{1:k})dx_{1:k}}{p(y_{1:k})} \quad \textbf{(5-7)}$$
$$= \frac{\int f(x_k)\frac{p(x_{1:k},y_{1:k})}{q(x_{1:k})}q(x_{1:k})dx_{1:k}}{\int p(x_{1:k},y_{1:k})dx_{1:k}}$$

By defining $\omega(x_{1:k}) = \frac{p(x_{1:k},y_{1:k})}{q(x_{1:k})}$, we have

$$E\big(f(x_k)\big) = \frac{\int f(x_k)\omega(x_{1:k})q(x_{1:k})dx_{1:k}}{\int \omega(x_{1:k})q(x_{1:k})dx_{1:k}} \quad \textbf{(5-8)}$$

Monte Carlo method is introduced here for solving the integration and for a large N, equation (5-8) is

$$E\big(f(x_k)\big) = \frac{\frac{1}{N}\sum f(X_k^{(i)})\omega(X_{1:k}^i)}{\frac{1}{N}\sum \omega(X_{1:k}^i)} \quad \textbf{(5-9)}$$

where $X_{1:k}^{(i)}$ are particles generated according to distribution $q(x_{1:k})$.

By defining $W\left(X_{1:k}^{(i)}\right) = \frac{\omega(X_{1:k}^i)}{\sum \omega(X_{1:k}^i)}$, the expectation of $f(x_k)$ is actually a weighted sum of $f(X_k^{(i)})$. Since the high dimension distribution $q(x_{1:k})$ is hard to sample and maintain an acceptable estimation variance, the weighted value $W\left(X_{1:k}^{(i)}\right)$ is determined by a brim distribution $q(x_k|x_{1:k-1})$. As a consequence, the sequential sampling method is applied.

$$\omega_n(x_{1:k}) = \frac{p(x_{1:k},y_{1:k})}{q(x_{1:k})} = \omega_{k-1}\frac{p(y_k|x_{1:k},y_{1:k-1})p(x_k|x_{1:k-1},y_{1:k-1})}{q(x_k|x_{1:k-1})} \quad \textbf{(5-10)}$$

Considering the HMM and the Markov characteristic of the system, the weight value in PF process can be rewritten as a recursion form:

$$\omega_n(x_{1:k}) = \omega_{k-1}(x_{1:k-1}) \frac{p(y_k|x_k)p(x_k|x_{k-1})}{q(x_k|x_{1:k-1})} \quad \textbf{(5-11)}$$

Besides, in order to increase the number of efficacious particles, resampling is introduced here. In resampling technic, particles are sampled from currently generated particles according to their weight value. A typical resample method is by roulette. It should be noted that after resampling, each particle has the same weight value $\frac{1}{N}$. The original weight of each particle is represented by its duplication quantities.

For a typical application, for example battery SOC estimation, $f(x_k) = x_k$ thus the expectation of current state is

$$E(x_k) = \sum W_k^{(i)} X_k^{(i)} \quad \textbf{(5-12)}$$

The implementation flowchart SOC estimation via PF method is shown in Figure 5-2.

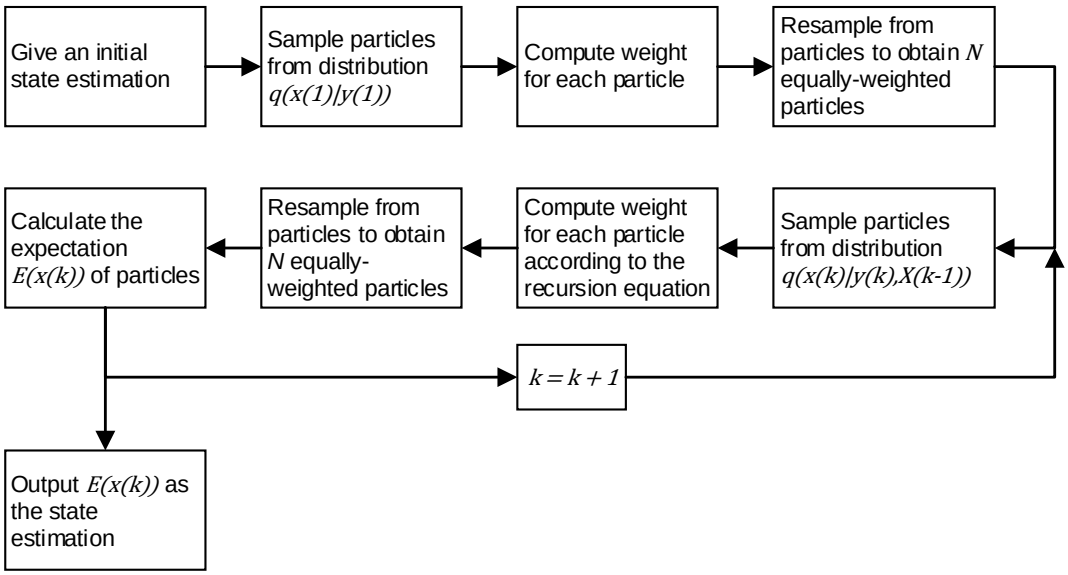

Figure 5-2: Implementation flowchart of the PF algorithm

5.3 Simulation study for SOC estimation algorithms

Two simulations are used to evaluate the performance of EKF based and PF based SOC estimation algorithm.

A square pulse current profile was applied to test the battery system. A white noise is added to the battery voltage to represent the measured voltage. EKF and PF were used for SOC estimation respectively in this simulation study.

5.3.1 Simulation of EKF based SOC estimation

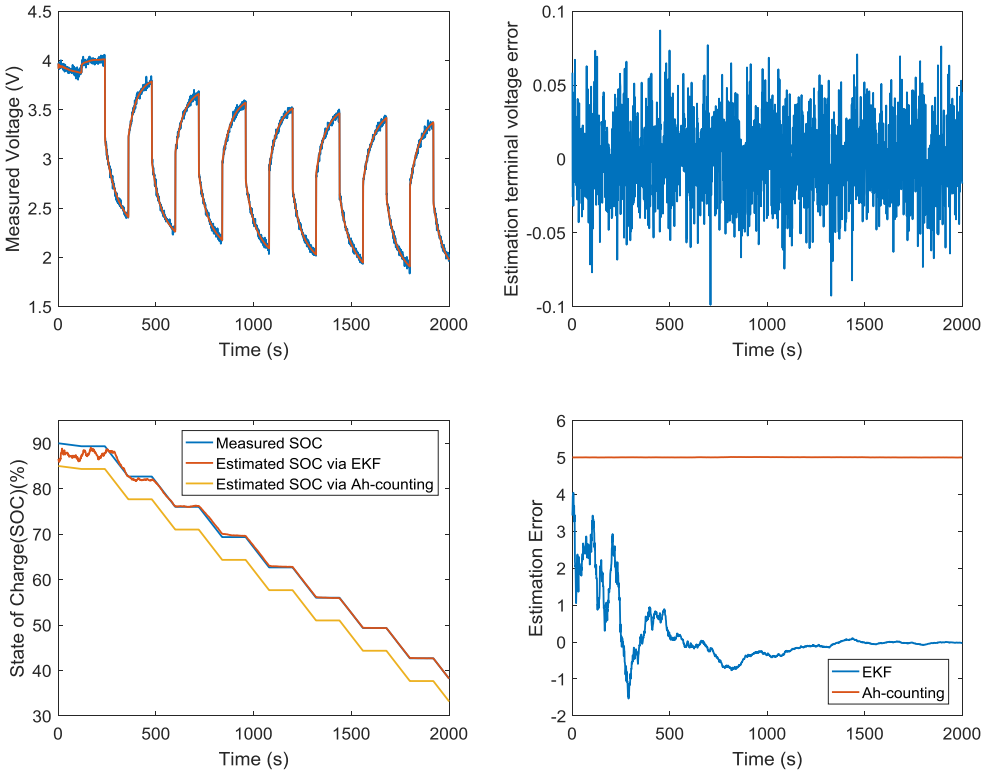

Figure 5-3: Battery SOC estimation via EKF

The simulation result of EKF based SOC estimation is shown in Figure 5-3. We can see that EKF has good stable estimation accuracy (< 2%). As a reference, SOC estimation via Ah-counting is also calculated. With the same initial error (5%), the Ah-counting method is not able to mitigate the initial error.

As a close-loop estimation method, EKF is able to converge to the optimal estimation and the estimation error of EKF will reduce during the process. This property relaxes the requirement of high precision SOC initial value estimation.

From Figure 5-4, we can see that EKF is able to have a good SOC estimation even the initial estimation of SOC is different to its real value.

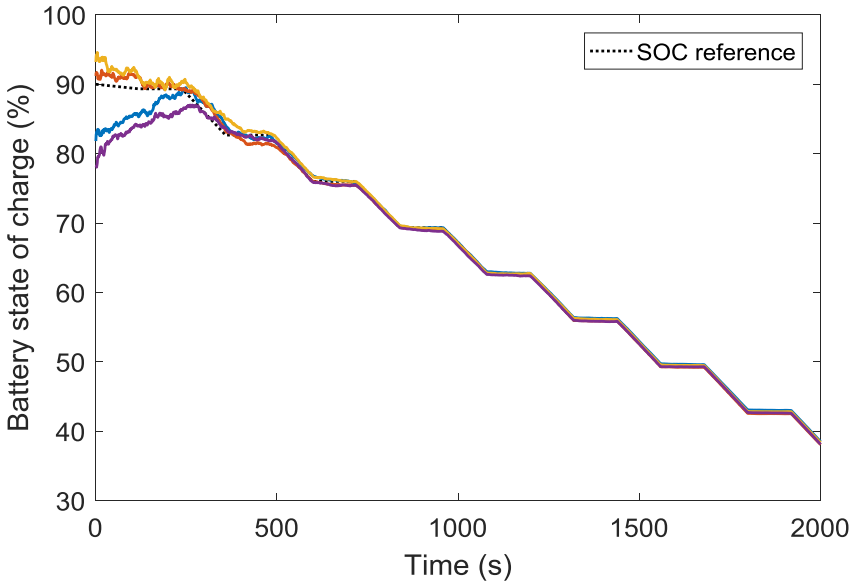

Figure 5-4: Battery SOC estimation via EKF with different initial values

5.3.2 Simulation of PF based SOC estimation

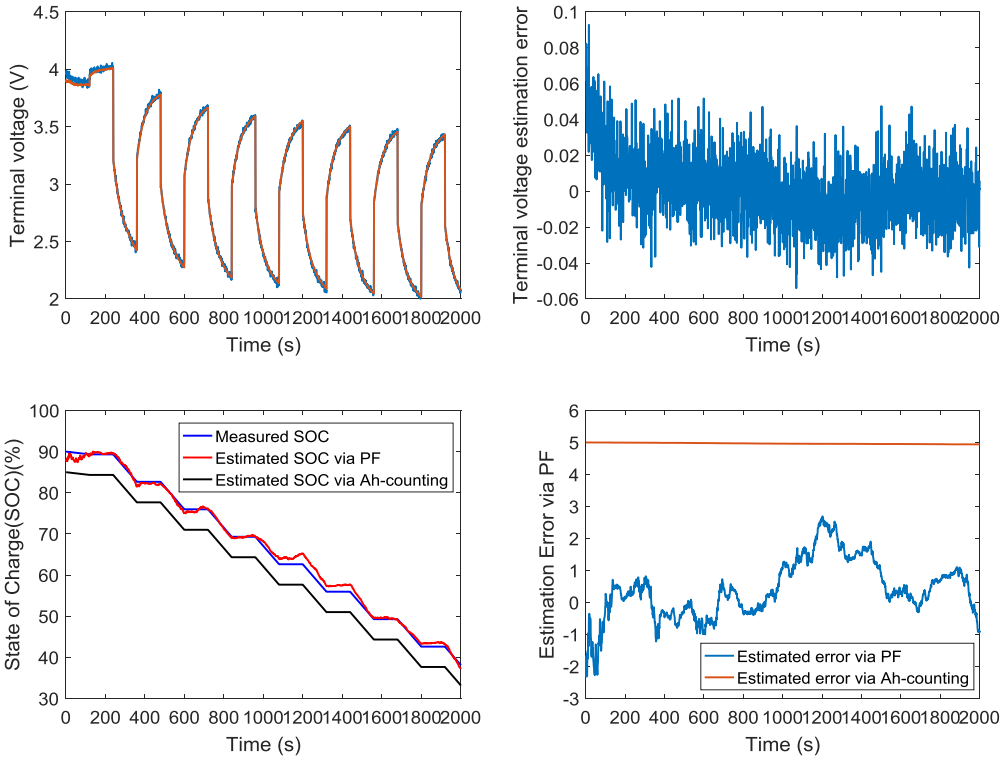

Figure 5-5: SOC estimation via PF

The simulation result of PF based SOC estimation is shown in Figure 5-5. It is safe to say that PF has acceptable estimation accuracy. Same with it in the EKF based SOC simulation, Ah-counting method is used as reference. A 5% initial estimation error is also used in this simulation and it can be found that comparing with EKF, PF has better performance in initial SOC estimation.

The effect of particle numbers is also studied in this section. From Figure 5-6, we can see that the performance of PF is related with particle numbers. With the increasing particle numbers, the average of absolute error decreases.

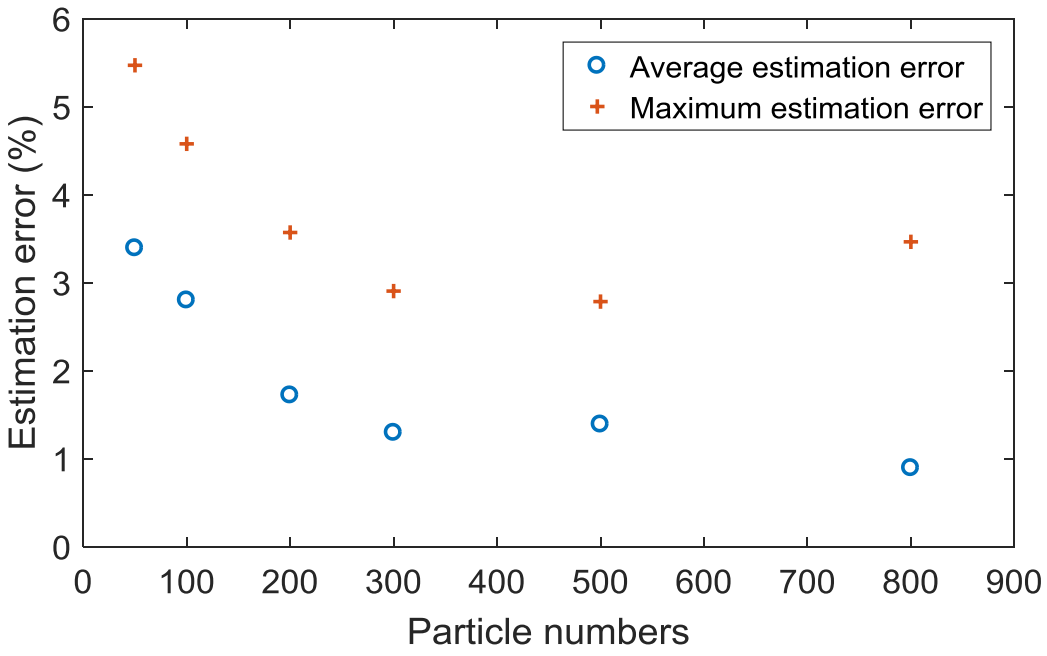

Figure 5-6: Estimation error of different particle numbers

5.3.3 Comparison

For the real-time application, the SOC estimation efficiency is of great importance. According to this consideration, the running time of the two SOC estimation algorithms is compared and the result is shown in Figure 5-7.

From Figure 5-7, with the same estimation error band (2%), we can see that PF will use three times computation time than EKF in one time complete estimation process. As a result, EKF is chosen in this research for battery SOC estimation. However, it should be noted that EKF is model relative. A better model can help

increase the estimation precision. Finally, the adaptive battery model-based EKF SOC estimation algorithm is proposed.

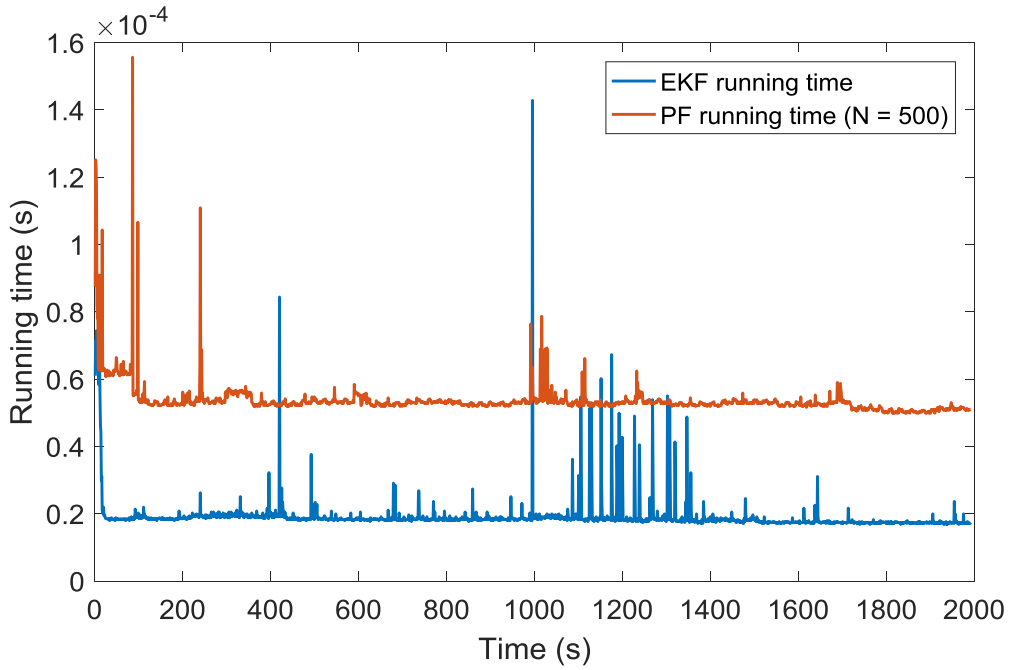

Figure 5-7: Running time comparison of EKF and PF

5.4 Experiment verification for the proposed SOC estimation.

This experiment is used to verify the performance of the proposed SOC estimation algorithm. A current profile was defined and used as the input. This profile includes charge and discharge phase at different current value thus it is able to represent a comprehensive battery operating conditions. In this test, the initial ambient temperature is 20℃. The SOC reference of is calculated via Ah-counting method according to the current profile and labelled battery capacity. The sample rate in this experiment is 50 Hz.

The procedure of this test can be listed as following. Firstly, before applying the current profile, a constant discharge period is used to adjust battery SOC to 70% and then a one hour rest is used for ensuring battery into its stable state. A 2% initial estimation error is set in order to verify the effect of initial SOC estimation error. The test result is shown in Figure 5-8.

The pre-defined current profile is shown in Figure 5-8 (a) and the corresponding output is plotted in Figure 5-8 (b). Figure 5-8 (c) exhibits the error between measured and estimated terminal voltage. Moreover, with the algorithm in section 4, the AGA running indication is shown in Figure 5-8 (d). When the signal equals “1”, it means that the AGA algorithm is called. It can be found that AGA parameter identification is not executed all the time, which can reduce the calculation burden. The EKF SOC estimation results with parameter update and without parameter update are shown in Figure 5-8 (e) and the estimation errors are also plotted in figure respectively. As expect, EKF is model parameter sensitive and the new proposed method has a smaller EKF estimation error.

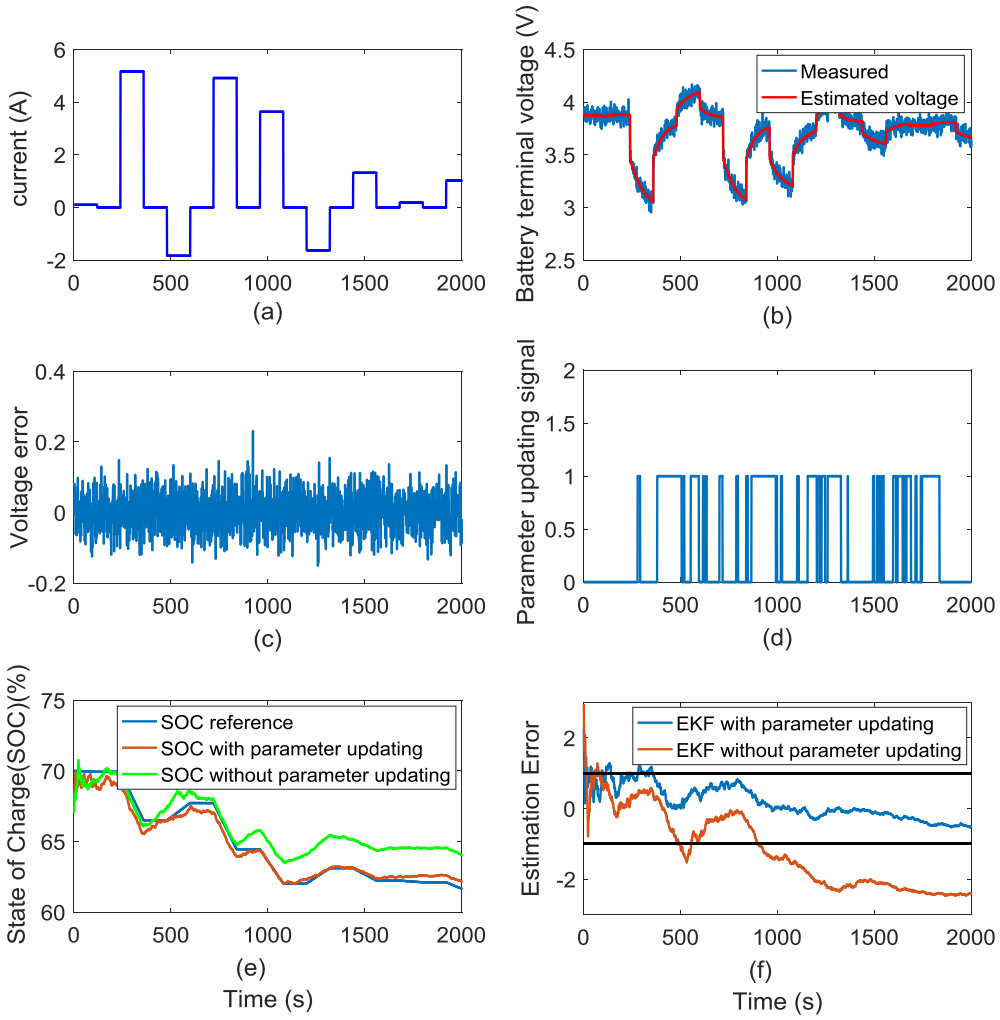

Figure 5-8: Experiment result for the proposed algorithm

5.5 Conclusion

In this chapter two model-based SOC estimation algorithms, EKF and PF, are introduced. Simulation results show that EKF and PF can both estimate battery SOC within an acceptable error band. Moreover, these methods are able to relax the requirement on initial SOC value estimation. However, EKF exhibits a better efficiency than PF thus is chosen as the SOC estimation method in this research.

The performance of EKF algorithm relays on the system model. As a consequence, adaptive battery model-based EKF SOC estimation is proposed. The adaptive battery model is introduced in Chapter 4. The feasibility of the proposed method is demonstrated by a hardware experiment. Experiment results show that the proposed method has a satisfying error band (≤ 1%).

6 Battery management system

Battery management system (BMS) design is an attractive topic in HEPS since it has tight connection with the whole system reliability and safety.

In this chapter, the single cell SOC estimation method is extended for battery pack SOC estimation via fuzzy logic and the effectiveness of this method is valid by a physical experiment. In addition, the battery cell balancing and fault detection method are also included in this chapter.

6.1 Battery pack SOC estimation

In the HEPS, batteries are usually connected in serial or parallel for satisfying voltage and capacity requirements [78] - [80]. The feedback value for HEPS supervisory controller should reflect the condition of the battery pack as entirety instead of a certain single cell. As a consequence, the battery pack SOC is emphasized here and used as the feedback value for HEPS. In this research, the battery pack SOC is defined as the average SOC of all cells. It should be noted that although for the battery management system in HEPS each cell can be monitored and the state can be obtained by its own sensor and model, this detailed cell-level management has significant hardware expense and computation burden [81]. On the contrary, with the development of manufacturing precision and cell balancing strategy, cell to cell variation may continue decrease. This trend makes it possible to predict battery pack conditions and performance with only monitoring few battery cells.

6.1.1 Fuzzy logic estimator

Fuzzy logic proposed by Zadeh in 1965 is a multi-value logic where the input of the system usually has some uncertainties. Due the inherent robustness, fuzzy logic is and has exhibited its feasibility and effectiveness in many fields.

The proposed Fuzzy Logic Estimator (FLE) has three phases which are fuzzification, fuzzy operation and defuzzification:

(1) Fuzzification: Numerical inputs are translated into membership values in this phase via membership functions which are built in terms of users'

experience and knowledge. In this research, Gaussian membership functions are chosen to calculate inputs' membership degrees for each fuzzy sets. The membership function is shown in left figure in Figure 6-1. The input of the FLE is the

$$\frac{v_a - v_l}{v_h - v_l} \tag{6-1}$$

where v_h is the maximum cell terminal voltage, v_l the minimum cell voltage, v_a the average cell voltage.

(2) Rule-based inference: Mamdani inference mechanism is used in this phase and the fuzzy rules in FLE can be described as right below:

IF v is high, *THEN* SOC is SOC_h

IF v is medium, *THEN* SOC is $(SOC_h + SOC_l)/2$ **(6-2)**

IF v is low, *THEN* SOC is SOC_l

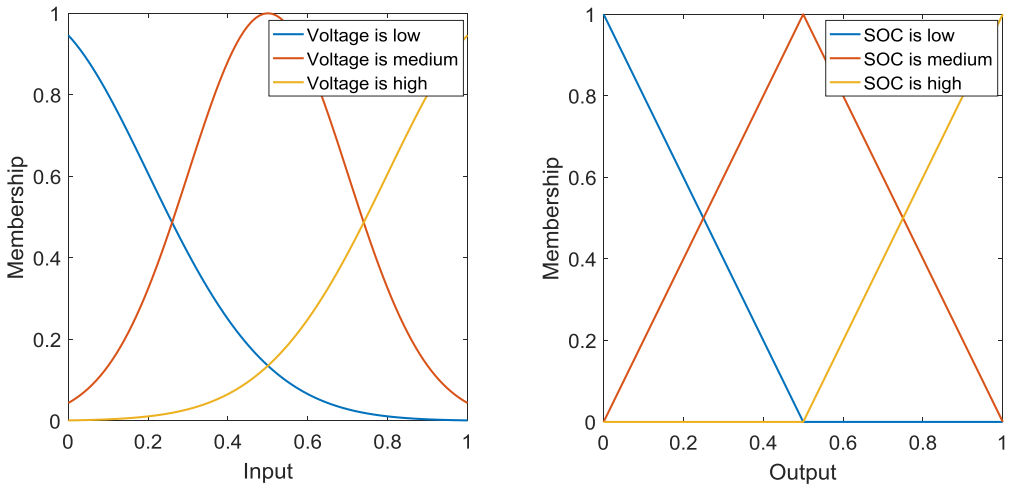

Figure 6-1: Membership function of fuzzy SOC estimator

(3) Defuzzification: In this battery pack SOC estimation application, centroid method is used for defuzzification. The defuzzification formula is:

$$z = \frac{\int \mu_b(z) \cdot z dz}{\int \mu(z) dz} \tag{6-3}$$

Output functions are plotted in the left figure in Figure 6-1. The output α is in the range of 0 to 1 and the battery pack SOC is

$$SOC = (1 - \alpha)SOC_l + \alpha SOC_h \quad \textbf{(6-4)}$$

6.1.2 FLE Simulink model and the simulation result

In order to validate the effectiveness of the proposed battery pack SOC FLE, a simulation model is built in Simulink and its architecture is shown in Figure 6-2. In this simulation model, five Li-Po batteries are connected in serial to represent the HEPS battery pack. A constant ambient temperature is used in this simulation and set as 20℃. Required cell SOC and battery voltage signals (according to (6-1)) are selected by the signal selection module.

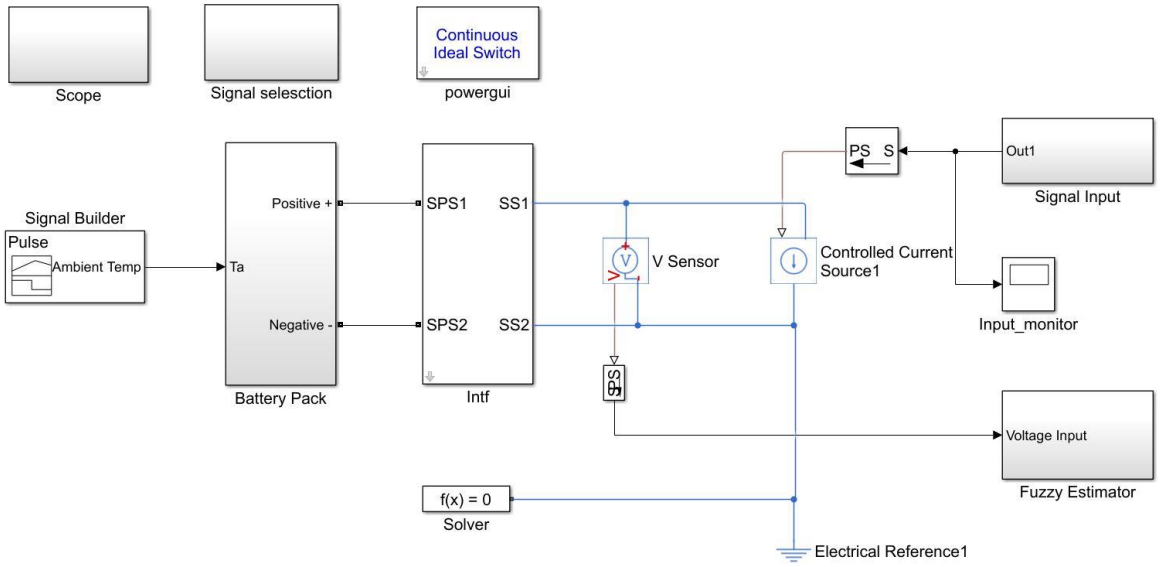

Figure 6-2: Fuzzy pack SOC estimator in Simulink

A pre-defined current test profile is plotted in Figure 6-3. This profile includes discharging and charging phases and in each phase different current values are used for simulating a comprehensive operation situation. In order to show that the FLE can effectively estimate the battery pack SOC, the initial SOC values of the five batteries are set as 92%, 92%, 92%, 91%, 90% respectively.

The simulation result is shown in Figure 6-4. The maximum/minimum cell SOC as well as the estimated battery pack SOC is plotted in the left figure. Taking

average battery pack SOC as the reference, we can calculate the FLE estimation error which is around 0.2%. The simulation result illustrates the feasibility of the proposed FLE.

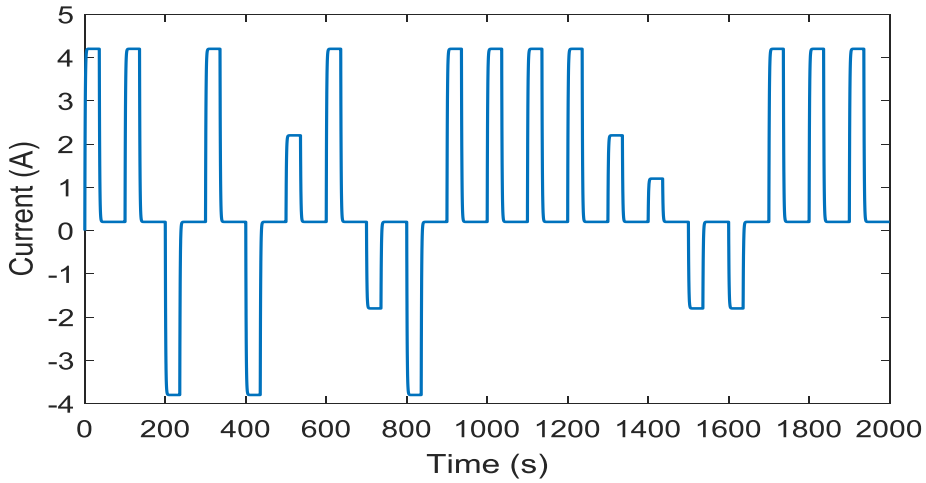

Figure 6-3: Current profile

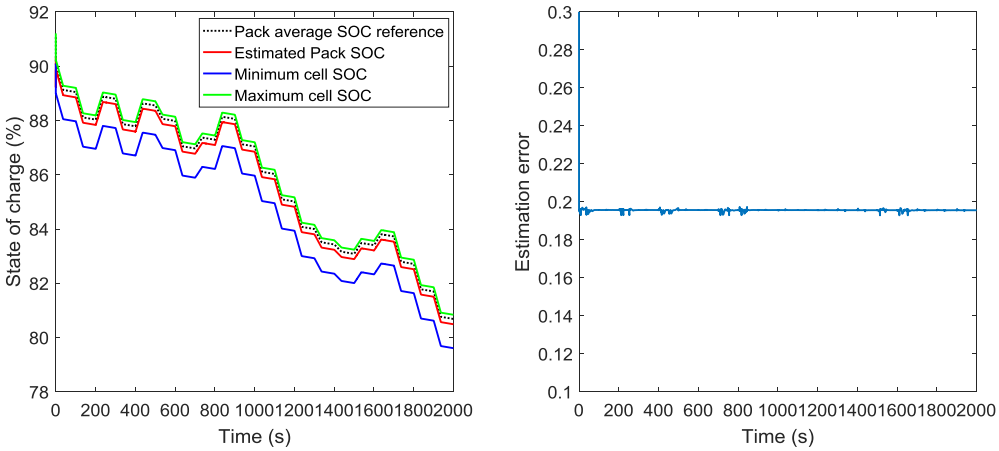

Figure 6-4: Simulation results of the fuzzy logic estimator

6.1.3 Battery pack SOC estimation algorithm

The proposed FLE and the EKF based single SOC estimation algorithm make up the complete battery pack SOC estimation method. The flow chart of the proposed EKF-fuzzy logic joint pack SOC estimator is shown in Figure 6-5.

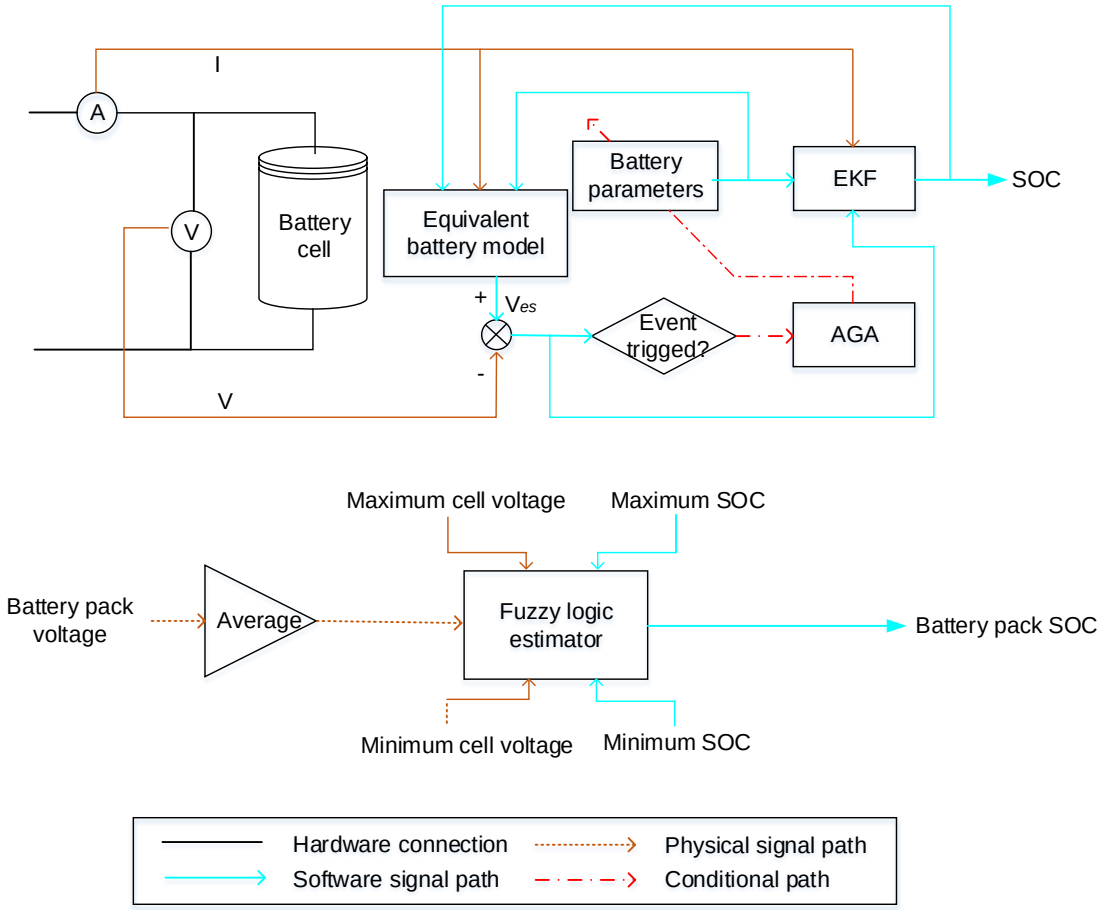

Figure 6-5: Flow chart of the proposed battery pack SOC estimator

In this EKF-fuzzy logic joint pack SOC estimator, the EKF is used for single cell SOC estimating according to the measured cell terminal voltage and load current. The converge property of EKF ensures that even the reference battery cell changes, the SOC can still converge to the real value of the reference battery cell. Taking maximum/minimum cell voltages and SOC, the FLE estimates the pack SOC based on the averaged battery pack terminal voltage.

6.1.4 Experiment verification

Five cells are connected serially for this pack SOC estimation experiment. Before the test, a constant current discharge process is applied to each battery cell to adjust its SOC. The initial SOC of the five cells at the beginning of this test are set as 82%, 80%, 80%, 75% and 80% respectively via a precision constant current discharge procedure. The reference SOC is the calculated via

Ah-counting method and the initial value of the reference is the average of the 5 cells' initial SOC values. At each sample time, the maximum and minimum of cell voltages are logged, and average battery pack value is obtained by measuring the pack terminal voltage and divided by five. The current profile in this test is as the same as we use in single cell SOC estimation test. The experiment result is shown in Figure 6-6.

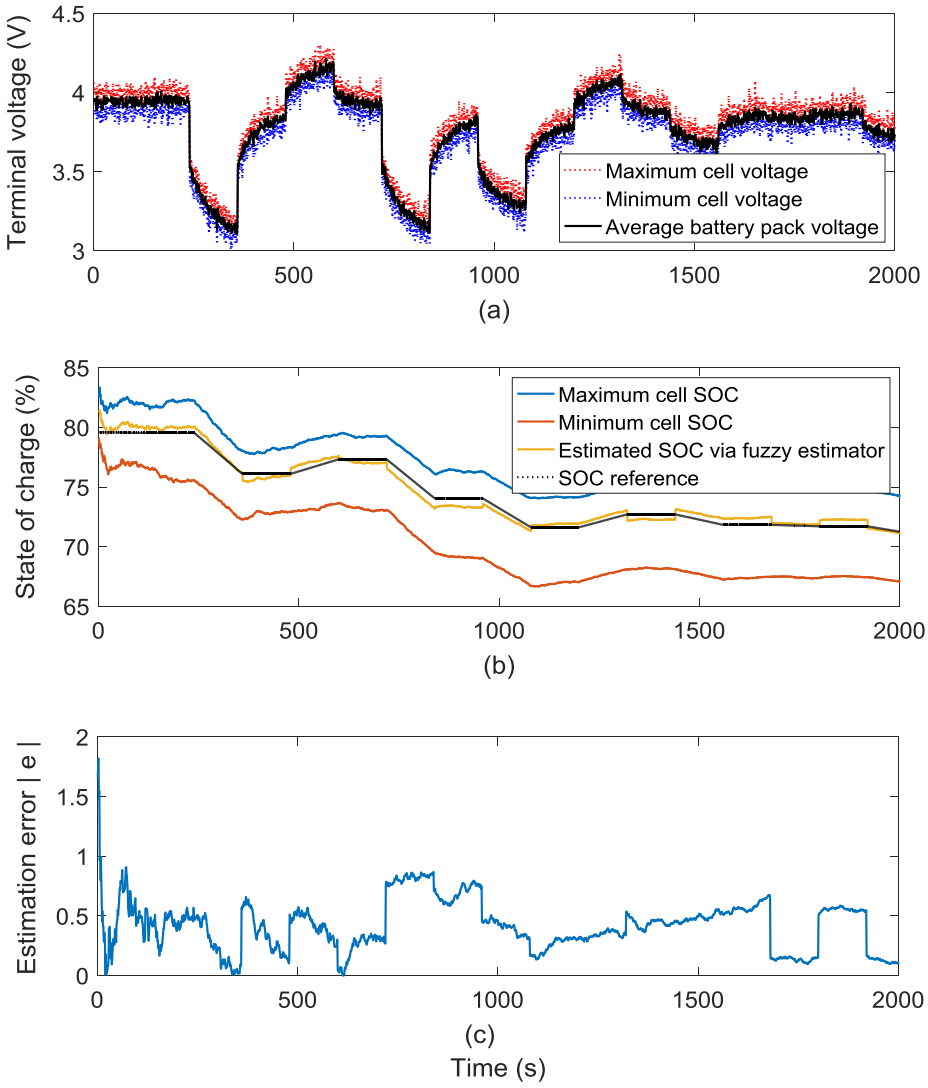

Figure 6-6: Pack SOC estimation result via fuzzy logic estimator

As it shown in Figure 6-6, fuzzy logic estimator is able to estimate the average SOC value for HEPS with an error within 1%. It should be noted that there may occurs estimation error saltation when voltage changes suddenly. This is

because the fuzzy logic output relays on the terminal voltage and the voltage changes will directly reflect in pack SOC estimation. This result shows that the proposed EKF-fuzzy logic pack SOC estimator can be used for high accurate battery pack SOC estimation.

6.2 Battery cell balancing

6.2.1 Bi-direction DC/DC converter based balancer model

The bi-direction converter-based battery balancing method is studied in this section. A simulation model is built in Simulink to evaluate the balancer's performance. The battery cell balancing Simulink model is shown in Figure 6-7.

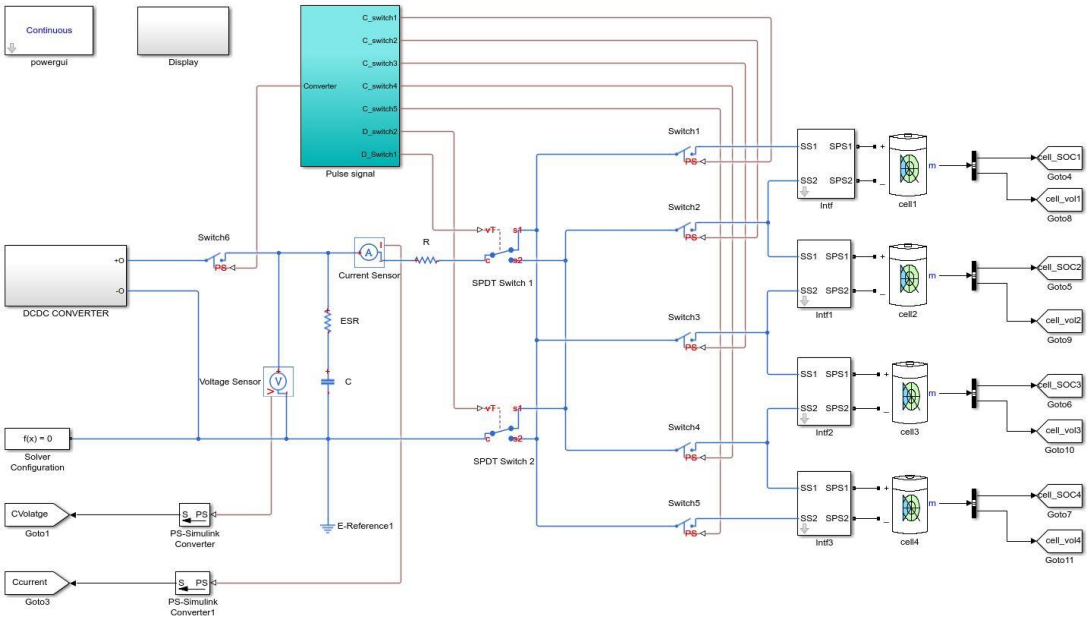

Figure 6-7: Cell balancing Simulink model

The workflow of this balancing model can be described as follow: Firstly, the high voltage battery cell is connected to the Single Switch Capacitor (SSC), the bi-direction DC/DC converter will help to maintain the capacitor voltage smaller than the cell to absorb energy and transfer the energy into a 12V backup battery. Secondly, the low voltage battery cell is connected to the SSC and the converter will boost the capacitor voltage to promote the energy transition from backup battery to the battery cell. The 12V backup battery works as a buffer in

this balancer architecture. The control logic in this four battery pack simulation is in shown in Table 6-1.

In Table 6-1, “1, 2” in SPDT switch column means the two position of the switch (shown in Figure 6-7) and “1” of cell switch means the switch is on.

Table 6-1: Control logic in battery cell balancing system

Cell Number	SPDT switch 1	SPDT switch 2	Cell switch 1	Cell switch 2	Cell switch 3	Cell switch 4	Cell switch 5
1	1	1	1	1	-	-	-
2	2	1	-	1	1	-	-
3	1	2	-	-	1	1	-
4	2	2	-	-	-	1	1

The bi-direction DC/DC converter is the key part in the converter based balancer. A simplified bi-direction DC/DC converter Simulink model is shown in Figure 6-8.

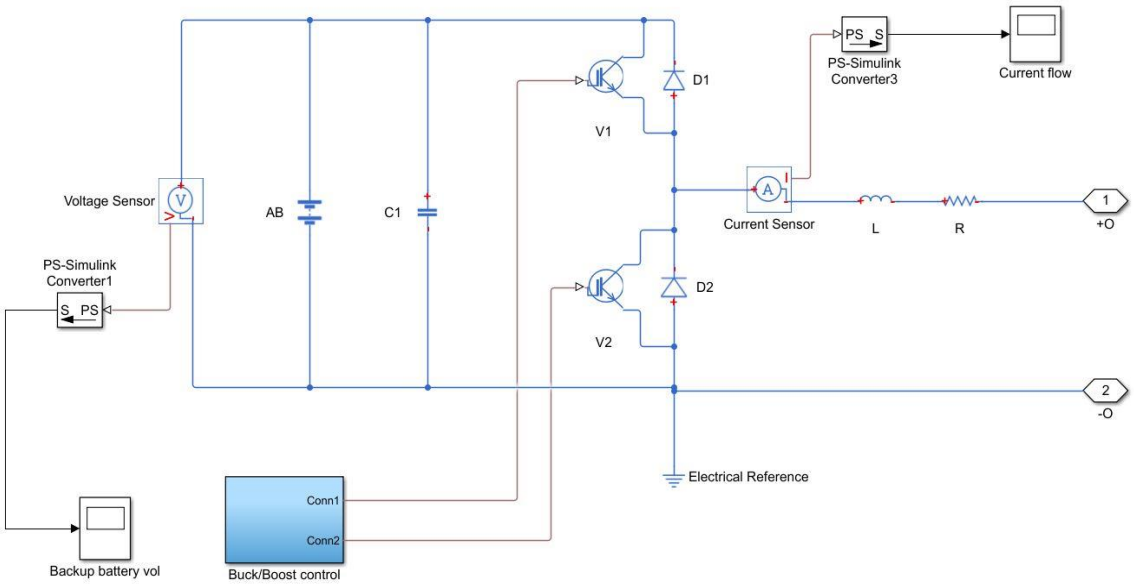

Figure 6-8: Bi-direction DC/DC converter in battery balancer

The bi-direction DC/DC converter is able to work in both “buck” and “boost” mode. The function of converter relays on two MOSFET mainly which are “V1” and “V2”. The bi-direction DC/DC converter works in “buck” mode when V1 is controlled by PWM signal while V2 is closed. In this case, backup battery AB is in discharging thus the energy is transferred to a low voltage battery cell in battery pack through SSC. On the contrary, the converter works in “boost” mode when V1 is closed and V2 is controlled by PWM signal. In this case, back battery AB is charged by high voltage battery cell.

6.2.2 Battery balancer simulation result

In the simulation, the initial SOC of the four battery cells are 95%, 90%, 90%, 85% respectively. The aims of that a relative large SOC differences among cells are applied in this test is to show the balancer performance. It is noteworthy that in the real application, SOC differences are usually less than 5%. The balancing result is shown in Figure 6-9.

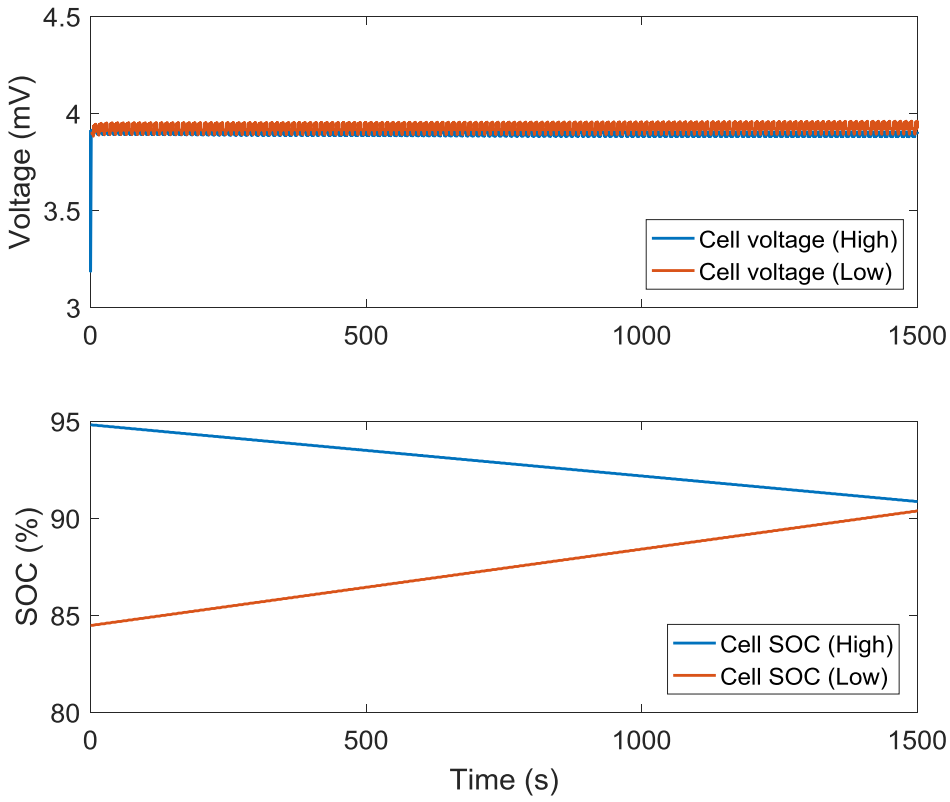

Figure 6-9: Battery cell balancing simulation result

It can be seen from above figure that the converter-based battery balancing system can balance battery cells effectively. Moreover, it should be noted that due to the Li-Po battery dynamic characteristics, even two cells have very similar terminal voltages their SOC values may still be different. However, in the converter based balancing method, the problem can be solved by buck/boost stage. In addition, MOSFET devices have a high switch frequency. Hence the balancing operation will not interface the HEPS controller whose control frequency is ten times less than it of the converter based balancer.

6.3 Battery fault detection

Although Li-Po batteries are known as long-service devices, their length of life depends on the environment and operating conditions. In order to ensure the satisfactory performance of the battery system, some protection methods need to be developed.

6.3.1 Overcharge and overdischarge management

It is necessary to detect the fault and predict remaining life to avoid accidents, some of which might be life-threatening. Among faults mentioned in section 2, overcharging or discharging deserve the most attention since they may shorten battery life or even cause serious accidents.

To avoid overcharge and over-discharge, the maximum/minimum SOC and voltages should be always monitored. Recall the proposed pack SOC estimation mechanism in Section 6.1. Note that the overcharge and over-discharge protection can be constructed according to the estimated maximum and minimum SOC values.

6.3.2 Circuit fault detection

Sparks may occur in a circuit due to a connection fault or environmental disturbance such as vibration. Normally, fault, disturbance, or other system characteristics causes frequency variation of the measured signal. Thus frequency information can be used for system fault detection.

6.3.2.1 Introduction of Wavelet

For non-stationary signals, the Fourier transform causes a loss in time information. Shift time Fourier transform can be used for addressing this problem by localising the signal using a time window function, but the size of the window is constant. However, wavelet analysis uses a variable time-frequency window which can provide good localization in property in both frequency and time domains.

The continuous wavelet transform (CWT) of function $x(t)$ is given in (6-5).

$$X(a,b) = \frac{1}{\sqrt{a}} \int x(t) \bar{\psi}(\frac{t-b}{a}) dt \quad \textbf{(6-5)}$$

where a is the scaling number determining the oscillatory frequency and length of wavelet function, b the translation parameters determining the shift position. Function ψ called the mother wavelet and is continuous in both the time and frequency domains. The main purpose of the mother wavelet is to provide a source function to generate the daughter wavelets which are simply translated and scaled versions of the mother wavelet. The short line above $\bar{\psi}(t)$ represents a complex conjugate.

The Discrete Wavelet Transform (DWT) is derived from the CWT and used for discrete signal process. It not only provides sufficient information for signal analysis but also reduces the computational time.

DWT can abstract time and frequency information simultaneously by a scaling function and wavelet function

$$\Phi_{i,k} = \sqrt{2}^{i} \Phi(2^{i}t - k)$$
$$\Psi_{i,k} = \sqrt{2}^{i} \Psi(2^{i}t - k) \quad \textbf{(6-6)}$$

where i, k are all integral values.

The scaling function $\Phi_{i,k}$ is associated with a low-pass filter while the wavelet function $\Psi_{i,k}$ is associated with a high-pass filter. For signal reconstruction, high-pass g and low-pass filter h should satisfy following equation:

$$g(n) = (-1)^n h(L-1-n) \tag{6-7}$$

where L is the filter length which is an even number.

A signal can be decompensated into:

$$x_L(i-1,n) = \sum_{k=0}^{\infty} h(2n-k)x(i,k)$$
$$x_H(i-1,n) = \sum_{k=0}^{\infty} g(2n-k)x(i,k) \tag{6-8}$$

In DWT analysis, any time series can be decomposed into one approximate signal and several detailed signals. The decompensation flow chart is shown in Figure 6-10.

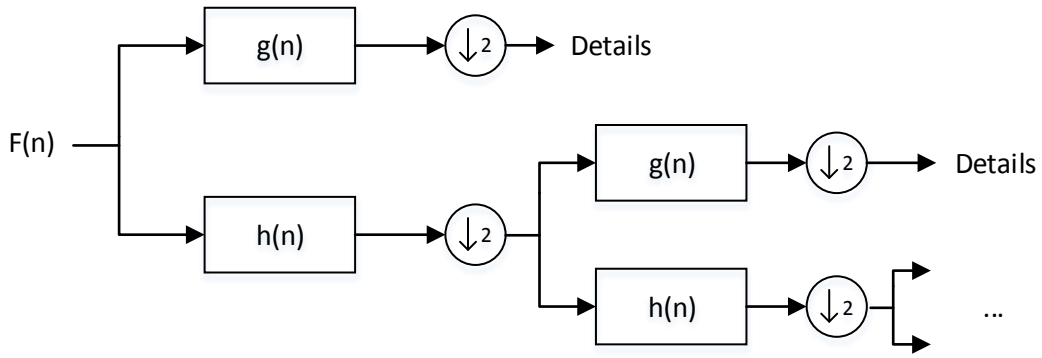

Figure 6-10: DWT signal flow

6.3.2.2 Simulation result

An analysis based on the physical HEPS electric signal was carried out to validate the proposed DWT fault detection method. The Haar wavelet base (shown in Figure 6-11) was chosen in this simulation. The simulation results of circuit fault detection are shown in Figure 6-12.

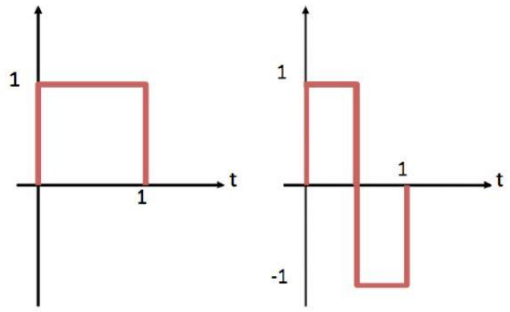

Figure 6-11: Haar wavelet base

In Figure 6-12, “s” is the source signal which is obtained by the HEPS hardware platform test. Two simulated spark signals were added afterward in the 450 seconds and the 2200 seconds. Three-level wavelet decomposition is used here for signal analysis. After decomposition, details signal “d1” and “d2” can be used to assess the fault by using a predefined threshold. In other words, the DWT is able to find the fault even if the fault does not cause great voltage variation (±1.5 volts in this simulation). From the simulation, it can be noted that the fault signal can be detected effectively.

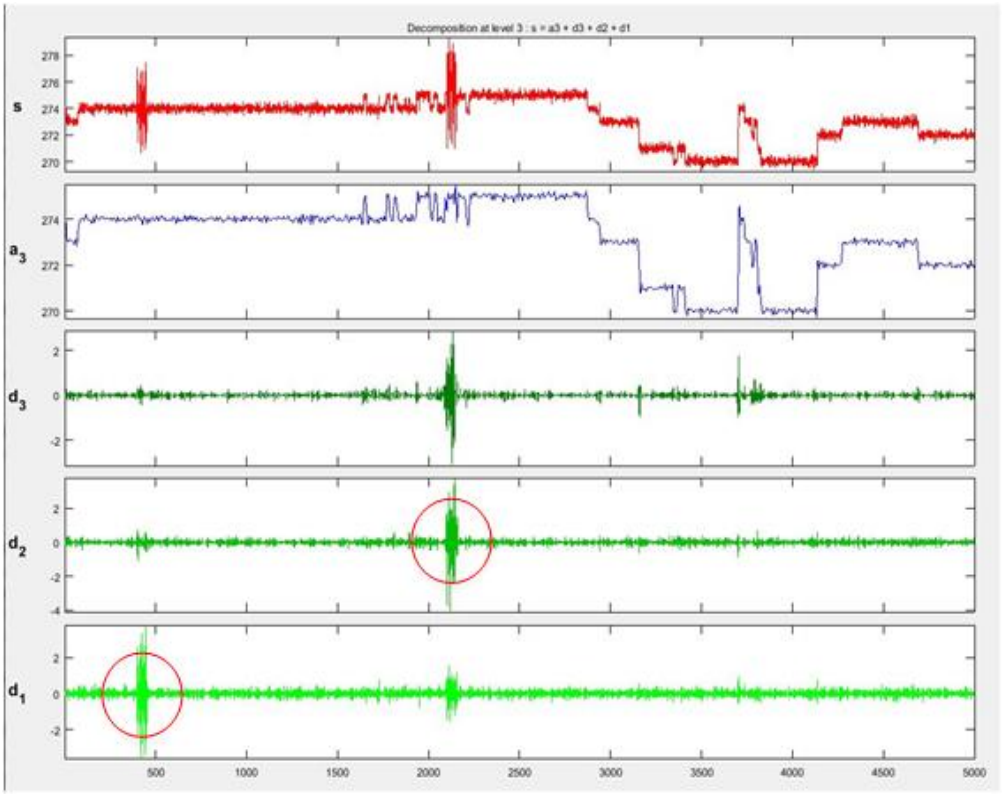

Figure 6-12: Signal decompensate via Haar wavelet

6.4 Conclusion

In this chapter, some functions of BMS have been investigated and it is concluded that:

(1) An EKF-fuzzy logic joint pack SOC estimator is proposed and used for battery pack SOC estimation. This pack SOC can be used as a feedback value for HEPS controller. An experiment was used for verification and its result shows that the maximum estimation error is around 1%.

(2) A converter based battery balancing method was investigated. The simulation result shows that it can effectively balance battery cells.

(3) Because a fault in the battery system usually causes signal frequency variation, the DWT was applied to the BMS for circuit fault detection. The experiment results show that after three-level decompensation, the fault can be seen clearly by comparing the details signal with a predefined threshold.

7 Conclusion and future work

Hybrid propulsion system nowadays is an attractive technology in developing next generation aircrafts and the electrification trend will probably continue in the foreseeable future. This chapter includes the conclusion of this research and recommends some works for future hybrid propulsion system development.

7.1 Concluding remarks

In this research, a hardware platform is built for the HEPS. Via feedback path and control output path experiments, the effectiveness of the HEPS hardware platform is verified so that it can be used for later control strategy validation.

The design of battery management system is another key part in this research. This part includes SOC estimation, battery cell balancing and battery system fault detection.

First, an adaptive battery model is proposed. This model adopts an event-triggered adaptive genetic algorithm for online battery parameter estimation. By experiment, it is shown that this online parameter method can effectively track parameter variations. Compared with other battery model, the proposed event triggered adaptive model is able to adjust itself according to the environment variation (online parameter update) with lower computation complexity (identification only happens when event is triggered).

Second, based on this adaptive battery model, an EKF-FLE joint method is proposed in this research for battery pack SOC estimation. In order to meet the requirement of real-time application and implementation, computation time is considered when design the algorithm. Experiment results indicate that the computation time for single cell SOC estimation needs is 0.02 s maximum while the estimation error less than 1%. Besides, This two-layer battery pack SOC estimation mechanism on the one hand is efficient since the fuzzy logic only relies on few inputs on the other hand can also be used to prevent overcharge and overdischarge.

In addition, considering the facts that inevitable manufacturing error and uneven operation conditions, a cell balancing method is also studied in this research. A bi-directional DC/DC converter based cell balancing model is built in Simulink and the simulation results show that this balancer can effectively balance cell SOC.

Moreover, periphery circuit faults are studied in this research and a discrete wavelet transform based method is used for fault detection. According to the simulation, this method is able to detect faults by comparing the decomposed details signal with a predefine threshold.

In this research, a relative complete battery management system is designed for practical applications. The performance of this system can be regarded as a benchmark for future development.

7.2 Recommendations for future work

The relationship between OCV and SOC is important in battery model because it is not only the basis for SOC initial value estimation but also works as the reference feedback in model based SOC estimation method. It is noteworthy that the OCV-SOC function in Chapter 4 can be replaced by some more complex functions. Although function selection is always a trade-off between complexity and accuracy, it is still worth developing different functions for different scenarios.

In some applications, higher power may be required. When the power requirement is high, even small power loss rates will generate significant heat. As a consequence, how to remove the heat or even reuse the heat via thermal devices is a key research direction.

Since there is an extra battery pack in the hybrid electric configuration, it is possible to utilize this battery pack and take advantage of it by developing a reconfigurable fault tolerant architecture hence improving aircraft’s reliability and residence.

In developing this reconfigurable structure, two main challenges will have to be overcome:

1) Integration. Due to the differing voltage and power levels, a suitable architecture should be designed for the new electric bus. This new structure should be reconfigurable for fault tolerant.
2) Fault detection. Faults are required be detected and isolated. This is still an open area of research -- more research is needed.

Compared to Li-Po batteries, Li-Sulphur batteries offer higher energy density, improved safety and a wider operational temperature range [73]. It is reported that Li-Sulphur battery has the potential to extend the electric vehicle operation range three times than it in now. In addition, since there are abundant sources of sulphur, Li-Sulphur batteries are promising in the commercial application. However, Li-Sulphur batteries represent a relatively new research area and they exhibit different characteristics from Li-Po batteries. For example, there is a flat area in the Li-Sulphur battery OCV-SOC curve. These facts mean that current battery model and state estimation methods may have to be adjusted for the Li-Sulphur battery scenario. Moreover, Li-Sulphur batteries have rapid fade due to battery cycling. This problem will require a more delicate battery management system design.

REFERENCES

[1] European Aviation Environmental report 2016. https://ec.europa.eu/transport/sites/transport/files/european-aviation-environmental-report-2016-72dpi.pdf

[2] https://en.wikipedia.org/wiki/Boeing_787_Dreamliner_battery_problems

[3] Lukic, S.M., Cao, J., Bansal, R.C., Rodriguez, F. and Emadi, A., 2008. Energy storage systems for automotive applications. IEEE Transactions on industrial electronics, 55(6), pp.2258-2267.

[4] Wang, Y., Yang, D., Zhang, X. and Chen, Z., 2016. Probability based remaining capacity estimation using data-driven and neural network model. Journal of Power Sources, 315, pp.199-208.

[5] Wang, Y., Chen, Z. and Zhang, C., 2017. On-line remaining energy prediction: A case study in embedded battery management system. Applied energy, 194, pp.688-695.

[6] Pop, V., Bergveld, H.J., Notten, P.H.L. and Regtien, P.P., 2005. State-of-the-art of battery state-of-charge determination. Measurement Science and Technology, 16(12), p.R93.

[7] Charkhgard, M. and Farrokhi, M., 2010. State-of-charge estimation for lithium-ion batteries using neural networks and EKF. IEEE transactions on industrial electronics, 57(12), pp.4178-4187.

[8] Lin, X., 2018. Theoretical Analysis of Battery SOC Estimation Errors Under Sensor Bias and Variance. IEEE Transactions on Industrial Electronics, 65(9), pp.7138-7148.

[9] El Din, M.S., Hussein, A.A. and Abdel-Hafez, M.F., 2018. Improved Battery SOC Estimation Accuracy Using a Modified UKF With an Adaptive Cell Model Under Real EV Operating Conditions. IEEE Transactions on Transportation Electrification, 4(2), pp.408-417.

[10] Yuan, Q., Zhao, F., Wang, W., Zhao, Y., Liang, Z. and Yan, D., 2015. Overcharge failure investigation of lithium-ion batteries. Electrochimica Acta, 178, pp.682-688.

[11] Hannan, M.A., Azidin, F.A. and Mohamed, A., 2014. Hybrid electric vehicles and their challenges: A review. Renewable and Sustainable Energy Reviews, 29, pp.135-150.

[12] Torres, J.L., Gonzalez, R., Gimenez, A. and Lopez, J., 2014. Energy management strategy for plug-in hybrid electric vehicles. A comparative study. Applied Energy, 113, pp.816-824.

[13] Montazeri-Gh, M. and Mahmoodi-k, M., 2015. Development a new power management strategy for power split hybrid electric vehicles. Transportation Research Part D: Transport and Environment, 37, pp.79-96.

[14] Sundstrom, O. and Guzzella, L., 2009, July. A generic dynamic programming Matlab function. In Control Applications,(CCA) & Intelligent Control,(ISIC), 2009 IEEE (pp. 1625-1630). IEEE.

[15] Malikopoulos, A.A., 2014. Supervisory power management control algorithms for hybrid electric vehicles: A survey. IEEE Transactions on intelligent transportation systems, 15(5), pp.1869-1885.

[16] Jiao, X. and Shen, T., 2014. SDP policy iteration-based energy management strategy using traffic information for commuter hybrid electric vehicles. Energies, 7(7), pp.4648-4675.

[17] Paganelli, G., Delprat, S., Guerra, T.M., Rimaux, J. and Santin, J.J., 2002. Equivalent consumption minimization strategy for parallel hybrid powertrains. In Vehicular Technology Conference, 2002. VTC Spring 2002. IEEE 55th (Vol. 4, pp. 2076-2081). IEEE.

[18] Gao, J.P., Zhu, G.G., Strangas, E.G. and Sun, F.C., 2009. Equivalent fuel consumption optimal control of a series hybrid electric vehicle. Proceedings of the Institution of Mechanical Engineers, Part D: Journal of Automobile Engineering, 223(8), pp.1003-1018.

[19] Sinoquet, D., Rousseau, G. and Milhau, Y., 2011. Design optimization and optimal control for hybrid vehicles. Optimization and Engineering, 12(1-2), pp.199-213.

[20] Won, J.S., Langari, R. and Ehsani, M., 2005. An energy management and charge sustaining strategy for a parallel hybrid vehicle with CVT. IEEE Transactions on Control Systems Technology, 13(2), pp.313-320.

[21] Rahimi-Eichi, H., Ojha, U., Baronti, F. and Chow, M.Y., 2013. Battery management system: An overview of its application in the smart grid and electric vehicles. IEEE Industrial Electronics Magazine, 7(2), pp.4-16.

[22] Tie, S.F. and Tan, C.W., 2013. A review of energy sources and energy management system in electric vehicles. Renewable and Sustainable Energy Reviews, 20, pp.82-102.

[23] Cheng, K.W.E., Divakar, B.P., Wu, H., Ding, K. and Ho, H.F., 2011. Battery-management system (BMS) and SOC development for electrical vehicles. IEEE Transactions on Vehicular Technology, 60(1), pp.76-88.

[24] Hannan, M.A., Lipu, M.S.H., Hussain, A. and Mohamed, A., 2017. A review of lithium-ion battery state of charge estimation and management system in electric vehicle applications: Challenges and recommendations. Renewable and Sustainable Energy Reviews, 78, pp.834-854.

[25] Li, Z., Huang, J., Liaw, B.Y. and Zhang, J., 2017. On state-of-charge determination for lithium-ion batteries. Journal of Power Sources, 348, pp.281-301.

[26] Lee, S., Kim, J., Lee, J. and Cho, B.H., 2008. State-of-charge and capacity estimation of lithium-ion battery using a new open-circuit voltage versus state-of-charge. Journal of power sources, 185(2), pp.1367-1373.

[27] Propp, K., Auger, D.J., Fotouhi, A., Longo, S. and Knap, V., 2017. Kalman-variant estimators for state of charge in lithium-sulfur batteries. Journal of Power Sources, 343, pp.254-267.

[28] Tang, X., Mao, X., Lin, J. and Koch, B., 2011, June. Capacity estimation for Li-ion batteries. In American Control Conference (ACC), 2011 (pp. 947-952). IEEE.

[29] Hu, C., Jain, G., Schmidt, C., Strief, C. and Sullivan, M., 2015. Online estimation of lithium-ion battery capacity using sparse Bayesian learning. Journal of Power Sources, 289, pp.105-113.

[30] Hu, C., Jain, G., Zhang, P., Schmidt, C., Gomadam, P. and Gorka, T., 2014. Data-driven method based on particle swarm optimization and k-nearest neighbor regression for estimating capacity of lithium-ion battery. Applied Energy, 129, pp.49-55.

[31] Becherif, M., Péra, M.C., Hissel, D. and Jemeï, S., 2012, October. Estimation of the lead-acid battery initial state of charge with experimental validation. In Vehicle Power and Propulsion Conference (VPPC), 2012 IEEE (pp. 469-473). IEEE.

[32] Zhang, Y., Song, W., Lin, S. and Feng, Z., 2014. A novel model of the initial state of charge estimation for LiFePO4 batteries. Journal of Power Source, 248, pp.1028-1033

[33] Tong, S., Lacap, J.H. and Park, J.W., 2016. Battery state of charge estimation using a load-classifying neural network. Journal of Energy Storage, 7, pp.236-243.

[34] Anton, J.A., Nieto, P.G., Viejo, C.B. and Vilan, J.V., 2013. Support vector machines used to estimate the battery state of charge. IEEE Trans. Power Electron, 28(12), pp.5919-5926..

[35] Seaman, A., Dao, T.S. and McPhee, J., 2014. A survey of mathematics-based equivalent-circuit and electrochemical battery models for hybrid and electric vehicle simulation. Journal of Power Sources, 256, pp.410-423.

[36] Gholizadeh, M. and Salmasi, F.R., 2014. Estimation of state of charge, unknown nonlinearities, and state of health of a lithium-ion battery based on a comprehensive unobservable model. IEEE Transactions on Industrial Electronics, 61(3), pp.1335-1344.

[37] Di Domenico, D., Fiengo, G. and Stefanopoulou, A., 2008, September. Lithium-ion battery state of charge estimation with a kalman filter based on a electrochemical model. In Control Applications, 2008. CCA 2008. IEEE International Conference on (pp. 702-707). IEEE.

[38] Lin, C., Mu, H., Xiong, R. and Shen, W., 2016. A novel multi-model probability battery state of charge estimation approach for electric vehicles using H-infinity algorithm. Applied Energy, 166, pp.76-83.

[39] Zhang, Y., Xiong, R., He, H. and Shen, W., 2017. Lithium-Ion Battery Pack State of Charge and State of Energy Estimation Algorithms Using a Hardware-in-the-Loop Validation. IEEE Transactions on Power Electronics, 32(6), pp.4421-4431.

[40] Chen, X., Shen, W., Dai, M., Cao, Z., Jin, J. and Kapoor, A., 2016. Robust adaptive sliding-mode observer using RBF neural network for lithium-ion battery state of charge estimation in electric vehicles. IEEE Transactions on Vehicular Technology, 65(4), pp.1936-1947.

[41] Xu, J., Mi, C.C., Cao, B., Deng, J., Chen, Z. and Li, S., 2014. The state of charge estimation of lithium-ion batteries based on a proportional-integral observer. IEEE Transactions on Vehicular Technology, 63(4), pp.1614-1621.

[42] Ye, M., Guo, H. and Cao, B., 2017. A model-based adaptive state of charge estimator for a lithium-ion battery using an improved adaptive particle filter. Applied Energy, 190, pp.740-748.

[43] Wang, Y., Zhang, C. and Chen, Z., 2015. A method for state-of-charge estimation of LiFePO 4 batteries at dynamic currents and temperatures using particle filter. Journal of power sources, 279, pp.306-311.

[44] Sepasi, S., Ghorbani, R. and Liaw, B.Y., 2014. Improved extended Kalman filter for state of charge estimation of battery pack. Journal of Power Sources, 255, pp.368-376.

[45] He, H., Xiong, R. and Peng, J., 2016. Real-time estimation of battery state-of-charge with unscented Kalman filter and RTOS μCOS-II platform. Applied Energy, 162, pp.1410-1418.

[46] Yang, F., Xing, Y., Wang, D. and Tsui, K.L., 2016. A comparative study of three model-based algorithms for estimating state-of-charge of lithium-ion batteries under a new combined dynamic loading profile. Applied Energy, 164, pp.387-399.

[47] Daowd, M., Omar, N., Van Den Bossche, P. and Van Mierlo, J., 2011. A review of passive and active battery balancing based on MATLAB/Simulink. J. Int. Rev. Electr. Eng, 6, pp.2974-2989.

[48] Wu, C., Zhu, C., Ge, Y. and Zhao, Y., 2015. A review on fault mechanism and diagnosis approach for Li-ion batteries. Journal of Nanomaterials, 2015, p.8.

[49] Belov, D. and Yang, M.H., 2008. Investigation of the kinetic mechanism in overcharge process for Li-ion battery. Solid State Ionics, 179(27), pp.1816-1821.

[50] Maleki, H. and Howard, J.N., 2006. Effects of overdischarge on performance and thermal stability of a Li-ion cell. Journal of power sources, 160(2), pp.1395-1402.

[51] Suresh, P., Shukla, A.K. and Munichandraiah, N., 2002. Temperature dependence studies of ac impedance of lithium-ion cells. Journal of applied electrochemistry, 32(3), pp.267-273.

[52] Ji, Y., Zhang, Y. and Wang, C.Y., 2013. Li-ion cell operation at low temperatures. Journal of The Electrochemical Society, 160(4), pp.A636-A649.

[53] He, Z., Gao, M., Wang, C., Wang, L. and Liu, Y., 2013. Adaptive state of charge estimation for Li-ion batteries based on an unscented Kalman filter with an enhanced battery model. Energies, 6(8), pp.4134-4151.

[54] Kaypmaz, T.C. and Tuncay, R.N., 2011, September. An advanced cell model for diagnosing faults in operation of Li-ion Polymer batteries. In Vehicle Power and Propulsion Conference (VPPC), 2011 IEEE (pp. 1-5). IEEE.

[55] Singh, A., Izadian, A. and Anwar, S., 2013, November. Fault diagnosis of Li-Ion batteries using multiple-model adaptive estimation. In Industrial Electronics Society, IECON 2013-39th Annual Conference of the IEEE (pp. 3524-3529). IEEE.

[56] Tröltzsch, U., Kanoun, O. and Tränkler, H.R., 2006. Characterizing aging effects of lithium ion batteries by impedance spectroscopy. Electrochimica Acta, 51(8), pp.1664-1672.

[57] Moebes, T.A., 2011, January. Lithium battery analysis: probability of failure assessment using logistic regression. In Reliability and

Maintainability Symposium (RAMS), 2011 Proceedings-Annual (pp. 1-5). IEEE.

[58] Kim, J. and Cho, B.H., 2014. An innovative approach for characteristic analysis and state-of-health diagnosis for a Li-ion cell based on the discrete wavelet transform. Journal of Power Sources, 260, pp.115-130.

[59] Becraft, W.R. and Lee, P.L., 1993. An integrated neural network/expert system approach for fault diagnosis. Computers & chemical engineering, 17(10), pp.1001-1014.

[60] Liu, J., Saxena, A., Goebel, K., Saha, B. and Wang, W., 2010. An adaptive recurrent neural network for remaining useful life prediction of lithium-ion batteries. NATIONAL AERONAUTICS AND SPACE ADMINISTRATION MOFFETT FIELD CA AMES RESEARCH CENTER.

[61] Virk, S.M., Muhammad, A. and Martinez-Enriquez, A.M., 2008, October. Fault prediction using artificial neural network and fuzzy logic. In Artificial Intelligence, 2008. MICAI'08. Seventh Mexican International Conference on (pp. 149-154). IEEE.

[62] Zhang, H., Zhang, Y. and Yin, C., 2016. Hardware-in-the-loop simulation of robust mode transition control for a series–parallel hybrid electric vehicle. IEEE Transactions on Vehicular Technology, 65(3), pp.1059-1069.

[63] Schlager, M., 2008. Hardware-in-the-Loop simulation: A scalable. time-triggered hardware-in-the-loop simulation framework.

[64] ENSTROJ., 2014. Owner’s manual for the brushless AC synchronous motor EMRAX.

[65] Voss, W., 2008. A comprehensible guide to controller area network. Copperhill Media.

[66] Samadi, M.F. and Saif, M., 2017. State-Space modeling and observer Design of Li-Ion batteries using Takagi–Sugeno fuzzy System. IEEE Transactions on Control Systems Technology, 25(1), pp.301-308.

[67] Zhang, C., Li, K., Mcloone, S. and Yang, Z., 2014, June. Battery modelling methods for electric vehicles-A review. In Control Conference (ECC), 2014 European (pp. 2673-2678). IEEE.

[68] He, Y., Liu, X., Zhang, C. and Chen, Z., 2013. A new model for State-of-Charge (SOC) estimation for high-power Li-ion batteries. Applied Energy, 101, pp.808-814.

[69] Bae, K.C., Choi, S.C., Kim, J.H., Won, C.Y. and Jung, Y.C., 2014, February. LiFePO4 dynamic battery modelling for battery simulator. In Industrial Technology (ICIT), 2014 IEEE International Conference on (pp. 354-358). IEEE.

[70] Shen, Y., 2010. Adaptive online state-of-charge determination based on neuro-controller and neural network. Energy Conversion and Management, 51(5), pp.1093-1098.

[71] Einhorn, M., Conte, F.V., Kral, C. and Fleig, J., 2013. Comparison, selection, and parameterization of electrical battery models for automotive applications. IEEE Transactions on Power Electronics, 28(3), pp.1429-1437.

[72] Zhang, X., Zhang, W. and Lei, G., 2016. A Review of Li-ion Battery Equivalent Circuit Models. TRANSACTIONS ON ELECTRICAL AND ELECTRONIC MATERIALS, 17(6), pp.311-316.

[73] Fotouhi, A., Auger, D.J., Propp, K., Longo, S. and Wild, M., 2016. A review on electric vehicle battery modelling: From Lithium-ion toward Lithium–Sulphur. Renewable and Sustainable Energy Reviews, 56, pp.1008-1021.

[74] Chen, M. and Rincon-Mora, G.A., 2006. Accurate electrical battery model capable of predicting runtime and IV performance. IEEE transactions on energy conversion, 21(2), pp.504-511.

[75] Wei, J., Dong, G. and Chen, Z., 2017. On-board adaptive model for state of charge estimation of lithium-ion batteries based on Kalman filter with proportional integral-based error adjustment. Journal of Power Sources, 365, pp.308-319.

[76] Dubarry, M., Truchot, C. and Liaw, B.Y., 2014. Cell degradation in commercial LiFePO 4 cells with high-power and high-energy designs. Journal of Power Sources, 258, pp.408-419.

[77] Chui, C.K. and Chen, G., 2009. Kalman Filtering: with Real-Time Applications.

[78] Xiong, R., Sun, F., Gong, X. and He, H., 2013. Adaptive state of charge estimator for lithium-ion cells series battery pack in electric vehicles. Journal of power sources, 242, pp.699-713.

[79] Zheng, Y., Lu, L., Han, X., Li, J. and Ouyang, M., 2013. LiFePO 4 battery pack capacity estimation for electric vehicles based on charging cell voltage curve transformation. Journal of Power Sources, 226, pp.33-41.

[80] Sun, F., Xiong, R. and He, H., 2016. A systematic state-of-charge estimation framework for multi-cell battery pack in electric vehicles using bias correction technique. Applied Energy, 162, pp.1399-1409.

[81] Hu, X., Li, S. and Peng, H., 2012. A comparative study of equivalent circuit models for Li-ion batteries. Journal of Power Sources, 198, pp.359-367.

Appendix A Comparison among different embedded development boards

NAME	Microcontroller	Register Bits	Clock Speed	Flash Memory	UART	Remark
Arduino UNO	ATmega328	8	16MHZ	32KB	1	
Arduino Zero	ARM Cortex M0+	32	42MHZ	256KB	2	
Arduino Ethernet	ATmega328	8	16MHZ	32KB	-	Ethernet Controller
Raspberry pi 3	ARMv8 CPU	64	1.2GHZ	Micro-SD	2	1 Ethernet port 4 USB ports
STM32 F207IE	ARM Cortex M3	32	120MHZ	512KB	2	2 CAN controller 1 Ethernet port
Atmel SAM4E16E	ARM Cortex-M4	32	120MHZ	1024KB	2	2 CAN controller 1 Ethernet port
STM32F207 ZG-NUCLEO	ARM Cortex M3	32	120MHZ	1024KB	4	2 CAN controller 1 Ethernet port
NXP LPC11C14	ARM Cortex M0	32	50MHZ	256KB	1	CAN controller

Appendix B CAN bus message data format

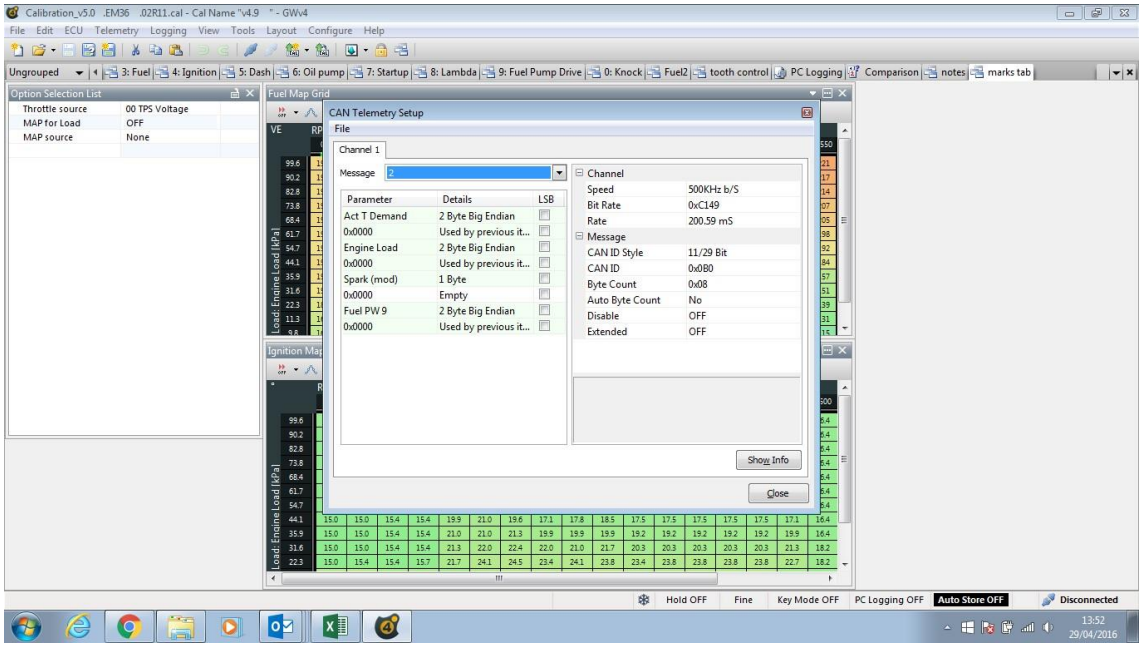

Figure B-1: Configuration of CAN bus message in ECU

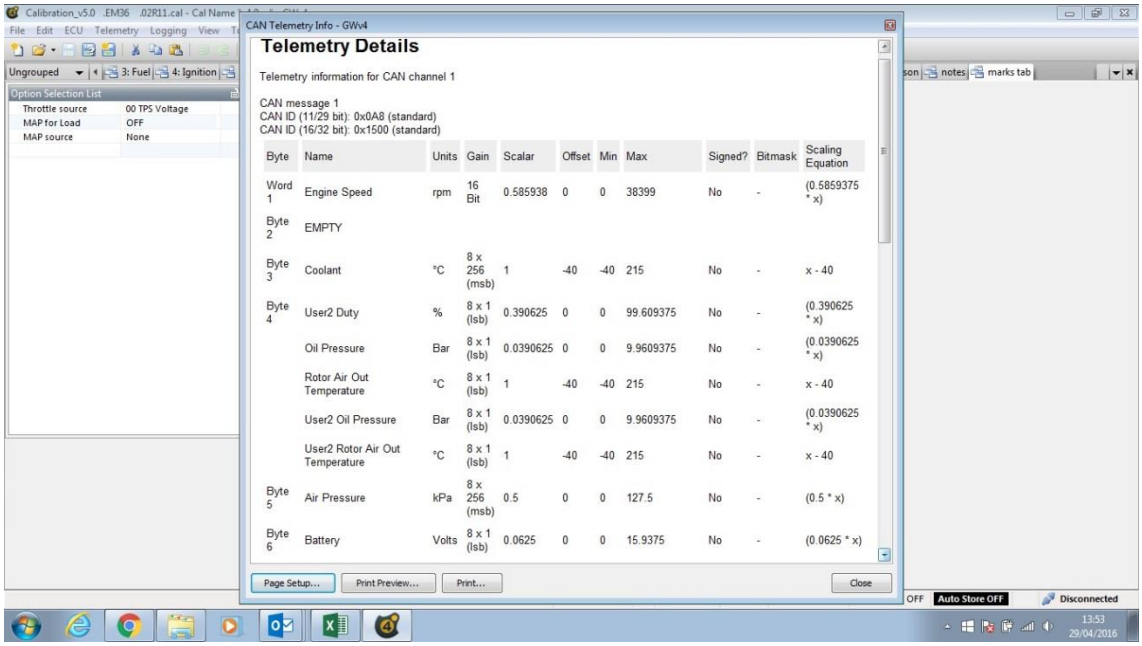

Byte	Name	Units	Gain	Scalar	Offset	Min	Max	Signed?	Bitmask	Scaling Equation
Word 1	Engine Speed	rpm	16 Bit	0.585938	0	0	38399	No	-	(0.5859375 * x)
Byte 2	EMPTY									
Byte 3	Coolant	°C	8 x 256 (msb)	1	-40	-40	215	No	-	x - 40
Byte 4	User2 Duty	%	8 x 1 (lsb)	0.390625	0	0	99.609375	No	-	(0.390625 * x)
	Oil Pressure	Bar	8 x 1 (lsb)	0.0390625	0	0	9.9609375	No	-	(0.0390625 * x)
	Rotor Air Out Temperature	°C	8 x 1 (lsb)	1	-40	-40	215	No	-	x - 40
	User2 Oil Pressure	Bar	8 x 1 (lsb)	0.0390625	0	0	9.9609375	No	-	(0.0390625 * x)
	User2 Rotor Air Out Temperature	°C	8 x 1 (lsb)	1	-40	-40	215	No	-	x - 40
Byte 5	Air Pressure	kPa	8 x 256 (msb)	0.5	0	0	127.5	No	-	(0.5 * x)
Byte 6	Battery	Volts	8 x 1 (lsb)	0.0625	0	0	15.9375	No	-	(0.0625 * x)

Figure B-2: CAN bus data format

Appendix C Work flow in the data exchange controller

C.1 Work flow of the main function

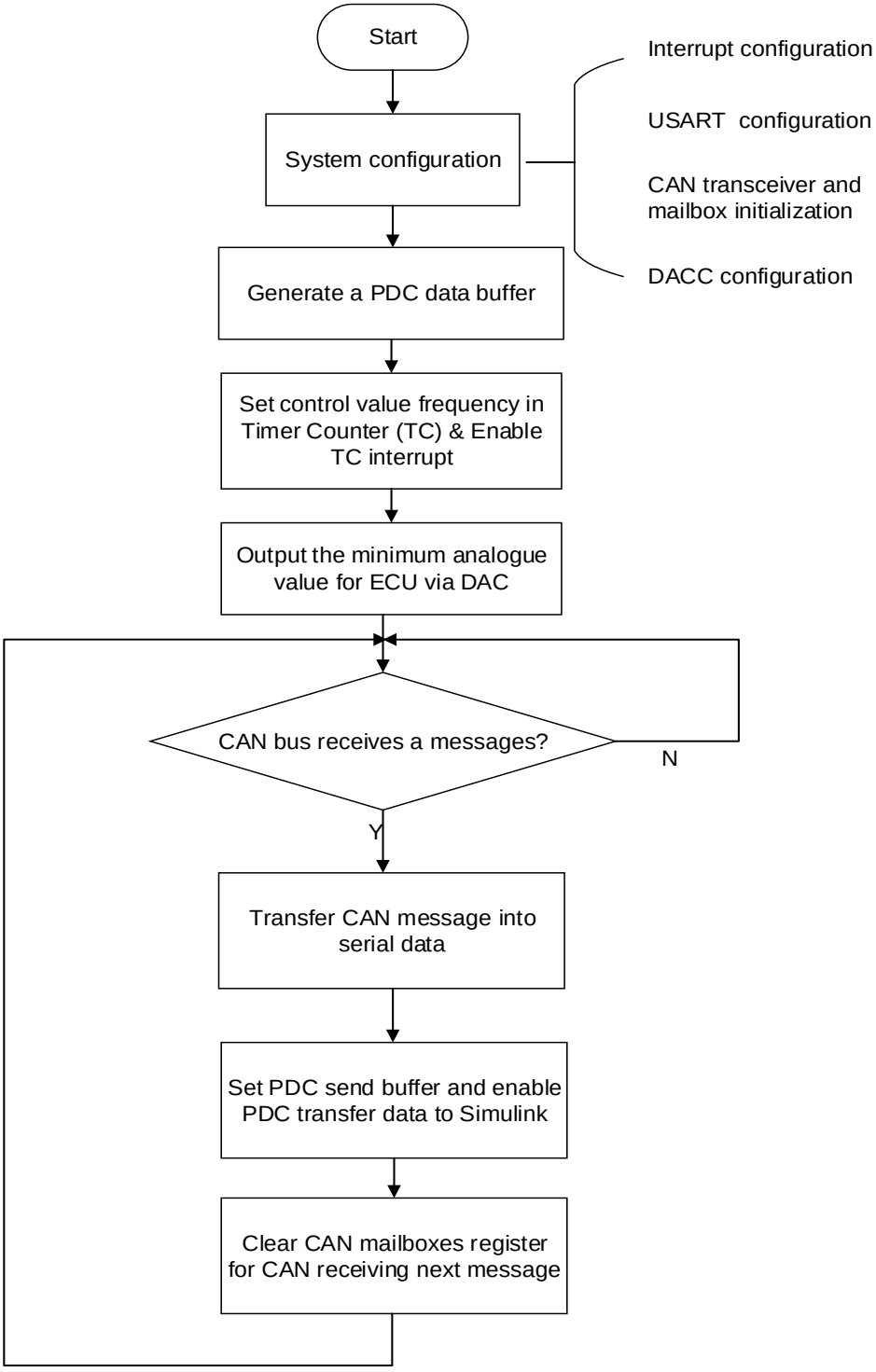

C.2 Work flow of the interrupt function

C.2.1 UART interrupt function

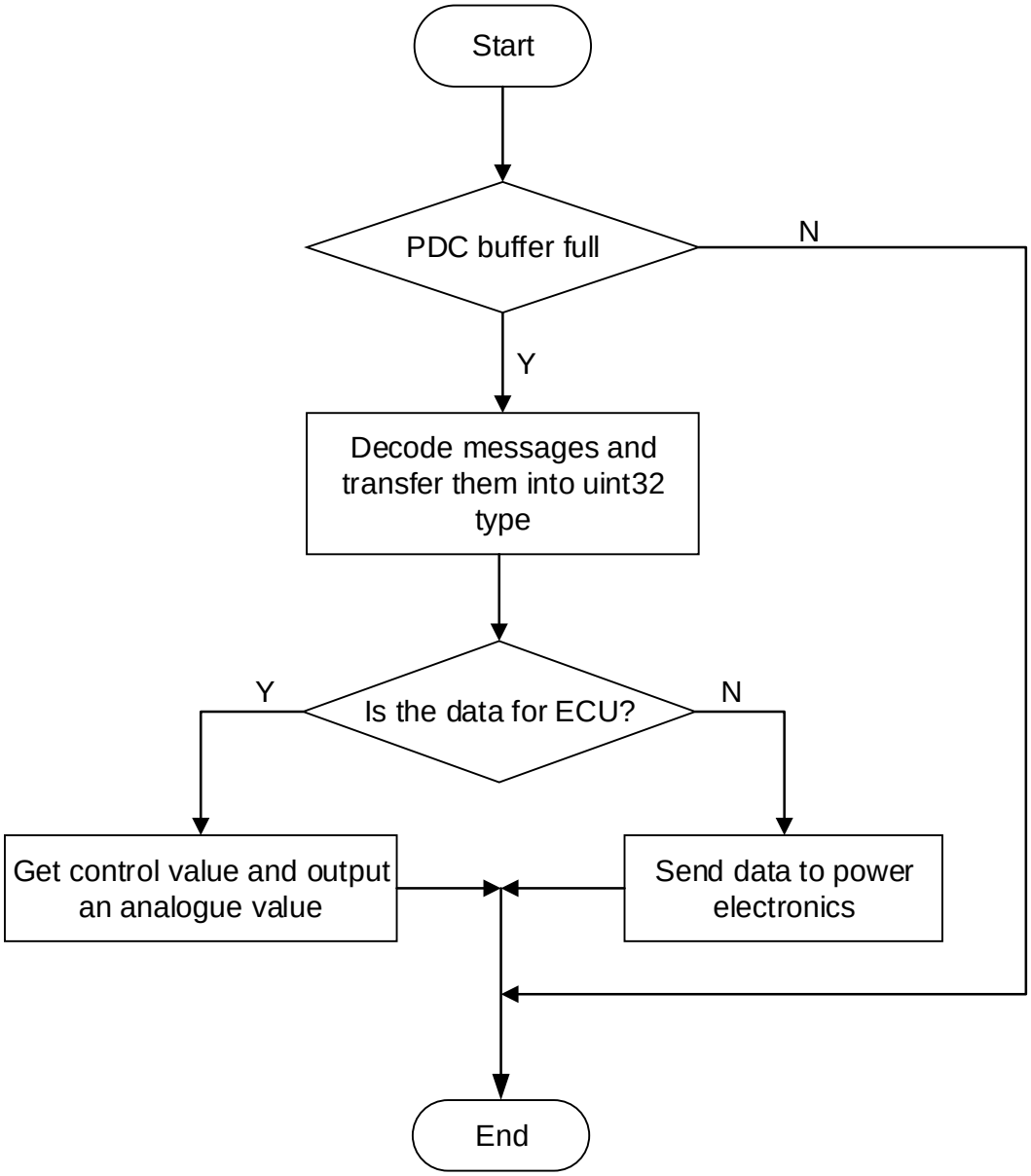

C.2.2 CAN interrupt function

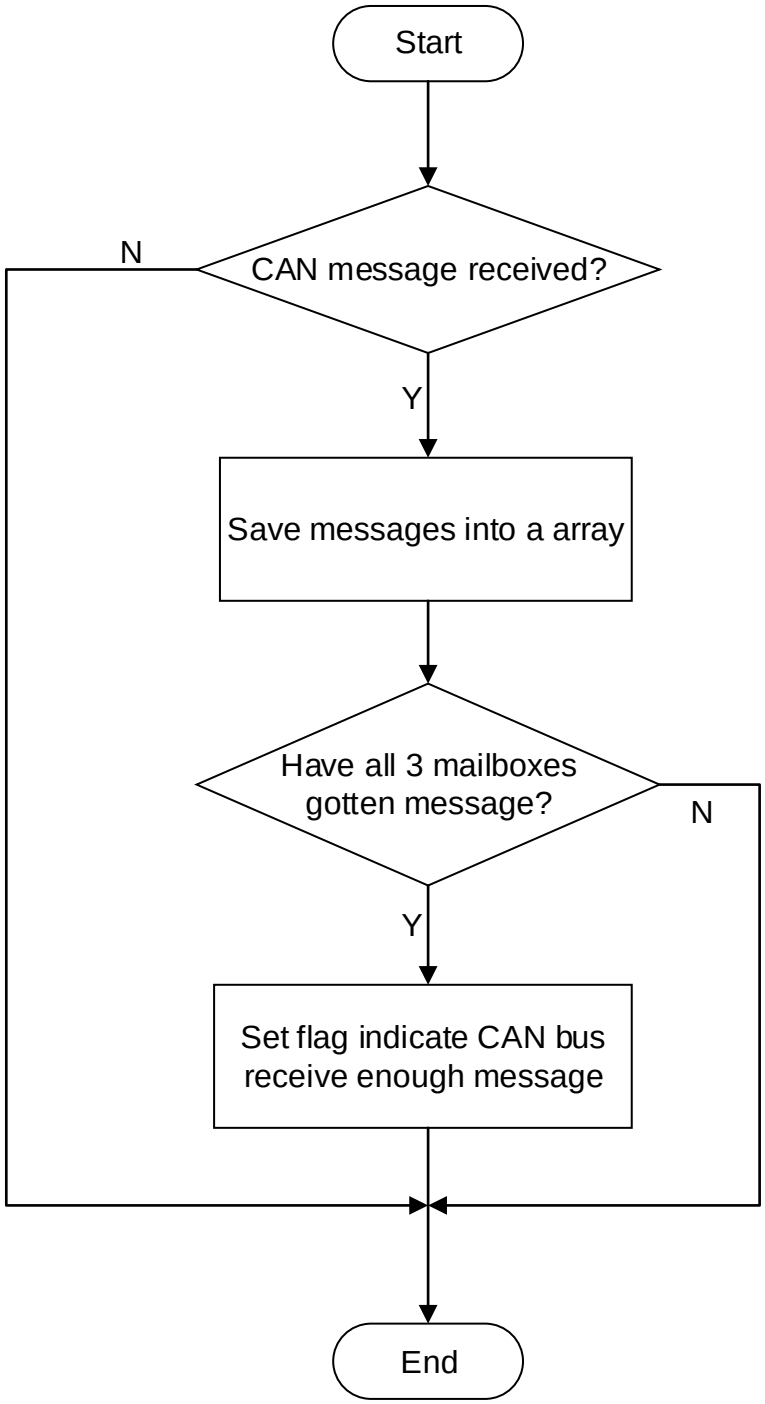

Appendix D SOC estimation flowchart